Waterflooding Management and Identifying IOR Opportunities in a Mature Reservoir

by
Yidan Zhu

A thesis submitted to the Department of Petroleum Engineering,
Cullen College of Engineering
in partial fulfillment of the requirements for the degree of

MASTER OF SCIENCES

in Petroleum Engineering

Chair of Committee: Dr. Ganesh C. Thakur

Committee Member: Dr. S.M. Farouq-Ali

Committee Member: Dr. Guan Qin

University of Houston
December 2019

ACKNOWLEDGMENTS

Firstly, I would like to express my sincere gratitude to my advisor, Dr. Ganesh Thakur (Distinguished Professor, Department of Petroleum Engineering & Director-Energy Industry Partnerships) for his patience, motivation, and immense knowledge. His guidance has helped me extensively in both conducting research and writing this thesis. I could not have imagined having a better advisor and mentor for my master's studies. Besides my advisor, I would like to give my special thanks to Dr. Syed Farouq-Ali and Dr. Guan Qin, who kindly served as my committee.

Secondly, I would like to express my appreciation to Dr. Peila Chen, Dr. Sriram Balasubramanian, and Dr. Zeinab Zargar. They have always been helpful in assisting and guiding various aspects of the project. Thanks to Dr. Sumantra Chatterjee for providing me a geological model for the reservoir of interest in this study.

I would like to also thank my parents for their support both emotionally and financially during my studies. Thanks to my friends for providing me the support to a successful completion.

ABSTRACT

This thesis has identified opportunities to improve production performance by utilizing secondary and tertiary recovery strategies in a mature oil reservoir. The identification techniques include analytical methods and simulation studies on field performance. Recommendations based on the field study and well performance were provided. A reservoir simulation study was carried out using Eclipse to conduct production predictions based on the recommendation. It can be concluded that infill drilling is the most effective way to develop this field and increase oil recovery. The result of this work will help the operator to improve reservoir management of the field and will also provide guidance in identifying areas that are suitable for a new infill drilling campaign.

TABLE OF CONTENTS

LIST OF TABLES

LIST OF FIGURES

NOMENCLATURE

B_g = gas formation volume factor (rb/Mscf)

B_o = oil formation volume factor at the start of waterflooding (rb/stb)

B_{oi} = initial oil formation volume factor (rb/stb)

B_w = water formation volume factor

E_D = displacement efficiency

E_I= vertical sweep efficiency

M_a = apparent molecular weight

N_p = current cumulative oil production

N_{p1} = cumulative oil production at the start of waterflooding (STB)

R_s = solution gas-oil ratio

S_{oi} = initial oil saturation

S_{or} = residual oil saturation

S_{wc} = connate water saturation

k_{ro} = oil relative permeability

k_{rw} = oil relative permeability

q_1 = production rate at the start of the decline

q_2 = production rate at the end of the decline

$q_{current}$ = current oil rate

q_{limit} = economic oil rate

q_o= oil production rate

q_w = water production rate

q_{wi} = water injection rate

t_1 = start of the decline

t_2 = end of the decline

μ_o = oil viscosity

μ_w = water viscosity

ρ_g = gas density (gm/cc)

ρ_o = oil density

μ_g = gas viscosity (cp)

h = depth

S_g = gas saturation at the start of injection

GOR = producing gas-oil ratio

M = mobility ratio

N = Original oil in place (STB)

T = temperature (˚R)

V = Dystra-Parsons permeability variation

d = decline rate

p = pressure (psi)

z = compressibility factor

CHAPTER 1: INTRODUCTION

Hydrocarbon reservoirs typically are developed through a series of stages: primary, secondary, and tertiary oil recovery. The ideal time to start managing a reservoir is at its discovery (*Thakur, 1990*). Therefore, it is of great significance to have decent reservoir management so that the life span of reservoirs can be extended with proper recovery techniques.

The field N-384 under study in this thesis has been under production since 1986 and is currently under waterflooding. It is critical to perform an analytical and simulation study to estimate the potential of the reservoir. Recommendations can be made on waterflooding management and surveillance as a method of putting principles into practice. A black oil simulation study on a sector of the entire field will be carried out for the prediction of infill wells' performance.

Data collection is the first step to have a better understanding of the reservoir. Field data such as production, completion, core flood, and PVT data were provided by the operator. In the analytical study, multiple diagnostic plots based on production data and pressure data were generated to assist in analyzing the performance of the field. Material balance study is one of the simplest and most straightforward mathematical techniques to study the basic physics behind reservoir production. Material balance study shows that the field under consideration has an aquifer support.

In the reservoir simulation study, the black oil model-based simulation was carried out using Eclipse (Petrel RE). The static geological model was built by the geologist in our research group. In the methodical history match runs, several

sensitivity cases were conducted to investigate the uncertainty and reliability of the geological model. It can be observed from the history match result that the field has strong aquifer support, which is consistent with the result from the material balance study. At the end of the history match, the oil phase productivity index was calibrated and the status quo case for the prediction was run before predicting any workover or infill drilling effect on recovery improvement. In all prediction cases, flowing bottomhole pressure (FBHP) was used as a constraint. A total of six prediction cases were conducted from 2019 to 2040. The simulation with two infill wells yields the highest ultimate oil recovery.

CHAPTER 2: BACKGROUND

This section provides a review of the analytical and numerical methods of reservoir management employed in this study.

2.1: Analytical method of reservoir management

In general, the main objective of reservoir management is to optimize profitable oil and gas recovery (*Satter, Varnon, and Hoang, 1994*). From an analytical aspect, diagnostic plots play an important role in reflecting the field conditions. For instance, production rate vs. time or cumulative production during secondary recovery can be used to extrapolate an estimation of ultimate recovery or may indicate improvement in the waterflooding performance (*Thakur, 1991*). In this study, the diagnostic plots used are as follows:

1. Oil rate vs. time
2. Oil rate, well count vs. cumulative production
3. Water oil ratio (WOR) vs. cumulative production
4. After – Before – Compare (ABC) plot
5. Voidage replacement ratio plot.

The utility of these plots will be discussed in Chapter 4 in detail.

For the field under the secondary recovery stage, investigating sweep efficiency can provide significant insight into the heterogeneity of the reservoir and a better understanding of the field geology.

Material balance calculations are useful methods for reservoir performance analysis (*Walsh, 1995*). Nowadays, this method has been integrated into reservoir engineers' toolbox for reservoir evaluation workflow. The material balance equation is

the simplest expression of the mass balance in the reservoir, and it assumes the reservoir as a tank. From the material balance study, the drive mechanism of the reservoir, original oil in place (OOIP), and other necessary parameters of the reservoir can be estimated. In this study, the software MBAL from IPM toolkit was used to estimate OOIP and inferred aquifer size.

2.2.: Reservoir Simulation

The Merriam-Webster Dictionary defines simulate as assuming the appearance of without the reality. Simulation of petroleum reservoir performance refers to the construction and operation of a model whise behavior assumes the appearance of actual reservoir behavior. The advantage of reservoir simulation is that it can identify "what if" scenarios. It can test not only various development alternatives but also the impact of uncertain reservoir parameters.

Reservoir simulation is an area of reservoir engineering in which computer models are used to predict the flow of fluids through porous media. Conventional finite difference simulation is underpinned by three physical concepts: conservation of mass, isothernal fluid phase behavior, and the Darcy approximation of fluid flow through porous media. Black-oil simulator is used thoughout the simulation study.

CHAPTER 3: FIELD DESCRIPTION

This section provides a field overview along with its conditions, geological properties and producing fluid properties. The field description assists in understanding the recovery status and future development strategies.

3.1: Reservoir Description

The field N-384 is a reservoir located in the northeastern part of India. It started production in 1986 and water injection was initiated in 2009. The production zone is consolidated sandstone formation at an average depth of 9665 feet (2946 meter). The oil zone interval thickness is 223 feet (68 meters). The field was developed with only vertical wells. A total of 15 wells has been drilled until now (See Figure 3-1). Currently, there are four active producers and one active injector. The initial reservoir pressure was 3900 psi and the bubblepoint pressure is 3500 psi with 39.93 MMSTB OOIP reported by the operator. The cumulative oil production until Apr. 2018 was 13.31 MMSTB, which corresponds to a recovery factor of 33.3%. Key parameters about the field are summarized in Table 3-1.

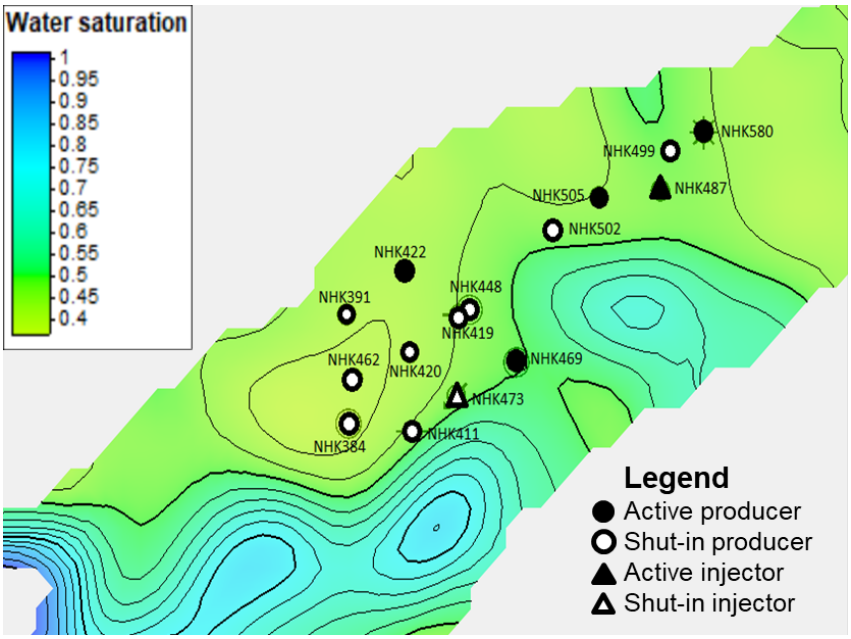

Figure 3-1. Field map with well location

Table 3-1. Field parameters

PARAMETER	VALUES
Field Name	N-384
Depth, ft.	-9665 (-2946 m.)
Formation	B 4th
Average Net Pay, ft.	88 (27 m.)
Original Oil in Place, MMSTB	39.94 (6.35 MMKLS)
Cumulative Oil Production, MMSTB	13.31 (2.116 MMKLS)
Initial Reservoir pressure, psi	3900
Current Reservoir Pressure, psi	3669
Cumulative Injection, MMSTB	10.46 (1.66 MMKLS)
No. of active producers	4
No. of active injectors	1

3.2: PVT Data and Core Data Review

3.2.1: PVT Data

PVT data was obtained from the measurement performance using the fluid samples collected from well N411 and N448. Table 3-2 provides a summary of the fluid properties from PVT analysis.

Table 3-2. PVT Data

Parameters	N411	N448
Bubblepoint Pressure, psi	3435	3490
Reservoir temperature, ˚F	181	186
API˚	30.1	31.6
B_o at bubblepoint pressure, rb/stb	1.4	1.44
Current B_g, rb/Mscf	0.836	0.842
R_s at bubblepoint pressure, Mscf/stb	0.864	0.887
Oil viscosity, Cp	0.56	0.46
Rock compressibility, 1/psi	3.69E-06	NA

Typically, when plotting B_o and viscosity data, the point at which the trend changes may be used to determine the bubblepoint pressure of the reservoir fluid. However, the data from two PVT reports are not consistent with each other.

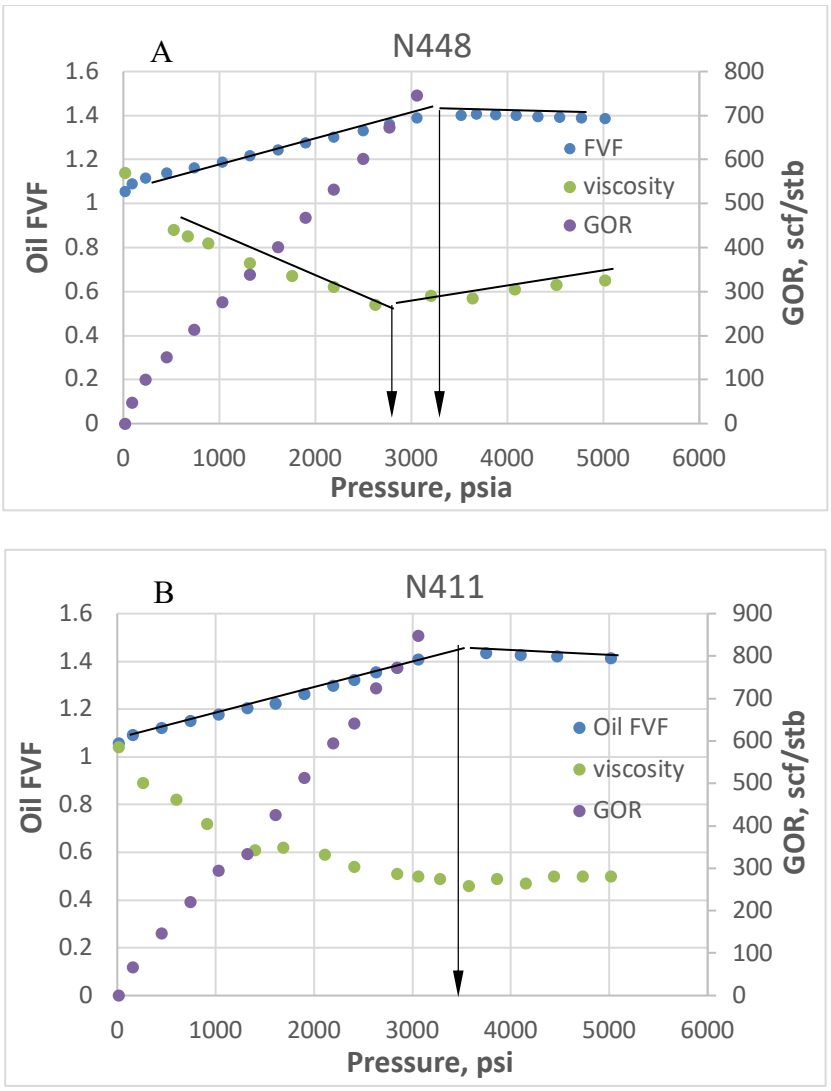

Figure 3-2. PVT data from two reports.

In figure 3-1A, B_o data indicates that the bubblepoint pressure is at 3500 psi, and the value from viscosity is much less than 3500 psi. In Figuer 3-1B, both B_o data and viscosity data indicate bubblepoint pressure is 3500 psi. In the following study, the bubblepoint pressure is assumed as 3500 psi.

Only the gas formation volume factor (B_g) data below bubblepoint pressure is available. For the data we need above bubblepoint pressure, the empirical equation is used. In the following plot, red dots stand for lab data, and blue dots are calculated by

the empirical equation. Below bubblepoint pressure, the data is overlapping, which means the calculated values are accurate enough for further consideration.

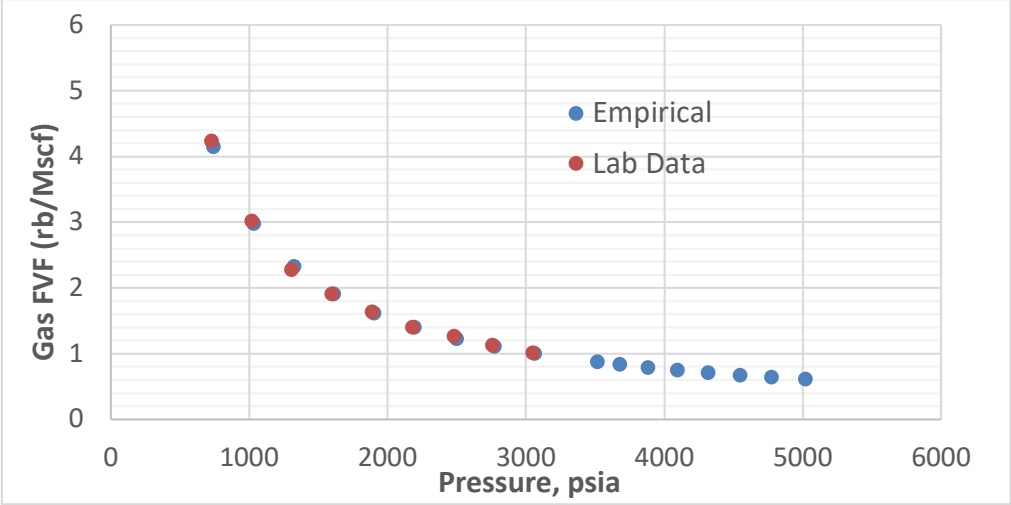

Figure 3-3. Gas formation factor.

The empirical equation used is

$$B_g = 5.036\frac{zT}{p}, \tag{3-1}$$

where

B_g = gas formation volume factor (rb/Mscf)

z = compressibility factor

T = temperature (˚R)

p = pressure (psi)

Gas viscosity (μ_g) is not available from the reports and all data was calculated with the empirical equations. The equations (taken from *Lee, Gonzales, and Eakin*, 1966) are:

$$\mu_g = A\, exp\left(B{\rho_g}^C\right)(10^{-4}), \tag{3-2}$$

$$A = \frac{(9.379+0.01607M_a)T^{1.5}}{209.2+19.26M_a+T}, \tag{3-3}$$

$$B = 3.448 + \frac{986.4}{T} + 0.01009M_a, \quad (3\text{-}4)$$

and

$$C = 2.447 - 0.2224B \quad (3\text{-}5)$$

ρ_g = gas density (gm/cc)

M_a = apparent molecular weight

T = temperature (˚R)

μ_g = gas viscosity (cp)

3.2.2: Core Analysis Data Review

Routine and special core analysis was conducted on the core samples retrieved from well N422. The air permeability, porosity, and relative permeability were determined and summarized in Table 3-3 and Table 3-4.

Table 3-3. Air Permeability Data

Depth Range, m	Permeability, MD		Porosity, %
	Horizontal	Vertical	
3054.72-3054.97	61.6	46.7	19.37
	57.3	27.3	
3052.38-3052.68	90.2	43.8	30.03
	42.3		
3051.13-3051.38	64.8	37	19.25
	37.5		
3049.95-3050.15	470.3	170.1	19.9

Table 3-4. Relative Permeability Summary

Core Depth, m	Porosity, %	S_{wi}, %	Effective k at S_{wi}, MD	k_{rg}	k_{ro}	k_{rw}
3049.95-3050.15	19.9	21.5	374	0.45	0.119	
3049.95-3050.15	19.9	24.89	116		0.47	0.08
3052.38-3052.68	30.03	39.8	16	0.29	0.08	
3052.38-3052.68	30.03	37.21	17	0.53	0.098	
3052.38-3052.68	30.03	39.8	16		0.49	0.12
304.72-3054.97	19.37	41.3	93	0.83	0.14	

From Table 3-3, a significant amount of uncertainty can be observed from the lab data results. One sample showed relatively high permeability while the other three were moderate. A conservative porosity value of 20% was chosen for the following studies. The range of initial water saturation is from 21.5% to 41.3%. 30% initial water saturation was deemed appropriate for further use. In water-oil relative permeability curves (See Figure 3-6), only two core samples were tested, and one of the sample gave high endpoint values. The water saturation start point of the other core is from 30%, therefore, 30% of initial water saturation was chosen. Due to the paucity of the sample, test specimens for the high permeability core could not be taken for the capillary test.

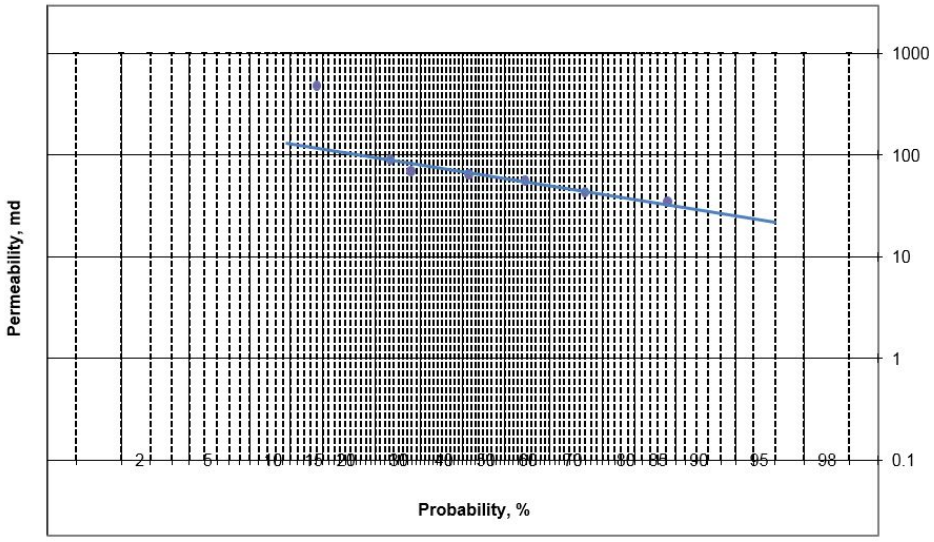

Figure 3-4: Permeability data for core sample.

Based on the available core data, heterogeneity of the reservoir could not be determined. The limited dataset is not enough to obtain a representative trend line for the whole reservoir. The calculated Dykstra-Parsons variation factor from Figure 3-3 is 0.31, which is not representative for this field due to its heterogeneous nature.

Dykstra-Parsons Coefficient is also calculated with the processed log data from the same well. The data was read every meter from the log. Figure 3-4 shows the data plotted on the probability log paper, and the calculated Dykstra-Parsons Coefficient from log data is 0.8 and it is used in the following calculation and study.

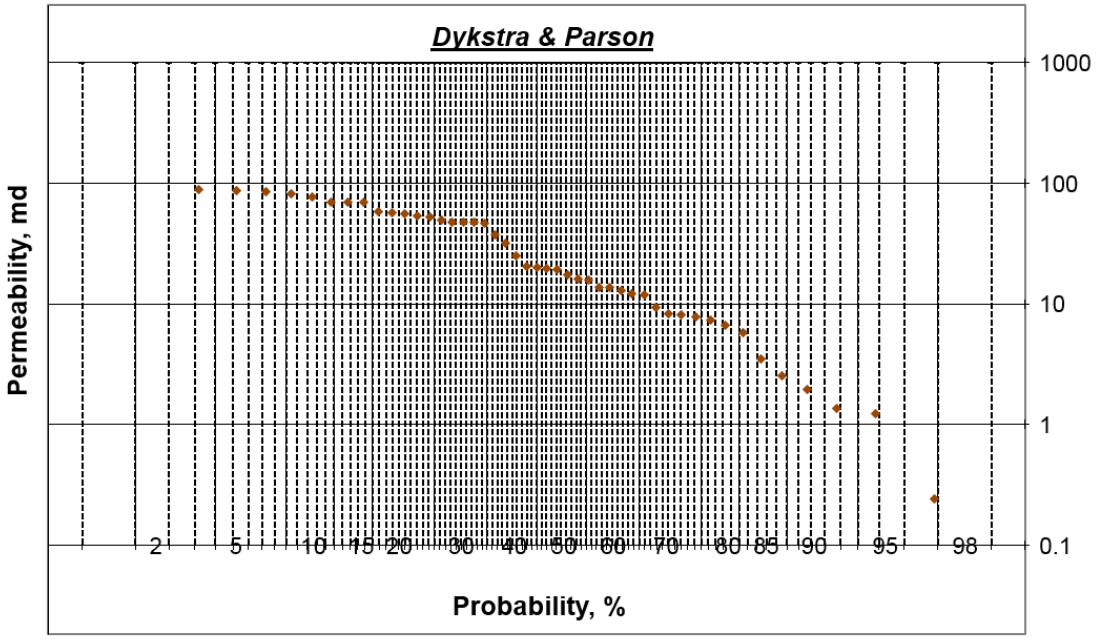

Figure 3-5. Permeability data from log.

The following two plots (Figure 3-4) show the relative permeability raw data. It can be observed that there is significant uncertainty from raw data.

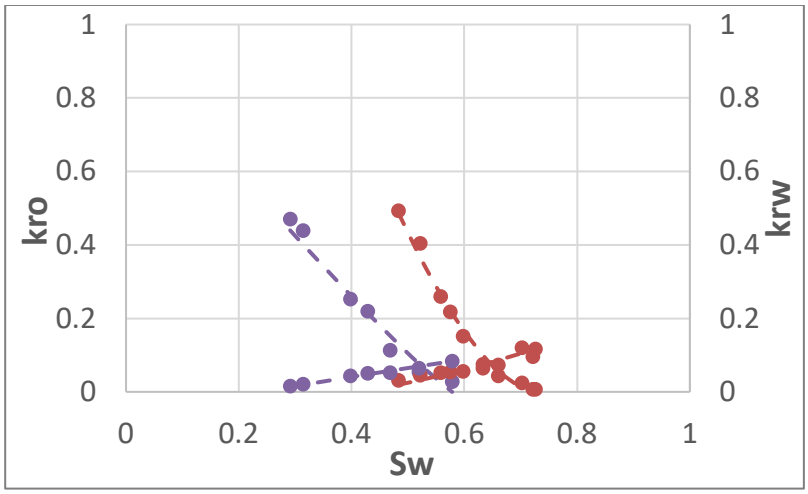

Figure 3-6. Water-oil relative permeability data from core sample.

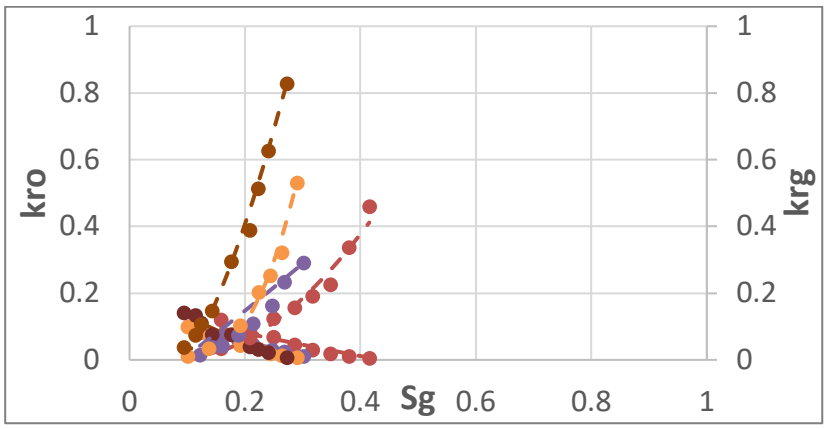

Figure 3-7. Oil-gas relative permeability data from core sample.

CHAPTER 4: ANALYTICAL METHODS FOR EVALUATION OF PRODUCTION PERFORMANCE

Before any secondary or tertiary recovery techniques are implemented, it is essential to evaluate field performance. The analytical method is to simply determine the estimated ultimate recovery (EUR) for a field, or a group of wells, or a single well in a development plan with production data only. This analysis process can not only help to gain a better understanding of the behavior of the reservoir but also provide guidance in the reservoir simulation.

In this chapter, production performance analysis will be discussed based on multiple diagnostic plots, and different analytical methods.

4.1: Diagnostic Plots for Evaluation of Waterflooding Performance

Diagnostic plots are powerful tools to reflect production history and trend with field operations. The plots can also help in the estimation of the ultimate recovery factor. Different types of diagnostic plots of the field under study will be discussed in the following sections in detail along with their usages.

4.1.1: Oil rate plot vs. time

A simple semilog plot of oil rate, water production rate, water injection rate, number of active producers vs. time serves as a very important tool in diagnosing field response (*Chen, Zhu, and Deka et al., 2019*).

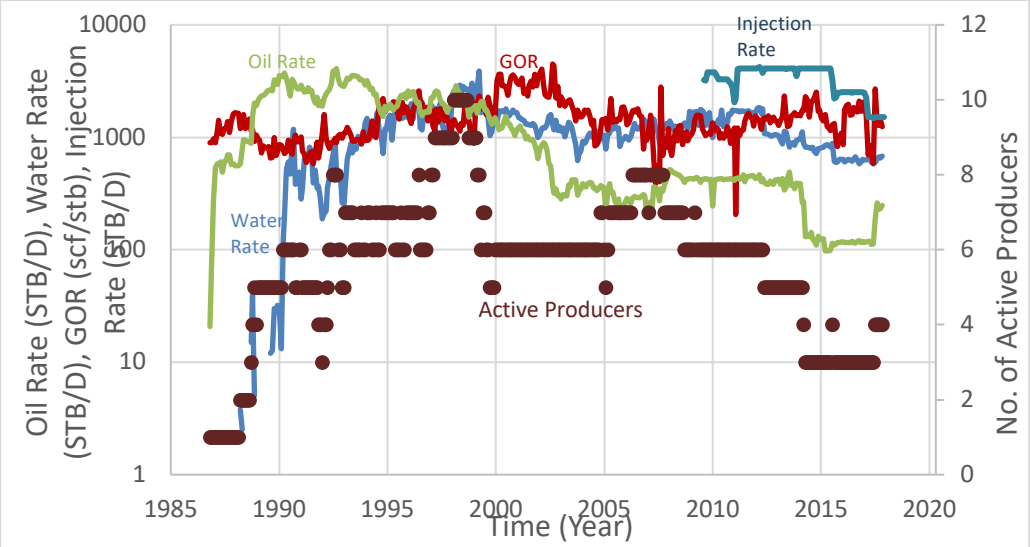

Figure 4-1. Field performance for N-384.

From the beginning of the production, Figure 4-1 clearly captures the trend that the oil rate increases with the increasing well count. Water injection started in 2009, and the injection rate was kept constant from 2011 to 2015. During this time period, the oil rate was kept constant as the injection rate was constant. The oil rate decreased 2015 onwards because of the closure of a few key wells. At the end of the last six months, the oil rate increased due to the addition of one more producer.

Since the field was initially undersaturated, the gas-oil ratio (GOR) should be constant before the reservoir becomes saturated. Additionally, the GOR should be consistent with the solution gas-oil ratio value from the PVT test report. In this case, GOR is around 900 SCF/STB at the beginning of depletion. Overall, oil production responds to the field operation quite well.

This semi log plot can also help estimate EUR. If only the oil rate curve from Figure 4-1 were selected and extrapolated, a trend line at the end of the production

(Figure 4-2) can be obtained. This trend line can be described by an exponential decline rate using equation 4-1

$$d = \frac{1}{t_2 - t_1} ln \frac{q_1}{q_2} \ , \qquad (4\text{-}1)$$

where

d = decline rate

t_1 = start of the decline

t_2 = end of the decline

q_1 = production rate at the start of the decline

q_2 = production rate at the end of the decline

For this particular case, no obvious exponential decline trend can be captured. Therefore, the previous decline trend was used for extrapolation. Figure 4-2 shows the detail.

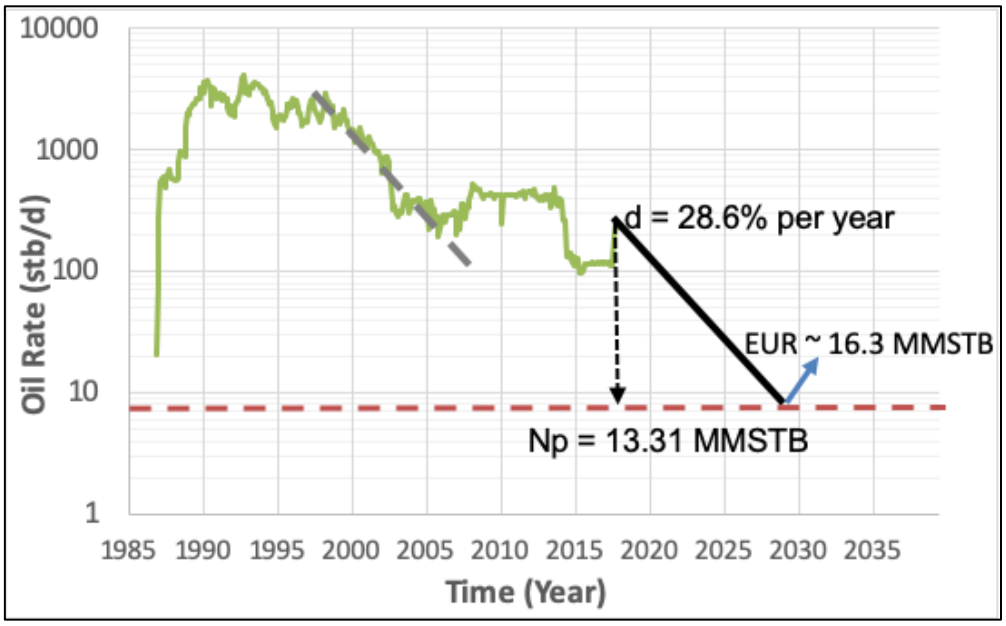

Figure 4-2. Decline Curve Analysis.

With the calculated decline rate, EUR can be determined with following the equation

$$EUR = N_p + \frac{q_{current} - q_{limit}}{d}, \quad (4\text{-}2)$$

where

N_p = current cumulative oil production

$q_{current}$ = current oil rate

q_{limit} = economic oil rate

d = decline rate

The result of decline curve analysis and EUR estimation are summarized in Table 4-1.

Table 4-1. Summary of Decline Curve Analysis

t_1, year	2020	d, %/year	28.6
t_2, year	2030	$q_{current}$, BOPD	247.16
q_1, BOPD	105	q_{limit}, BOPD	10
q_2, BOPD	6	EUR, MMSTB	16.33

4.1.2: Oil rate vs. cumulative oil production

The oil rate vs. cumulative oil production plot is a modification of oil rate vs. time plot. The only input needed in this Cartesian plot is historical oil production. Figure 4-2 shows a correlation between oil production rate, well count and water injection rate. It can be concluded that if any operation in the field were not effective, the production would follow the declining trend as the grey dash line indicates. There are four noticeable incremental productions through depletion history. Every time when oil production increased, it was due to the opening of the new wells before the onset of water injection. After water injection was implemented, production performance responded to waterflooding.

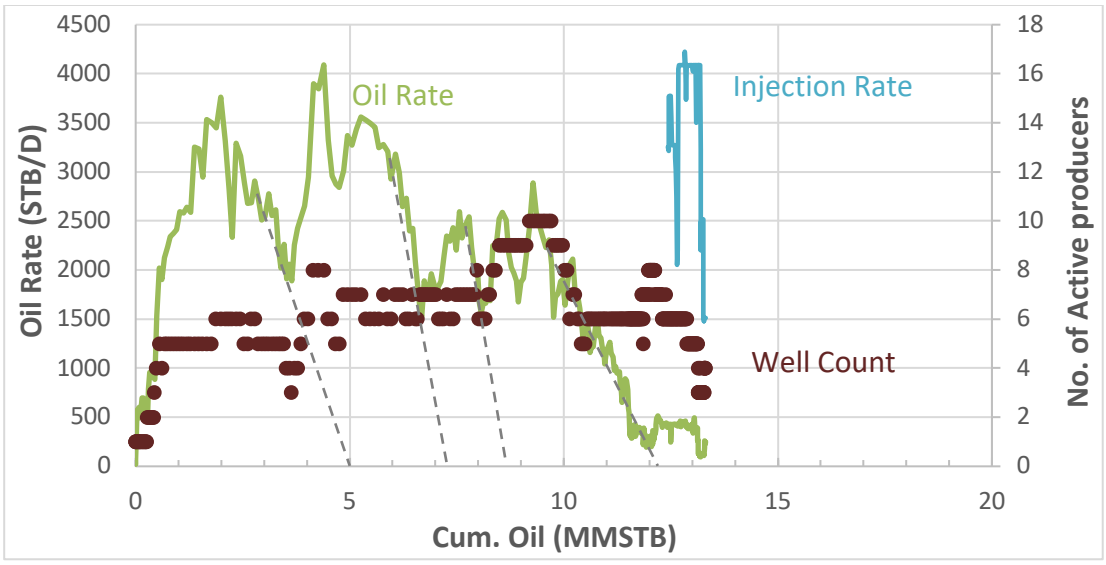

Figure 4-3. Production plot of field N-384 (Oil rate vs. cumulative oil).

4.1.3: Water oil ratio (WOR) vs. cumulative oil production

The semi log plot of WOR vs. cumulative oil is a good indicator of channeling and heterogeneity. Extrapolation of the WOR vs. cumulative oil plot is useful in determining the incremental recovery due to infill drilling or operational changes (*Baker, 1998*). Even though water injection rate decreases in the last few months, it has not arrested the oil production decline. Waterflooding is managed well, and WOR dropped in the most recent months, which can be inferred in the following figure. For the field under study, Economic limit was set as a WOR of 50, which is equivalent to 98% water cut. If the field was managed well and followed current WOR trend, it would yield a cumulative oil production of 16 MMSTB (40% of OOIP could be recovered).

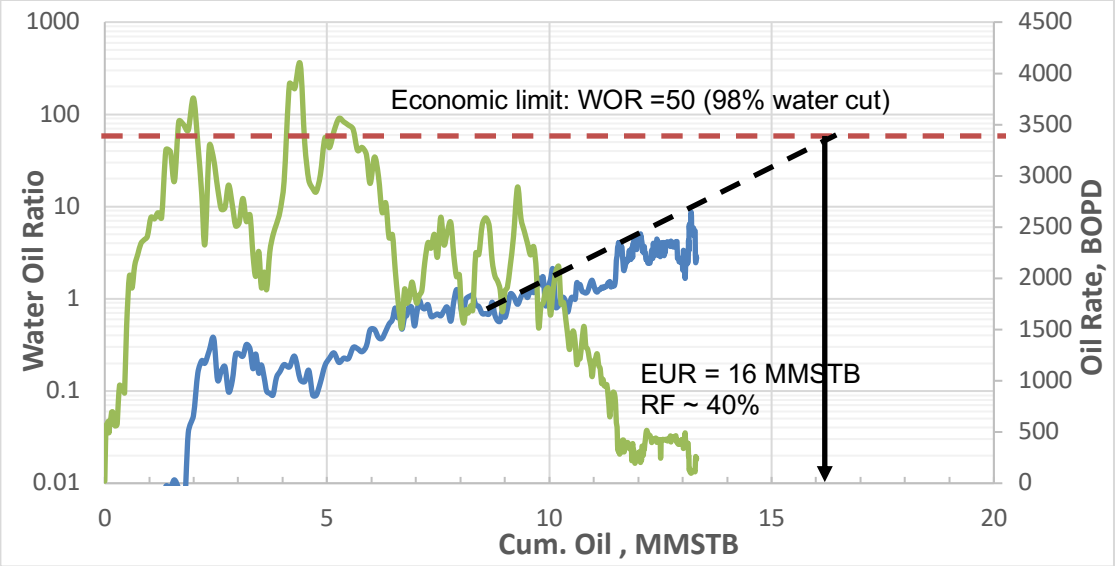

Figure 4-4. WOR vs. cumulative oil production of field N-384.

4.1.4: After-Before-Compare (ABC) Plot

This plot uses production data from two distinct dates and compares oil and water rate between those dates. The same dates are used for all wells (*Terrado, Yudono, and Thakur, 2006*). ABC Plot is a convenient tool for well-scale production performance. The changes can be used to assist in adjusting the operation of the well and identifying the region for IOR/EOR opportunities (*Chen et al. 2019*).

The x-axis and y-axis of ABC plot cross at the point (1, 1). If the wells fall on this point, it means there is no change on these wells. If the total liquid rate of the well increases, the well will fall on the slope line above (1, 1). If the well falls on the slope line below (1, 1), the total liquid of the well decreases and there might be an out-of-zone injection or well damage may exist. For wells in the first quadrant, water sweeps the oil like a leaky piston. Water displaces the oil towards the wellbore, and bypasses a small amount of oil resulting in a high sweep efficiency. For wells in the second quadrant, oil bank is forming in the formation. If the wells fall in the third quadrant,

they might have low injectivity or channeling problem. If the wells fall in the fourth quadrant, it could be a sign of a poor displacement flood in the field.

ABC Plots of N-384 field were generated with production data at one year, six months, three months and one month ago from up-to-date data. The changes can be observed noticeably between the comparison of three-month plot and a one-month plot.

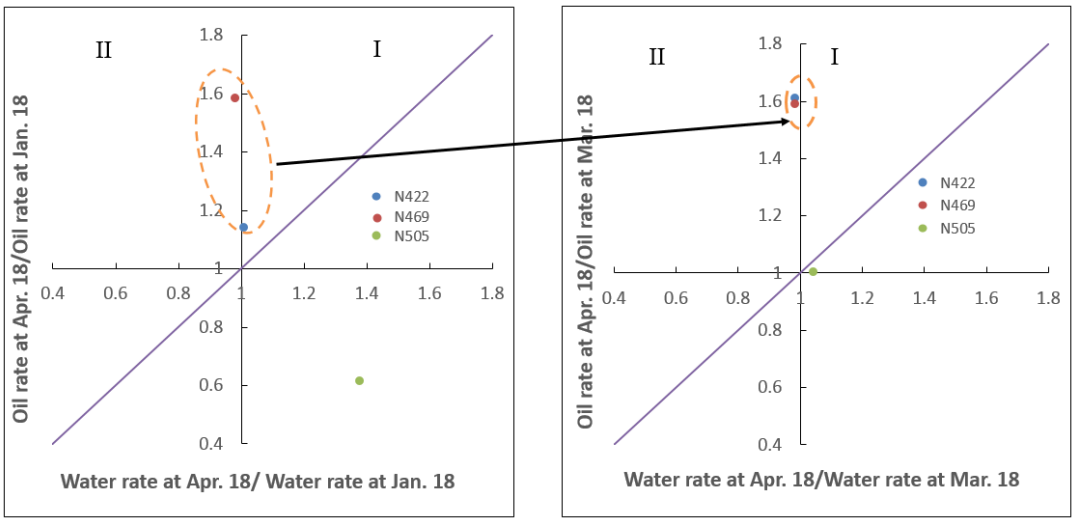

Figure 4-5. ABC plot comparison with three-month data and one-month data of field N-384.

From the comparison of the ABC plot between two different time periods, the performance of all three active producers improved with a decreasing water cut.

4.1.5: Alternative ABC Plot

In this section, I briefly discuss the new findings based on ABC Plot (See Sec. 4.1.4) in this study. In this study, I introduced a new analytical technique for waterflooding performance evaluation. This new findings was inspired by After-Before-Compare (ABC) plot invented in 2006. In the previous ABC plot, the oil rate

ratio is presented in y-axis and the water rate ratio is shown in the x-axis. Oil rate ratio and water rate ratio for all the wells are calculated individually from two distinct dates.

In the alternative plot, the x-axis is replaced by the FBHP ratio from two distinct dates. The advantages of this modified ABC plot are:

1. Filtering down the number of wells that need analysis and required immediate actions
2. Positioning of the wells in various quadrants for identification of specific issues for individual wells.

Figure 8-1 illustrates the differences between the previous ABC plot and the modified ABC plot.

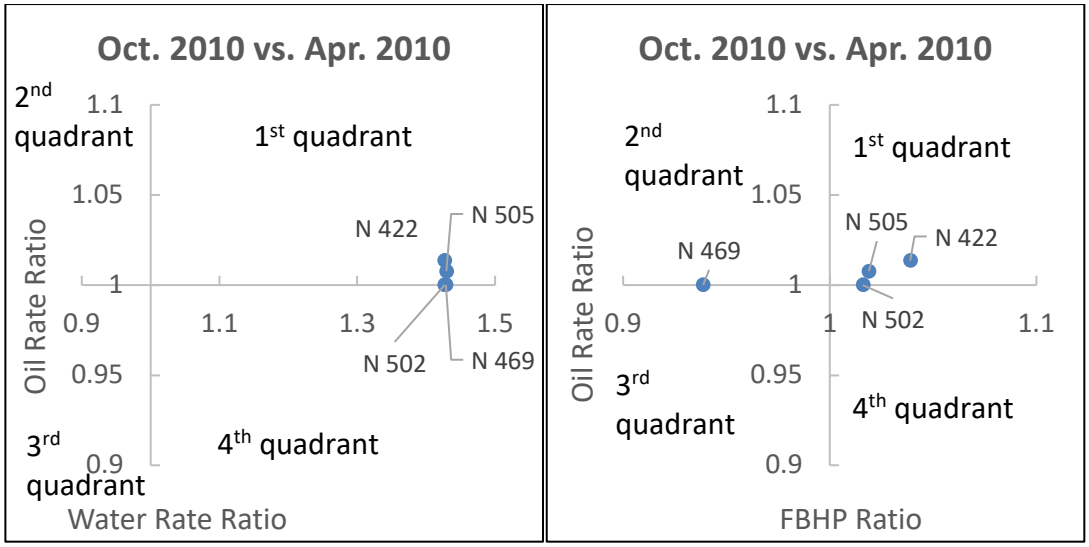

Figure 4-6. Comparison of the original and alternative ABC plot.

In the modified ABC plot, each point stands for each individual well, in which some features and properties can be quickly identified:

1. 1st quadrant: Both FBHP and oil rate ratios of the wells are greater than one. This observation implies that both the oil rate and FBHP are increasing as a

function of time. The surrounding well may be shut in or water injection supports surrounding pressure. It is an indication that a good pressure support from the aquifer or water injection

2. 2nd quadrant: Positioning of the wells in this quadrant implies an increasing oil rate and falling FBHP is decreasing as normally expected for a well. These wells do not require much attention if they were frequently tested throughout the selected period.
3. 3rd quadrant: The wells fell in this quadrant are facing some challenges as FBHP and oil rate ratios are both decreasing. This means that this portion of the reservoir requires more pressure support.
4. 4th quadrant: Wells fell in this quadrant have increasing FBHP but decreasing oil rates. There are two different scenarios in this quadrant. First, if the wells have an increasing water cut trend, it may because of breakthrough problems. Secondly, if water cut of the well is constant or decreasing, it is a good indication that by lowering FBHP, oil production will increase.

Figure 4-7 shows examples of the field N-384.

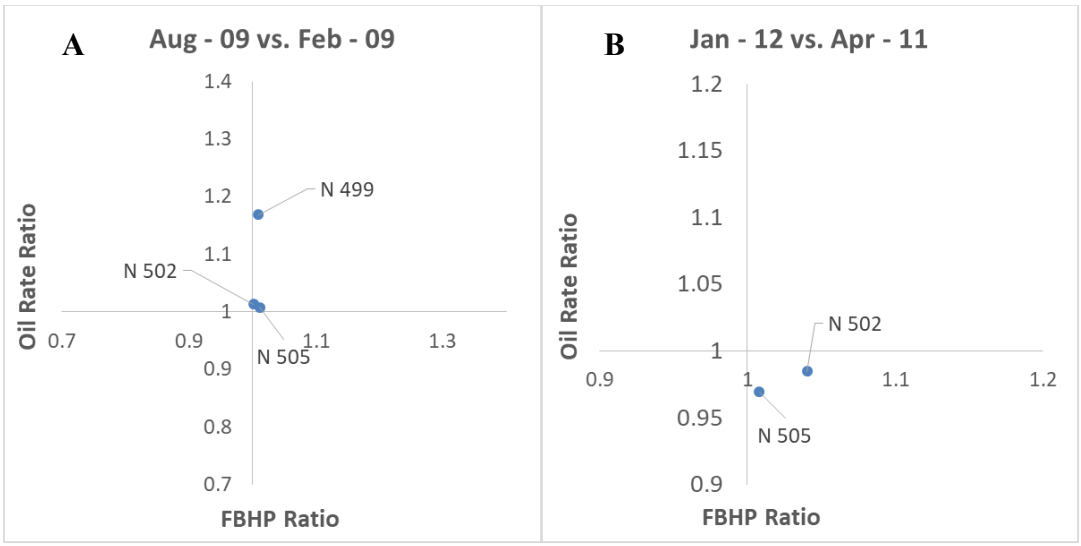

Figure 4-7. Alternative ABC plot for N-384 field.

In Figure 4-7A, all wells fall in the first quadrant, which indicates that the oil rate increases in all the wells. The reason for FBHP increase might be because of one surrounding well N580 being shut in July 2019.

In Figure 4-7B, we noticed that both wells fall in the 4th quadrant, and they are in the first scenario that they have an increasing water cut trend. These wells probably are the low performers in the field.

The limitation of the alternative ABC plot is that FBHP measurements are not always available and this method is not based upon any theortical concepts. It is recommended that this technique should be further tested in other fields.

4.1.6: Voidage Replacement Ratio (VRR) vs. time

Voidage replacement ratios on both a field basis as well as a pattern basis should be calculated in the following manner

$$VRR = \frac{injected\ reservoir\ volumes}{produced\ reservoir\ volumes} = \frac{B_w q_{wi}}{B_o q_o + B_w q_w + q_o (GOR - GOR) B_g}, \qquad (4\text{-}3)$$

where

B_w = water formation volume factor

B_o = oil formation volume factor

B_g = gas formation volume factor

q_{wi} = water injection rate

q_w = water production rate

q_o= oil production rate

GOR = producing gas-oil ratio

R_s = solution gas-oil ratio

The computation should be done cumulatively as well as instantaneously (e.g., monthly) and plotted versus time, providing another tool for monitoring waterflooding performance (*Baker, 1998*).

When monthly VRR is greater than 1.0 and reservoir pressure is not increasing, out-of-zone injection loss from the target zone or severe thieving is suspected. When monthly VRR is less than 1.0 and reservoir pressure is not decreasing, an influx of fluids is suspected (e.g., aquifer influx into the control area). Plotting the oil rate vs. time along with VRR vs. time helps one understand the relationship between these variables.

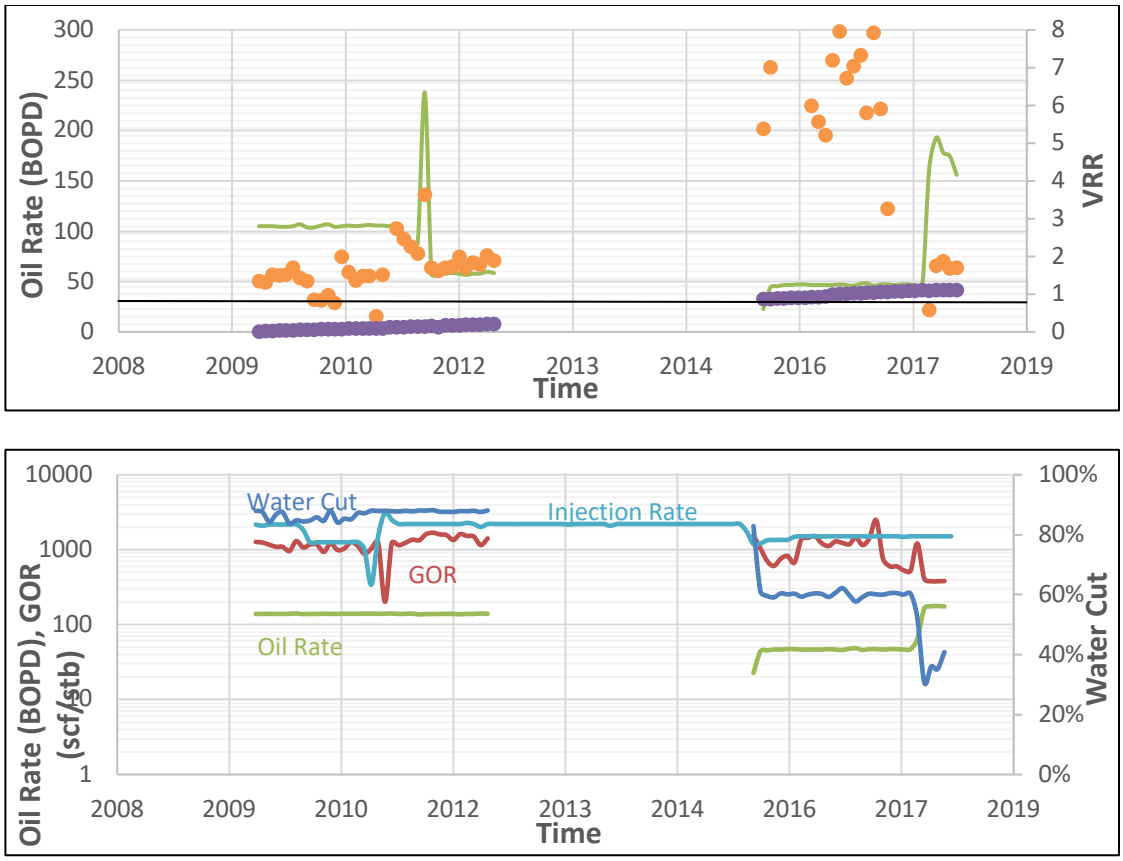

Figure 4-8. Regional VRR plot including three active producers and one injector.

Figure 4-8 shows an area in the field N-384 with three active wells; N505, N580, and N487 (See Figure 3-1), where a direct relationship between VRR and oil production rate is observed. The VRR behavior shows the presence of aquifer support because when VRR equals zero there was a high oil production rate at the beginning. From Oct. 2012 to Nov. 2015 all producers in this region were shut in. Current VRR is in a decreasing trend with an increasing oil production. Both instantaneous and cumulative VRR are close to 1, which is a good response from water injection.

4.2: Recommendations for future development

In section 4.1, diagnostic plots for production performance were discussed and recommendations can be provided with well performance analysis of each well. The following graph shows single-well performance from the same region as the regional VRR plot shown, which will assist in making development recommendations.

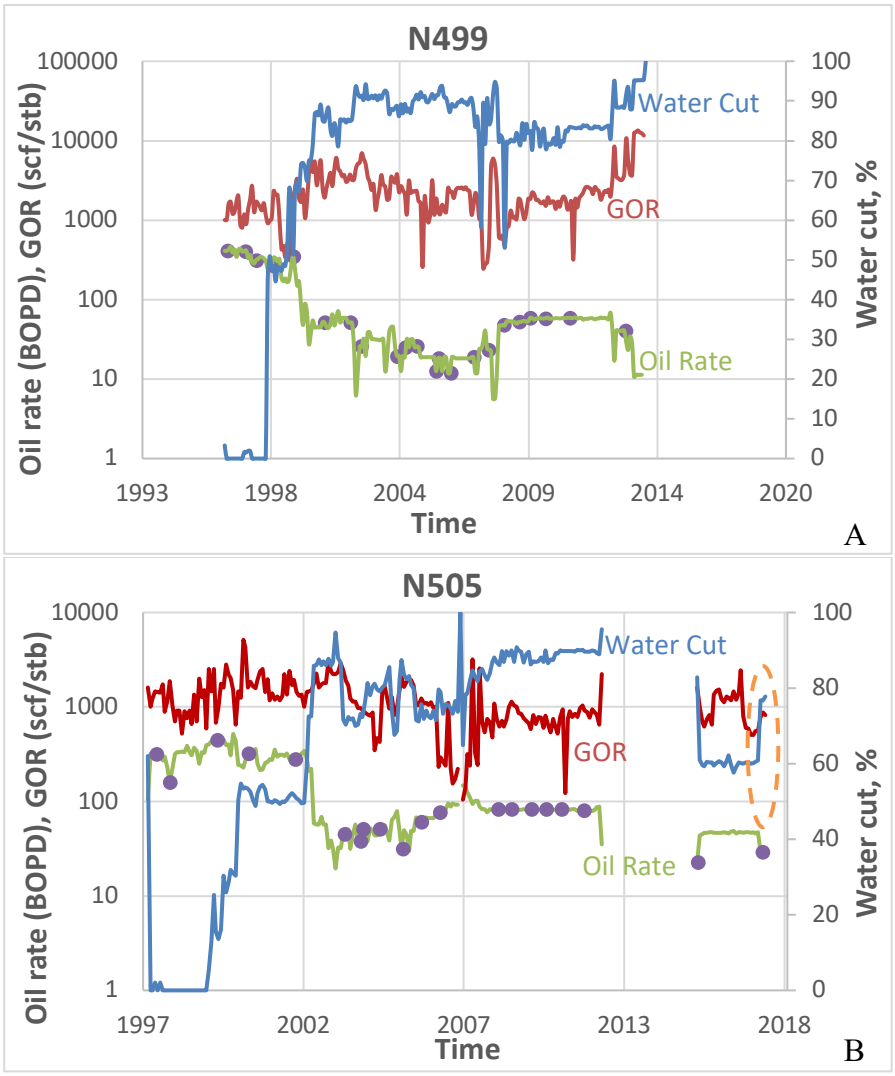

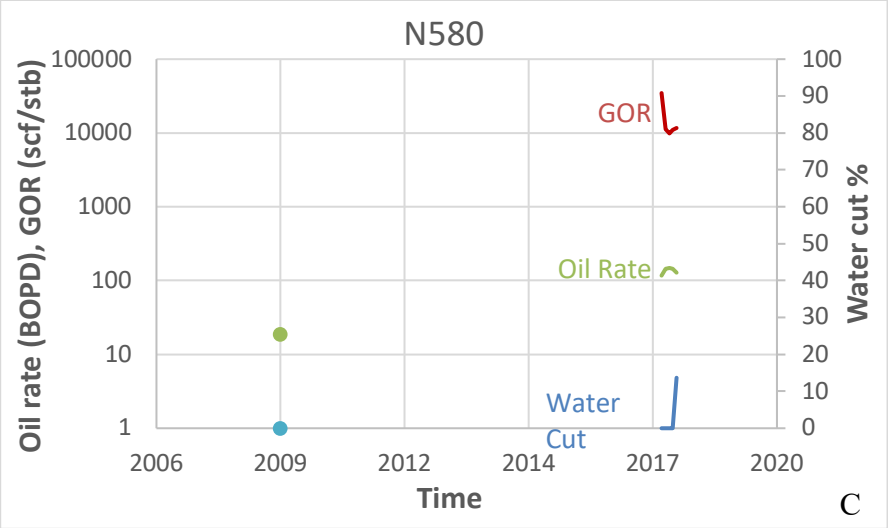

Figure 4-9. Single well production performance in VRR calculation region

These three wells are producers in VRR calculation area. Water injection started in Nov. 2009 and well N499 was shut in in Jul. 2014. The other two producers are still active.

As shown in Figure 4-7, after water injection, oil production did not respond rapidly in all three wells and the oil rates from well N499 and well N505 were stable. Until Jul. 2014, well N499 was shut in due to a 100% water cut. For well N505, the production data is not available from Oct. 2012 to Nov. 2015. It is not mentioned whether this well was shut in in that time period. From Figure 4-7B, there is an abrupt oil decline from N505 at the end of production history (labeled in the circle). It is recommended to find the reason causing this decreasing oil rate. Well N580 produced in Jul. 2009 and then shut due to a high gas rate. Until Dec. 2017, well N580 was re-opened as a gas well with a decent oil production after moving perforations down.

Figure 4-10 shows the production performance of the other two active producers not VRR calculation region. These wells are N422, and well N469.

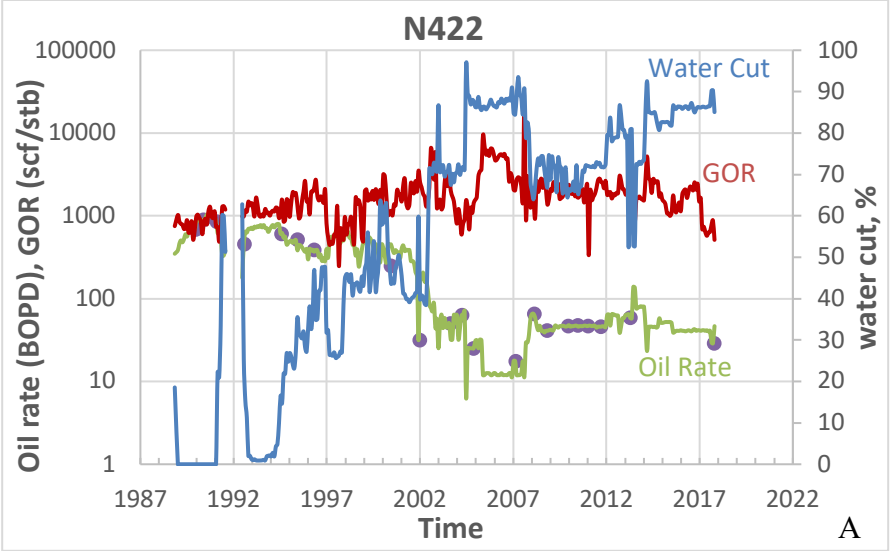

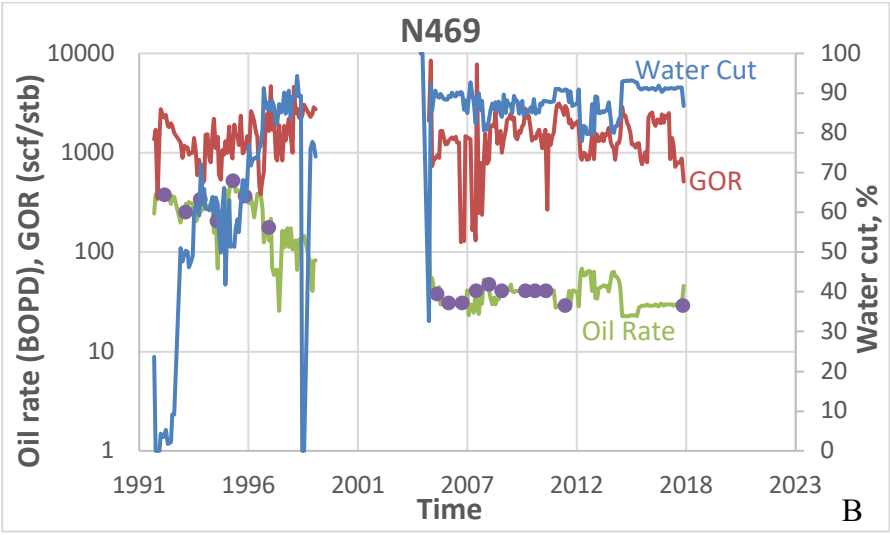

Figure 4-10. Two active producers not in VRR calculation region

Both wells N422 and N469 have a decreasing water cut trend and increasing oil rate. This is a positive sign for reservoir management. It is recommended that to keep the current status to reach a higher recovery.

Table 4-2 is a summary for all active producers and the injector at the end of available production data.

Table 4-2. Active well summary

Well Name	Oil rate, BOPD	Water Cut, %	GOR, scf/stb
N422	46.5	85	512.7
N469	45.9	87	512.4
N505	28.9	78	816.8
N580	127	13.68	1857.9
	Injection rate, BWPD	Cum. Injection, MMSTB	4493.5
N487	1509.4	5.86	

The recommendations for future development are:

1. Well N422 and well N469: Keep current status for future development to reach a higher recovery.
2. Well N505: Initially control the abrupt increasing water cut (from 60% to 77%) before move to waterflooding implementation. The reason for an abrupt decrease in oil rate at the end of history is needed. (Increasing GOR and water cut might be the reasons)
3. Well N580: The well was reopened in Dec. 2017. Production data for only 5 months is available. A longer observation is needed to make further recommendations. A decreasing water cut indicates a positive response of waterflooding management.

CHAPTER 5: SWEEP EFFICIENCY CALCULATIONS

Estimating sweep efficiency in a mature waterflooding project is of great significance. It provides an indication of the fraction of the reservoir which has been swept or not swept by the injected water (*Cobb and Marek, 1997*).

This chapter demonstrates the calculation of areal, vertical, volumetric and displacement sweep efficiency, as well as the ultimate recovery factor estimation. With the estimation of the sweep efficiency, a better understanding of the heterogeneity of the field can be achieved.

5.1: Displacement Efficiency

Displacement efficiency represents the fraction of oil been displaced from a zone swept by waterflooding. Lab data was used in the estimation of displacement efficiency for the field N-384 under study, assuming minor effects of changing B_o. The displacement efficiency can be calculated from the equation below

$$E_D = \frac{S_{oi}-S_{or}}{S_{oi}}, \tag{5-1}$$

where

E_D = displacement efficiency

S_{oi} = initial oil saturation

S_{or} = residual oil saturation

The result is listed in the following table.

Table 5-1. Displacement efficiency

Parameters	Values
S_{oi}	0.7
S_{oi}	0.3
E_D	0.57

The ultimate displacement efficiency of field N-384 is 57%.

5.2: Areal Sweep Efficiency – Fassihi Method (Fassihi, 1986)

Areal sweep efficiency of an oil recovery process primarily depends on two factors: the flooding pattern and the mobilities of the reservoir fluids (*Lyons, Plisga, and Lorenz, 2016*).

Fassihi (1986) provided correlations for areal sweep efficiency by means of nonlinear regression using Dyes et al. (1954)'s data. The plot was curve-fitted and the resulting equation is

$$\frac{1-E_A}{E_A} = [a_1 \ln(M + a_2) + a_3]f_w + a_4 \ln(M + a_5) + a_6, \qquad (5\text{-}2)$$

where E_A is the areal sweep efficiency which is the fraction of the pattern area contacted by water and M is the mobility ratio. Mobility ratio is calculated with the equation:

$$M = \frac{k_{rw}\mu_o}{k_{ro}\mu_w}, \qquad (5\text{-}3)$$

where,

M = mobility ratio

k_{ro} = oil relative permeability

k_{rw} = oil relative permeability

μ_o = oil viscosity

μ_w = water viscosity

Coefficients are listed in Table 5-2 for the 5-spot direct line drive and staggered line drive patterns. The use of equations with adjustable coefficients are very useful. These coefficients are valid both before and after breakthrough and can apply to mobility ratios between zero and ten, which is within the range observed in the majority of waterflooding projects (*William et al., 2016*). This mobility ratio range restriction is caused by the limitation of the experiment.

Table 5-2 shows the calculated areal sweep efficiency using this approach for the field N-384.

Table 5-2. Coefficients in areal sweep efficiency correlations and results

Coefficients in Areal Sweep Efficiency Correlations			
Coefficient	Five-spot	Direct line	Staggered line
a_1	-0.2062	-0.3014	-0.2077
a_2	-0.0712	-0.1568	-0.1059
a_3	-0.511	-0.9402	-0.3526
a_4	0.3048	0.3714	0.2608
a_5	0.123	-0.0865	0.2444
a_6	0.4394	0.8805	0.3158
f_w = 0.7335, current			
(1-E_a)/ E_a	0.026	0.050	0.144
E_a	0.974	0.952	0.874
f_w= 0.98, ultimate			
(1-E_a)/ E_a	-0.028	-0.044	0.138
E_a	1.028	1.046	0.879

Where f_w in Table 5-2 stands for water cut which is obtained from production data. The current water cut is 73.35%. Water cut of 98% is set as the economic limit to estimate ultimate areal sweep efficiency.

Since we do not have a staggered-like pattern (or any patterns), we are discounting the areal sweep efficiency by 10%. Therefore, areal sweep efficiency is 79% (0.879 × 0.9).

5.3: Vertical Sweep Efficiency

The determination of vertical sweep efficiency is an important step in the forecast of the performance of any waterflooding project. Two methods will be discussed in this section for the calculation of vertical sweep efficiency.

5.3.1: Vertical Sweep Efficiency – Dykstra-Parsons Method

This method was introduced by Dykstra and Parsons which has been widely used in the oil industry. The vertical sweep efficiency, in this approach, is a function of mobility ratio, WOR, and Dykstra-Parsons permeability variation. (*Fassihi, 1986*).

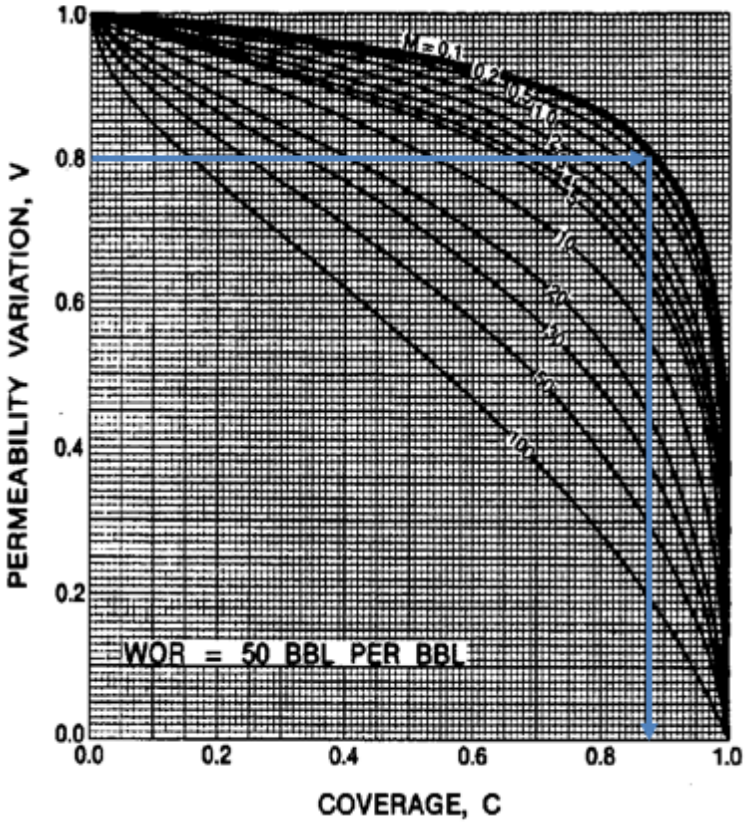

Figure 5-1. Coverage as a function of permeability variation and mobility ratio (Fassihi, 1986).

For field N-384, Dykstra-Parsons permeability variation (V) and mobility ratio (M) are calculated to be 0.8 and 0.314 respectively. So, as shown in Figure 5-2, the coverage (vertical sweep efficiency) is estimated to be 0.87.

5.3.2: Vertical Sweep Efficiency – deSouza Method

The second method was introduced by deSouza and Brigham (1995) by grouping the coverage curves for $0 \leq M \leq 10$ and $0.3 \leq V \leq 0.8$ into one curve by regression analysis. The equation they proposed is as:

$$Y = a_1 {E_I}^{a_2} (1 - E_I)^{a_3}, \tag{5-4}$$

where $a_1 = 3.334088568$, $a_2 = 0.7737348199$ and $a_3 = -1.225859406$.

The equation for Y was given by

$$Y = \frac{(WOR+0.4)\times(18.948-2.499V)}{(M+1.137-0.8094V)\times 10^{f(V)}}, \quad (5\text{-}5)$$

where,

$$f(V) = -0.6891 + 0.9735V + 1.6453V^2 \quad (5\text{-}6)$$

M = mobility ratio

V = Dystra-Parsons permeability variation

E_I= vertical sweep efficiency

Table 5-3. Result of vertical sweep efficiency calculations

	Current	**Ultimate**
WOR	2.75	49
M	0.314	0.314
$f(V)$	1.142692	1.142692
V	0.8	0.8
Y	5.91	92.72
E_I	0.563	0.93

In Table 5-3, WOR was set as the economic limit to estimate vertical sweep efficiency. And current vertical sweep efficiency and the ultimate vertical sweep efficiency are both listed in the table based on different WOR.

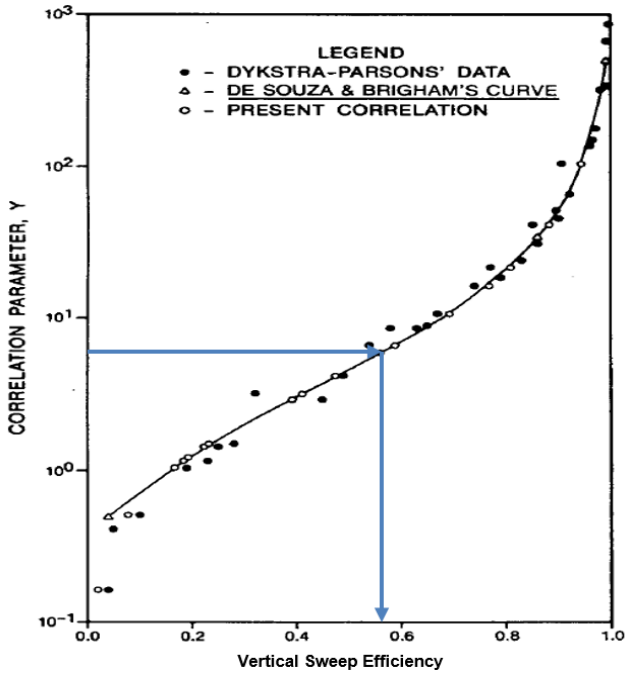

Figure 5-2. Vertical Sweep Efficiency Correlation (Fassihi, 1986).

In vertical sweep efficiency estimation, a conservative value was chosen as 87% from Dykstra-Parsons' method.

The ultimate recovery factor estimation with sweep efficiency (Dykstra-Parsons' method) is calculated as

$$E_A \times E_V \times E_D = RF. \tag{5-7}$$

The ultimate recovery factory calculated from this method is 39.2% (15.64 MMSTB).

5.4: Volumetric Sweep Efficiency

It is useful to compute the volumetric sweep efficiency of the injected water for evaluating the waterflooding performance. There are several correlations available to calculate volumetric sweep efficiency. The equation proposed by Cobb *et al*. (1997) is used for this study.

$$E_{vw} = \frac{\frac{\Delta N_p B_o}{V_p} + 1 - S_o - S_{wc}}{\bar{S}_w - S_{wc}}, \quad (5\text{-}8)$$

where ΔNp is the cumulative oil production since the start of the waterflooding, which means the difference between current cumulative oil production (STB) and the cumulative oil production (STB) when water injection started. S_o is the residual oil saturation when water injection started, and it can be determined by the equation as shown below

$$S_o = \left(1 - \frac{N_{p1}}{N}\right)\left(\frac{B_o}{B_{oi}}\right)(1 - S_{wc}), \quad (5\text{-}9)$$

where,

N_{p1} = cumulative oil production at the start of waterflooding (STB)

N = Original oil in place (STB)

B_o = oil formation volume factor at the start of waterflooding (rb/stb)

B_{oi} = initial oil formation volume factor (rb/stb)

S_{wc} = connate water saturation

V_p is pore volume (rb) defined by

$$V_p = \frac{(N - N_{p1})B_o}{S_o}. \quad (5\text{-}9)$$

$\bar{S}w$ is average water saturation in the water-swept portion of the pore volume, fraction. It can be obtained from fractional flow analysis. However, in a moderately low viscosity oil system (less than 2 to 3 cp), $\bar{S}w \cong 1 - S_{orw}$, where S_{orw} is the waterflood residual oil saturation.

Table 5-4 shows the values of each parameter used in the calculation.

Table 5-4. Summary of volumetric sweep efficiency result

N_{p1}, MMSTB	12.42
N_{p2}, MMSTB	13.31
B_{oi}, rb/stb	1.43
B_o, rb/stb	1.42
N, MMSTB	39.93
S_{wc}, fraction	0.3
S_o, fraction	0.48
S_g, fraction	0.22
V_p, MMBBL	81.57
$\bar{S}_W$, fraction	0.7
E_{vw}, fraction	0.58

The volumetric sweep efficiency calculated for the field N384 is 58%. If $\bar{S}_W$ can be assumed as being a constant as in the case of piston-like displacement, equation 7 becomes the equation of a straight line relating E_{vw} and ΔN_p. That is

$$E_{vw} = A + B\Delta N_p, \tag{5-10}$$

where

$$A = \frac{1-S_{wc}-S_o}{\bar{S}_w-S_{wc}} = \frac{S_g}{\bar{S}_w-S_{wc}}, \tag{5-11}$$

$$B = \frac{B_o}{V_p(\bar{S}_w-S_{wc})}, \tag{5-12}$$

and

$$S_g = 1 - S_o - S_{wc}, \tag{5-13}$$

where

S_g = gas saturation at the start of injection

If the ultimate oil recovery under current waterflood operations can be estimated from a decline curve analysis, the volumetric sweep efficiency plot can be extrapolated to yield ultimate volumetric sweep efficiency (*Cobb et al., 1997*).

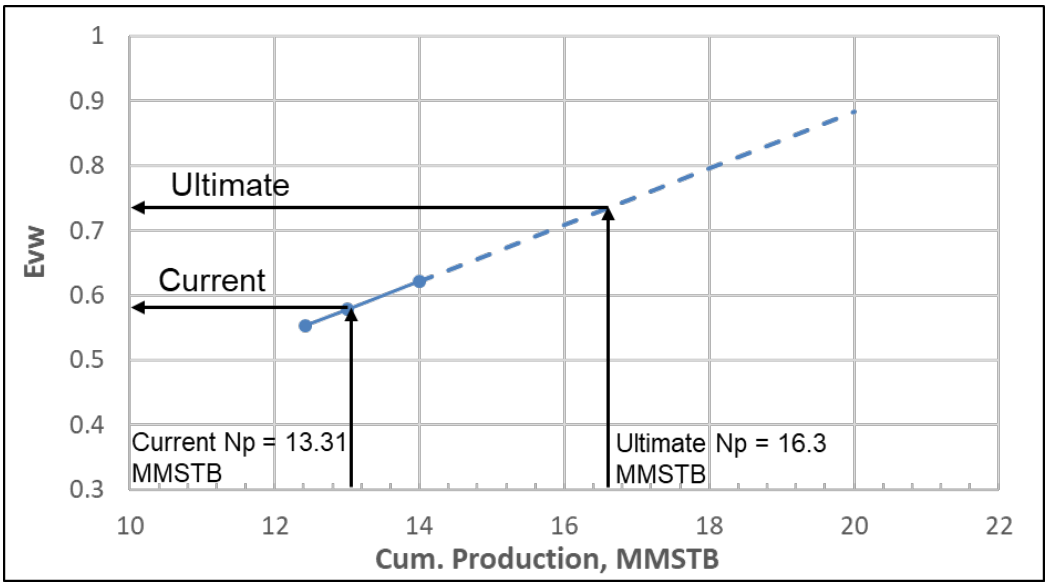

Figure 5-3. Ultimate volumetric sweep efficiency estimation.

The advantage of this method to estimate volumetric sweep efficiency is that only field production data is required.

From the decline curve analysis for the field N-384, EUR is around 16.3 MMSTB. The ultimate volumetric sweep efficiency would yield 72%.

Based on this method, the ultimate recovery factor will be

$$E_V \times E_D = RF \tag{5-14}$$

The ultimate recovery factor for the reservoir under study is calculated to be 41% (16.37 MMSTB).

5.5: Oil Recovery Prediction using Dykstra-Parsons' Method (V vs. M)

This is a semi-empirical and convenient method to predict oil recovery, which can be applied to all formations with initial oil saturation of 45% or greater. However,

it is cumbersome for practical use. The purpose is to provide a simplified method for making Dykstra-Parsons predictions (*Johnson, 1956*). For field N-384, the initial oil saturation from core analysis is 70%. Other required inputs are water-oil ratio (WOR), permeability variation (V), and initial water saturation (30%). It is worth mentioning that the plots are not provided for all different WOR values in their work because of experimental data limitations.

For the field under study, the current WOR value is 2.75 and 49 is set as an economic limit, which is equivalent to 98% water cut. Plots for the WOR of 25 and 100 are used for interpolation to estimate oil recovery.

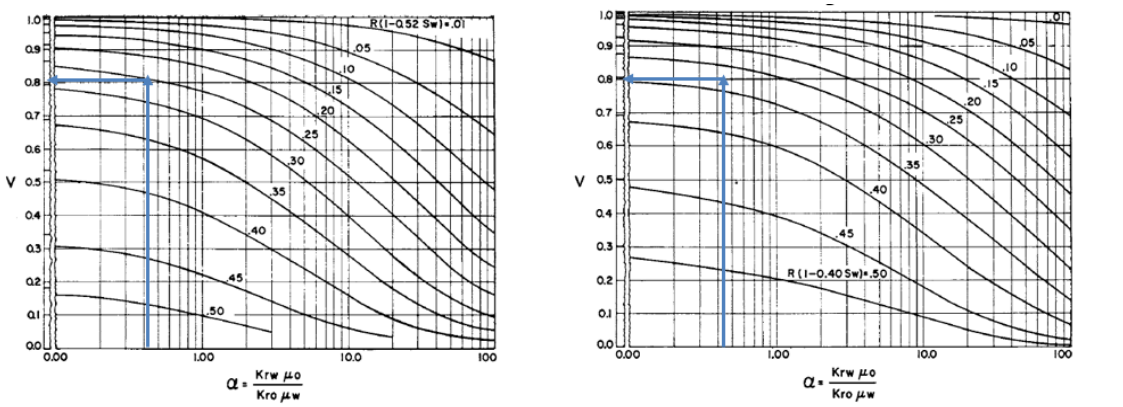

FIG. 3—PERMEABILITY VARIATION PLOTTED AGAINST MOBILITY RATIO SHOWING LINES OF CONSTANT $R(1 - 0.52\ S_w)$ FOR A PRODUCING WATER-OIL RATIO OF 25.

FIG. 4—PERMEABILITY VARIATION PLOTTED AGAINST MOBILITY RATIO SHOWING LINES OF CONSTANT $R(1 - 0.40\ S_w)$ FOR A PRODUCING WATER-OIL RATIO OF 100.

Figure 5-4. Oil recovery estimation for the Dykstra-Parsons Method (Johnson, 1956).

Table 5-5 shows the estimation of oil recovery for the WOR of 49.

Table 5-5. Interpolation of oil recovery

WOR	water cut	RF, %
25	96%	31.9
100	99%	37.5
49	98%	35.6

Interpolating from the WOR of 25 and 100, the ultimate recovery factor from this method is 35.6%. However, the current recovery factor from this method is only 21.6%, which is lower than production performance (33.3%).

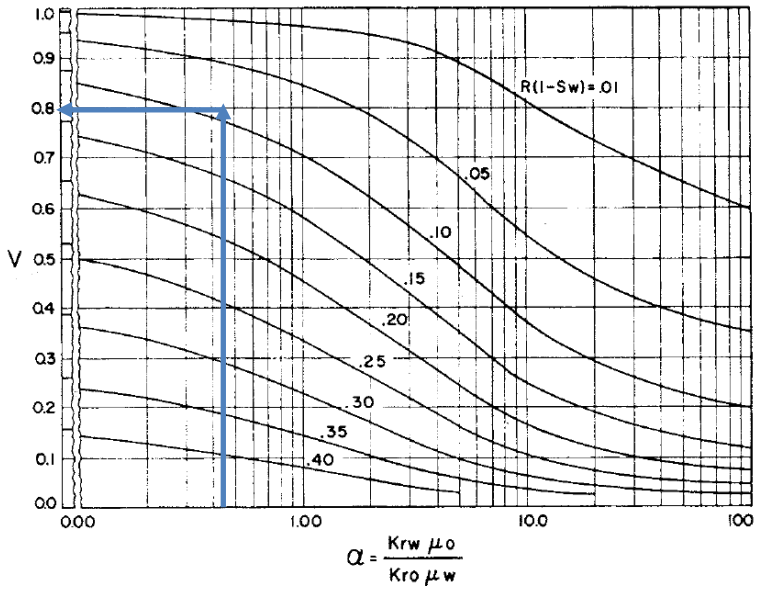

FIG. 1—PERMEABILITY VARIATION PLOTTED AGAINST MOBILITY RATIO SHOWING LINES OF CONSTANT $R(1 - S_w)$ FOR A PRODUCING WATER-OIL RATIO OF 1.

Figure 5-5. Oil Recovery Estimation at breakthrough (Johnson, 1956).

Since the plot at breakthrough is not available, the plot at WOR = 1 was used to estimate the recovery at breakthrough. In the plot, recovery factor is 12% (4.8 MMSTB). However, from Figure 4-4 (WOR vs. cumulative oil production), when WOR equals 1, recovery factor is 17.7% (7.07 MMSTB). Thus, oil recovery correlation with the permeability variation method tends to give lower estimates.

5.6: Summary of Recovery Factor Estimated from Different Methods

The following table illustrates the ultimate recovery factor from different methods discussed in the previous sections.

EUR estimation from sweep efficiency (Cobb's method) gives the highest ultimate recovery factor. Interpolation from the Dykstra-Parsons method (V vs. M) gives the lowest estimation.

Table 5-6. Summary of oil recovery estimation by different methods

Method	Ultimate Recovery factor, %	EUR, MMSTB
Decline Curve Analysis with production data	40.8	16.3
WOR vs. Np plot from field performance	40.04	16
Sweep Efficiency – Dykstra-Parsons' method	39.2	15.64
Sweep Efficiency – Cobb's method	41	16.37
Dykstra-Parsons – Permeability variation vs. Mobility ratio plot	35.6	14.21

Current recovery factor: 33.3%, current water cut: 73.35%.

CHAPTER 6: MATERIAL BALANCE STUDY

Material Balance studies were performed on the field N-384. A material balance model was built using MBAL software from Petroleum Experts for the entire field. The data was fed on a tank basis and utilized to understand the reservoir drive mechanism. This study assists in the understanding of reservoir drive mechanisms and the size of the aquifer.

The material balance study resulted in OOIP of 39.79 MMSTB with the aquifer size of 184710 MMRCF, compared with 39.93 MMSTB reported by the operator volumetric estimates with strong aquifer support. This aquifer volume resulted in a reasonable pressure match. The currently declared in-place volumes used in all calculation is 39.93 MMSTB.

6.1: Model Input

Table 6-1 summarizes the PVT parameters used in the MBAL model for the field N-384. The results of the best case material balance studies performed are shown in Table 6-1.

Table 6-1. PVT parameters summary in MBAL

Parameters	Values
R_S at P_b scf/STB	864
Oil gravity API	30.1
Gas Gravity sp. Gravity	0.796
Water salinity ppm	100,000
Temperature ˚F	183
Pressure, psi	3500

Table 6-2. Input summary of MBAL model for the best result

Parameters	Best Case Input
Initial Pressure psi	3900
Temperature, °F	183
Porosity	0.2
Initial Water Saturation	0.3
Initial Gas Cap m(m Ratio)	0
Water Compressibility 1/psi	3.50E-06
Aquifer Model	Carter-Tracy
Outer/Inner Radius Ratio	20
Encroachment Angle degree	180
Aquifer Permeability, MD	40
Rock Compressibility 1/psi	3.69E-06

6.2: Model Output and interpretation

The output from the MBAL study is presented below. The pressure history match before water injection is shown in Figure 6-1 which shows a reasonable pressure match.

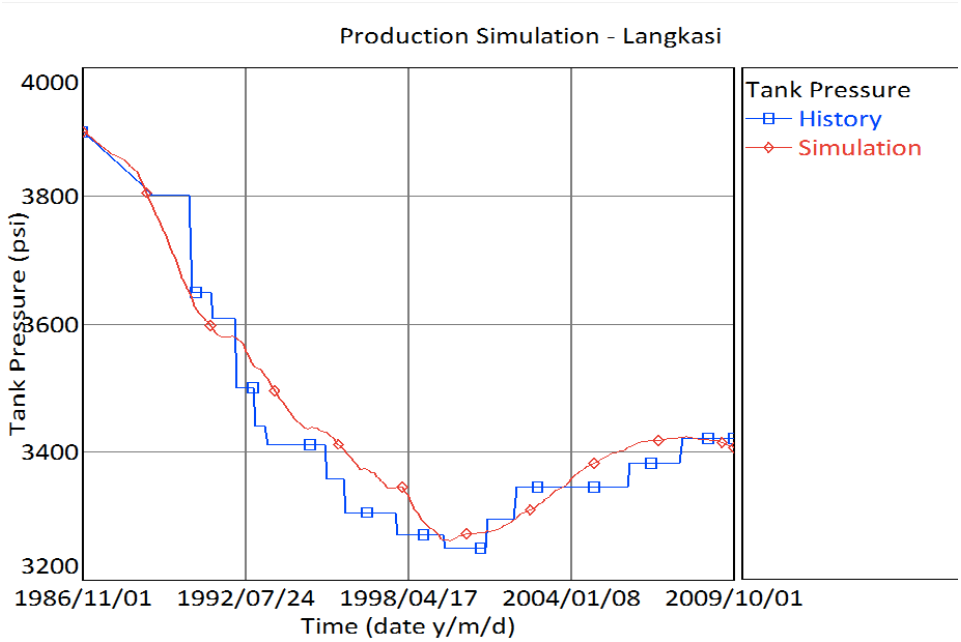

Figure 6-1: Pressure match before water injection.

The drive mechanism plot is shown in Figure 6-2. It indicates that the drive mechanism for the field N-384 is the combination of water influx, pore volume compressibility, and fluid expansion. At the beginning of depletion, fluid expansion had more contribution to the drive mechanism compared with that ten years later.

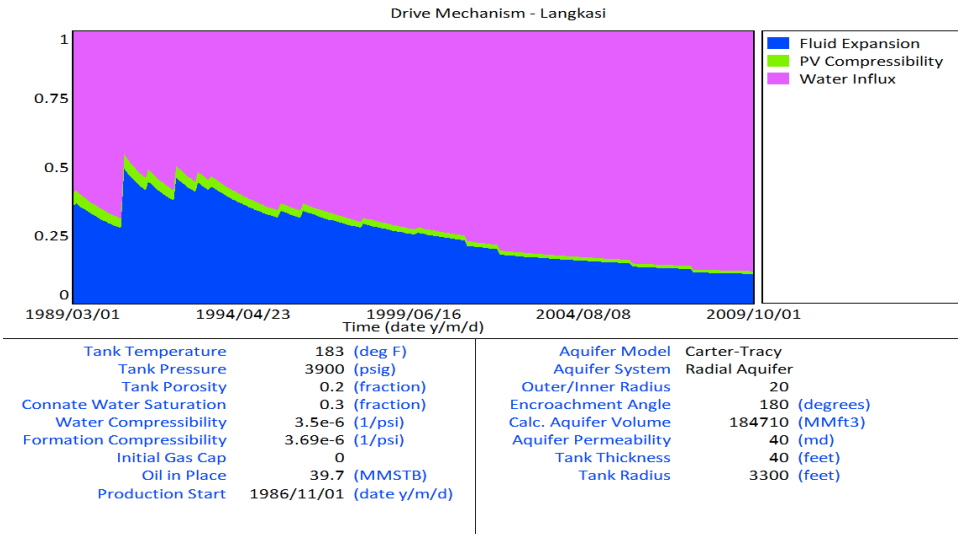

Figure 6-2: Drive mechanism plot.

Havlena-Odeh plot is shown in Figure 6-3. In this graphical method, reservoir voidage (F) is a function of oil expansion (E_o). In the plot, OOIP can be estimated from the intercept of the line and y-axis. As indicated from the plot, OOIP is close to the reported value (39.9 MMSTB) by the operator.

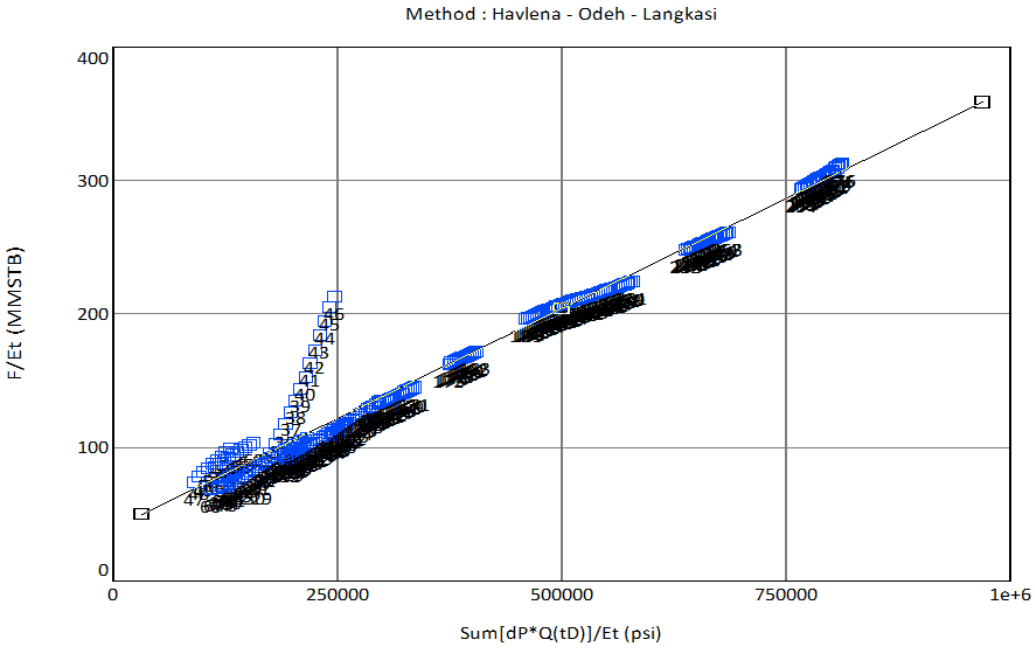

Figure 6-3. Havlena-Odeh Plot.

CHAPTER 7: RESERVOIR SIMULATION STUDY

Besides evaluating a hydrocarbon reservoir using analytical approaches, a reservoir simulation study can give a better understanding of the fluid flow in porous media and saturation and pressure distributions in the reservoir. However, the main application of this tool is to predict the field performance under various producing strategies as shown in this chapter. Additionally, finding the optimum recovery scheme for the field from reservoir simulation result will help in making engineering decisions.

In this chapter, the procedures used to input static data, reservoir rock and fluid properties for initialization, history match study, sensitivity study, and prediction will be discussed in detail to help make recommendations for future development.

The commercial simulator used in this study is ECLIPSE100 on the Petrel Platform to better visualize reservoir simulation results.

7.1: Overview of the geological model

The geological model used in this reservoir simulation study is a simplistic model. The property modeling including porosity, permeability, initial water saturation was performed using the geostatistical method of closest neighbor which honors the property distribution in the reservoir based on the distance from the wellbore with available data. The well distance in the Field N-384 is more than 900 ft. This well distance makes the uncertainty while upscaling the properties in the whole geological model. Additionally, the absence of seismic data and the nonexistence of log data in a few wells limited our understanding of the reservoir.

The total number of grid cells is 203433 (83×57×43 in I, J, K direction). The dimension of each cell is 50×50×2 meter. The average porosity is 14% including shale, and average permeability is 80 md. The average water saturation in the model is 30%.

Gas-Oil Contact (GOC) and Oil-Water Contact (OWC) are located at the depths of 2912 and 2980 meters respectively. Properties including initial water saturation, porosity, permeability, and facies are provided with the geological model.

7.2: Initialization

The determination of pressures and saturations for each phase in each grid cell is called initialization. The main input includes fluid property (PVT), relative permeability, compressibility, initial temperature, and initial pressure of the reservoir.

7.2.1: Water Saturation Initialization

When defining any case on Petrel before running the simulation, water saturation can either be input in the grid with keyword SWATINIT or running the simulation without using the saturation property from the geological model.

Equilibration will be used if running a simulation without a saturation property from the model. In this method, the contacts, a datum depth, and pressure are specified, and the phase saturation is calculated by the phase density. Hydrostatic equilibrium is assumed. If the pressure is known at a datum depth in the oil zone, then the black oil equation of state (EOS) for oil is:

$$\rho_o^{(r)} = \frac{\rho_o^{(s)} + R_s \rho_g^{(s)}}{B_o} \tag{7-1}$$

and the hydrostatic pressure of the oil phase:

$$P_o(h_2) = P_o(h_1) + \int_{h_1}^{h_2} \rho_o g dh, \quad (7\text{-}2)$$

where (r) and (s) denote reservoir and surface condition respectively,

ρ_o = oil density

h = depth

In the transition zone, capillary pressure governs phase saturation.

In this simulaton study, the keyword SWATINIT was used. The keyword SWATINIT means that initial water saturation for capillary pressure scaling. The water saturation property from the geological model input will be honored in capillary pressure scaling. Below OWC, water saturation is 1, and above OWC, if the water saturation input is less than S_{wc}, the input water saturation will be reset to S_{wc} and capillary pressure will be scaled according to this value in order to keep the same P_c value. The following illustration explains how the Pc curve is scaled.

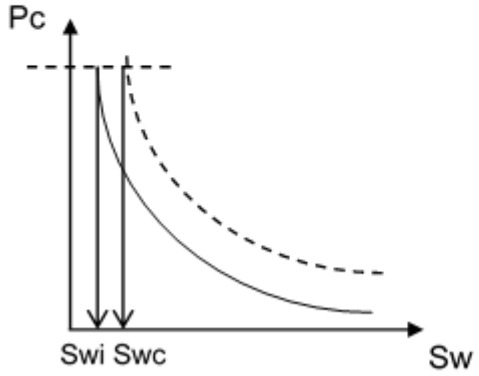

Figure 7-1. Capillary pressure scaling

If SWATINIT saturation is less than the connate water saturation for a cell, the initial water saturation will be reset to the connate saturation and the capillary pressure will be scaled according to this value.

7.2.2: Fluid Data Initialization

PVT data from wells N448 and N411 was analyzed and a single PVT model was developed to represent the whole field for simulation. The plots for oil and gas fluid properties are shown in the following plots.

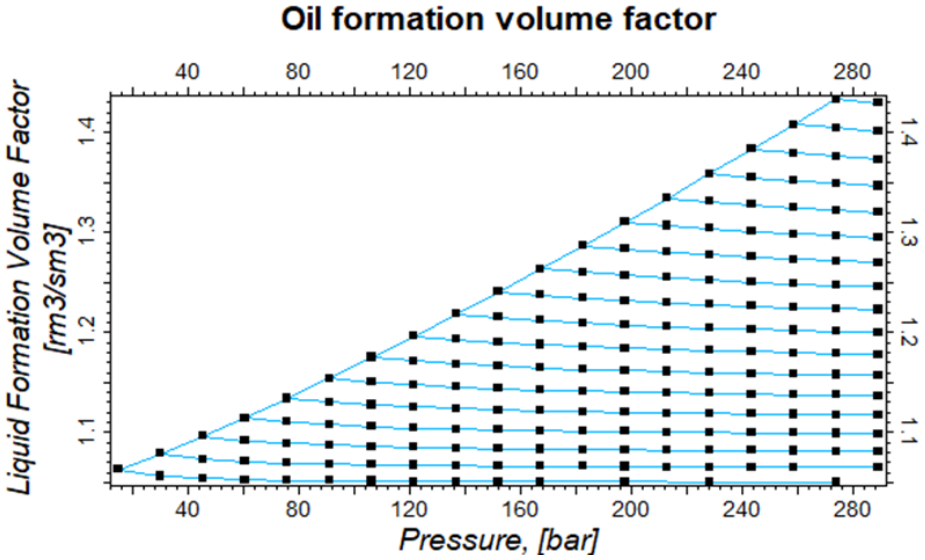

Figure 7-2. Oil formation volume factor vs. pressure.

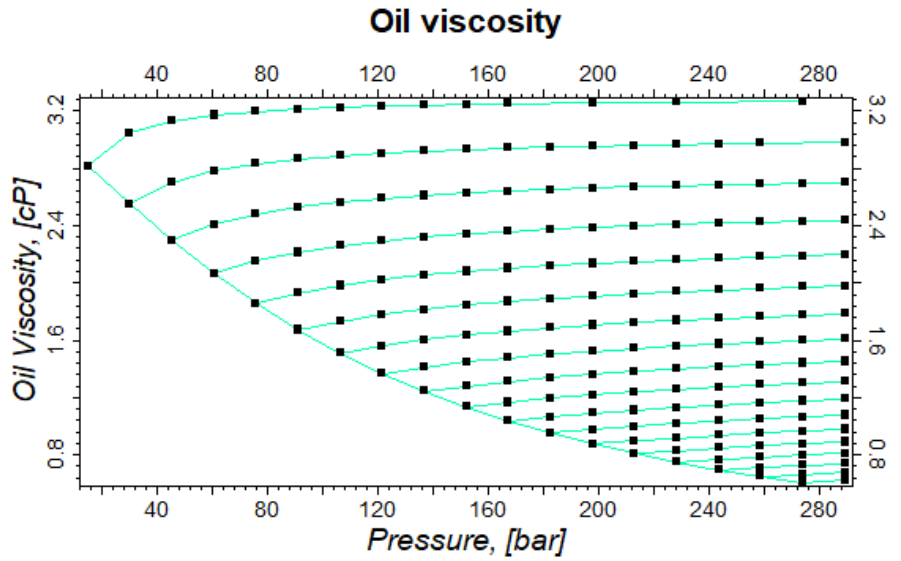

Figure 7-3. Oil Viscosity vs. pressure.

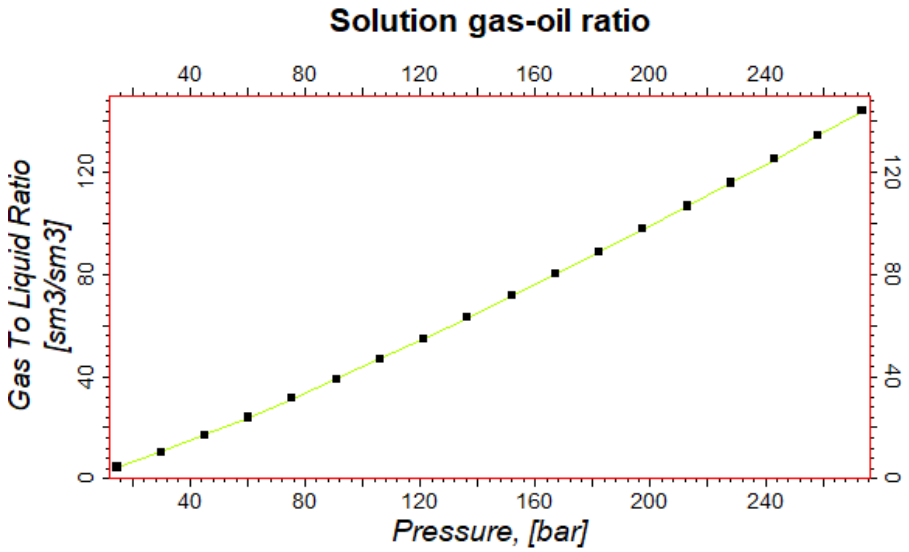

Figure 7-4. Solution gas-oil ratio vs. pressure.

7.2.3: Relative Permeability Curve

The relative permeability raw data from lab report has significant uncertainty, but lab data is honered. Therefore, in the simulation study, the raw data was tuned to reasonable values.

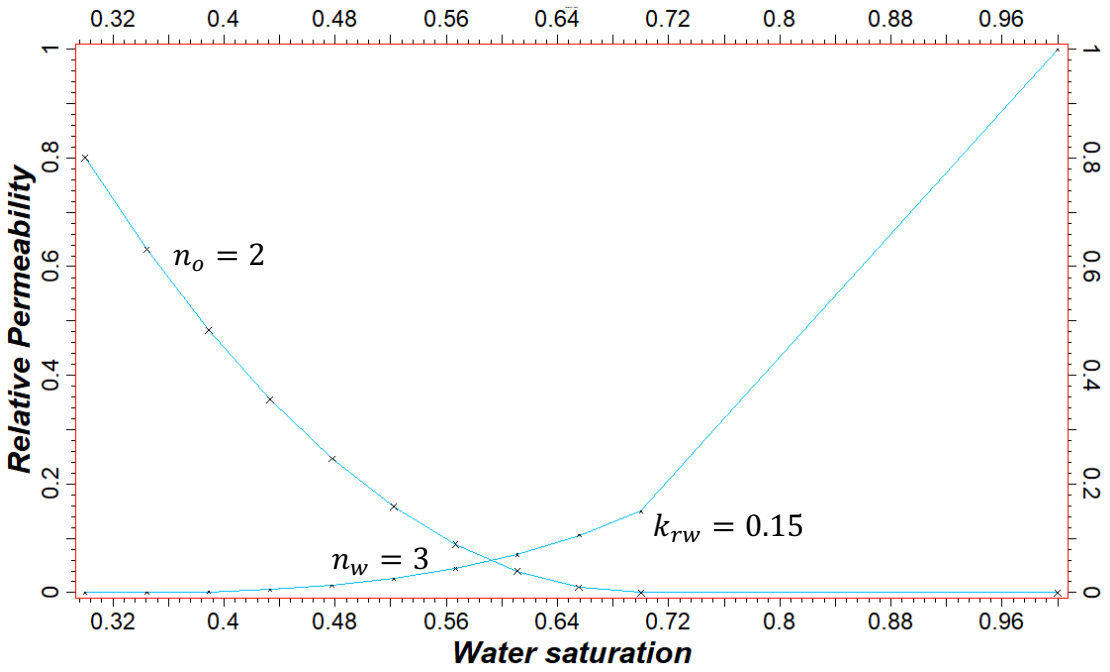

(a)

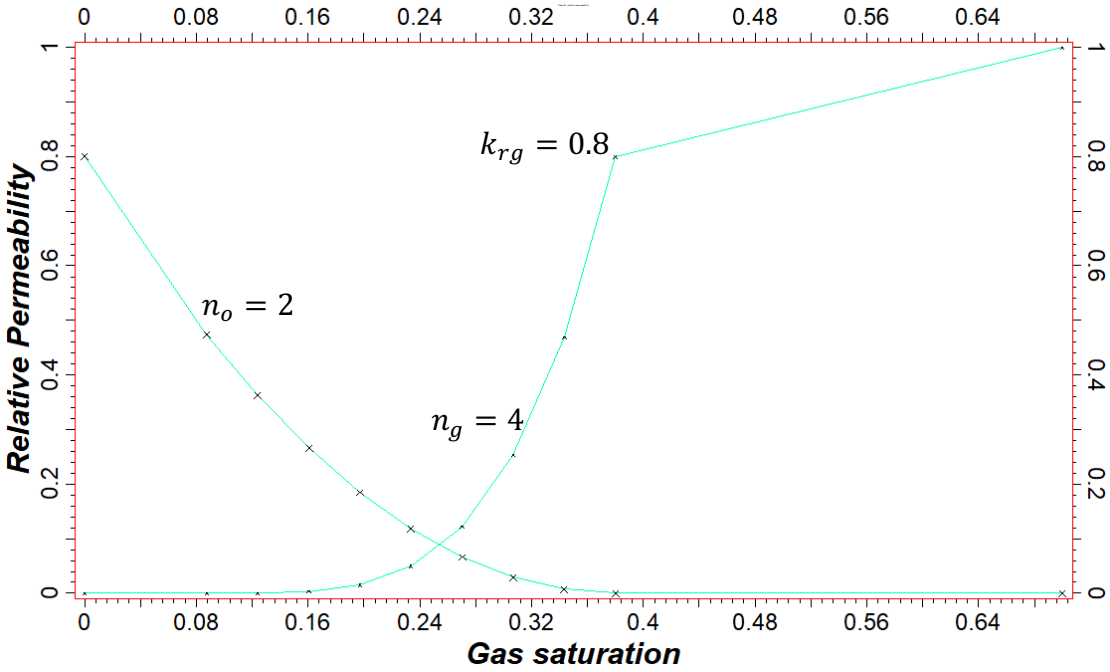

(b)

Figure 7-5. Relative permeability.

7.2.4: Water and Gas Contacts

Based on the map provided by the operator (Figure 7-6), gas and oil contacts are indicated for field N-384. The following picture is the screenshot of the field N-384 from the all assets. In the map, it can be observed that gas-oil contact (red line) is close to 2910 m. contour line and the oil-water contact (blue line) is 2980 m. In the simulation study, 2912 m is chosen for gas-oil contact and 2980 m is chosen for water-oil contact.

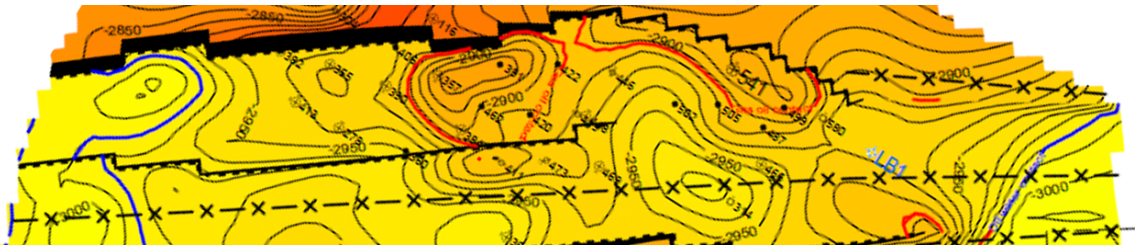

Figure 7-6. Gas and water contacts.

7.3: Volume Calculation

In the volumetric calculation, the required input is a 3D grid, contacts (GOC, and OWC), fluid properties, net-to-gross ratio (NTG), porosity and phase saturation.

In this reservoir study, the facies model is available and used in the volumetric calculation instead of NTG.

Average values are assumed for B_o and gas-oil ratio (R_s) based on the PVT report. Using these input data, the estimated OOIP in the sand is 9.6 MMKLS (60.37 MMSTB) for volumetric calculation, and 11.2 MMKLS (70.44 MMSTB) in both sand and shale. The following figure shows the volumetric calculation report results.

Case	Bulk volume[*10^3 m3]	Net volume[*10^3 m3]	Pore volume[*10^3 rm3]	HCPV oil[*10^3 rm3]	HCPV gas[*10^3 rm3]	STOIIP (in oil)[*10^3 sm3]
Facies						
Shale	33559	33559	3759	2229	0	1570
Sand	133080	133080	20745	13669	0	9626

Figure 7-7. Volumetric calculation result.

There are many uncertainties in the input data. As mentioned in the geological model description section, the property distribution in the geo-model is based on a geostatistical method considering the distance between wells. The seismic data is not available. This model does not fully represent the real geological conditions.

Table. 7-1.OOIP from simulation and volumetric calculation.

	OOIP, MMSTB
Volumetric	60.5
Simulation	65.7

In Table 7-1, OOIP is different from volumetric calculation and simulation, and it needs to be reconciled further. Moreover, the exact boundary of the field is unknown. The operator did not mention the procedure applied to estimate the OOIP. As a result, there is a difference between the reported OOIP by the operator and the volumetric calculation of this study. It is recommended that the EIP research team contact the operator to understand the exact boundary used in their OOIP calculation.

7.4: History Matching

History matching is one of the most significant and time-consuming parts in reservoir simulation study and an important step in reservoir management. A decent and reasonable match guarantees the reliability of the prediction. During history match, a better understanding of the geological model and the reservoir can be achieved. History matching is a good way to test the reliability of the geological

model. Some properties are needed to be slightly modified in order to get a close match. For the field under study, the producing time interval for the history match is from Nov. 1986 to Apr. 2018.

Sensitivity studies on the uncertainties were done on the model to analyze the effect of certain properties on the result. An attempt was made to modify the initial model parameters in a way to get a reasonable match of the field production data also, to be as consistent as possible with the original geological description of the reservoir. However, in this simulation study, due to the lack of log information for a few key wells, and the simplistic model, the OOIP from the initialization case is not close to the value reported by the operator.

As a common practice, in this simulation study, the field-scale pressure match is the first step to be taken. In the next step, the field-scale production data (cumulative gas, oil, and water production and gas, oil, water production rate individually) needs to be matched. The final step is focusing on individual well performance to assist in problem identification. During the history match the oil rate was set to be a constraint.

7.4.1: Base case history match

The so-called base case in this simulation study means running the simulation case with only the properties in the geological model. PVT properties and relative permeability are consistent with the lab data.

Table 7-2. Comparison of the base case and field data

Property	Output from simulation	Field Data	% Error
Oil Rate (BOPD)	184.68	246.90	25.20
Water Rate (BWPD)	122.62	679.89	81.96
Gas Rate (Mcf/d)	149.57	309.95	51.74
Cumulative Oil Production (MMSTB)	11.66	13.83	15.67
Cumulative Water Production (MMSTB)	3.39	12.79	73.45
Cumulative Gas Production (MMSCF)	15.14	19.31	21.58

Table 7-2 shows that there are significant errors between simulation output and field data. Water production has the biggest error and adding pore volume multiplier could help increase the support from the aquifer. Oil production should also increase. Gas production is not a big concern for the first match because a 30% error in gas measurement was confirmed by the operator.

By checking the production performance and log information of each individual well, it was found that a few wells have the problem of log data continuity. In some cases, no log data is available. This causes the inaccuracy in the upscaling of the reservoir properties assigned to each grid cell in the reservoir model. Therefore, some local modifications are necessary. Water saturation below OWC is manually set to be 1 and a pore volume (PV) multiplier is used to increase the pressure support from the aquifer.

Sensitivity study of the important parameters was performed. In the following sections, the effect of different parameters on the simulation results will be discussed.

After modifying properties in the model, the output from the simulator comes closer to observed field data.

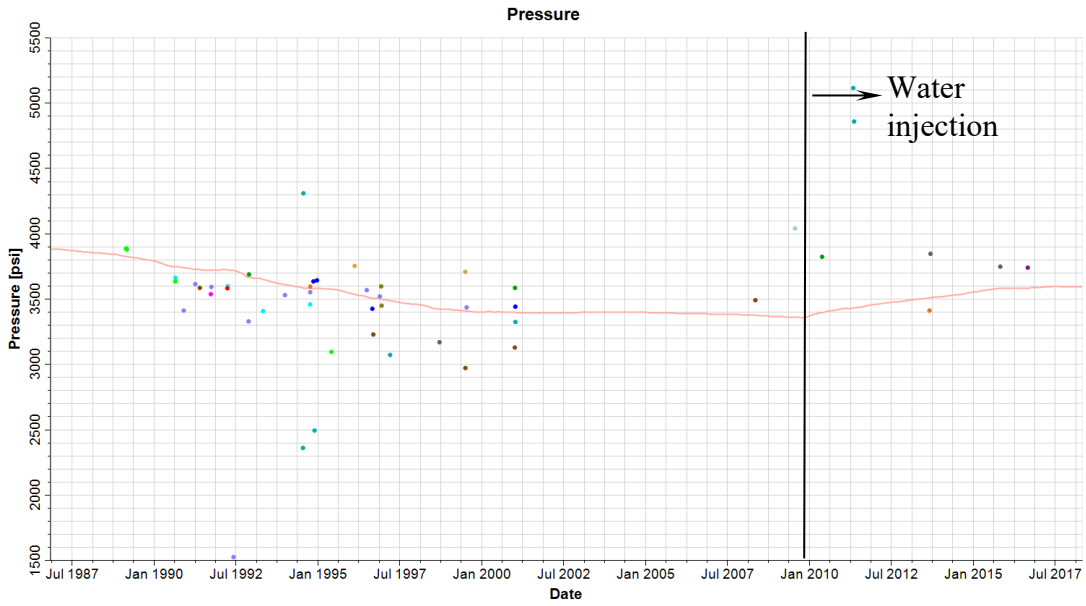

Figure 7-8. Pressure match.

Figure 7-8 illustrates the field-scale pressure match. The dots represent the static bottomhole pressures reported from each well in the field, and the solid curve is the output from the simulator. Before water injection, there was not a big drop in pressure, because the aquifer gives a strong pressure support. In Nov. 2009, water injection was initiated in the field resulting in the pressure increase (See Figure. 7-8).

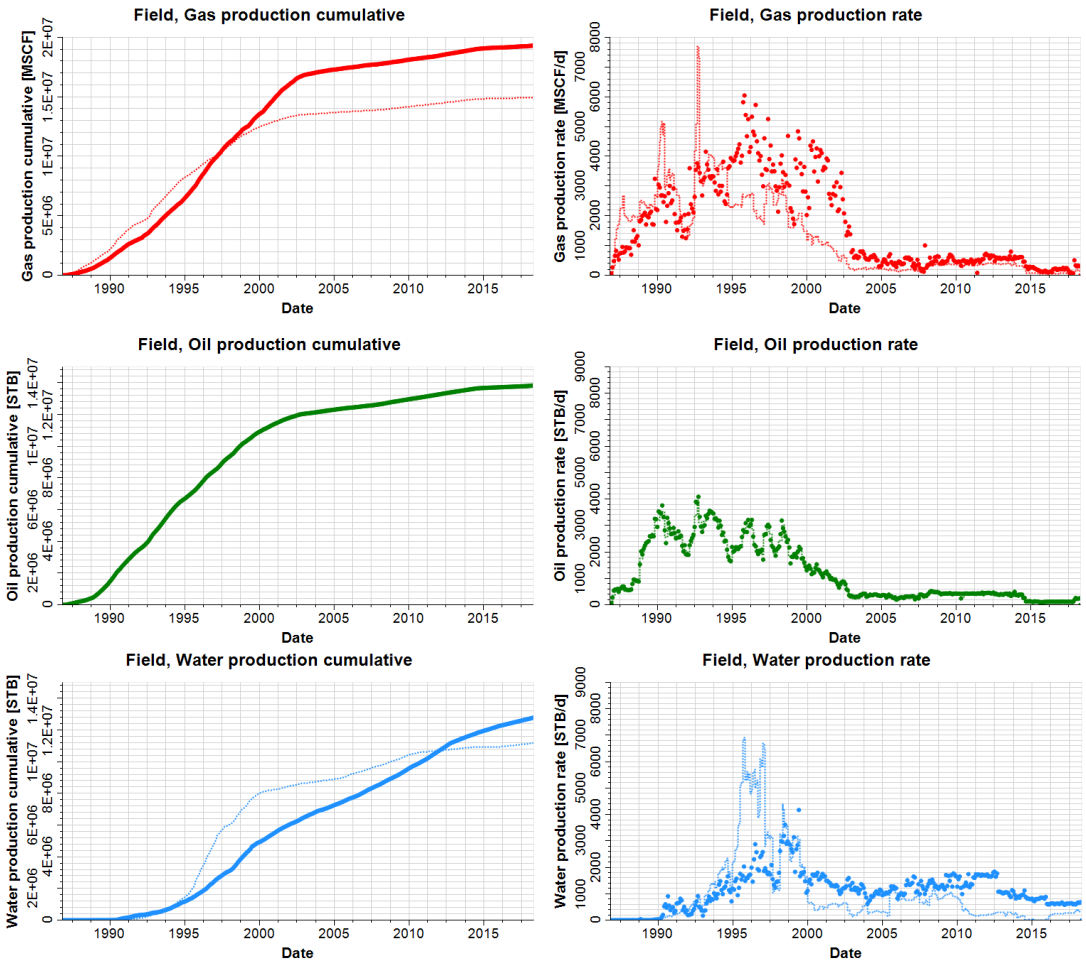

Figure 7-9. Field-scale production match for oil, water, and gas phases.

From the field-scale production match, cumulative oil production and oil production rates match well with the observed data. Figure 7-9 shows the final history match result. Gas production match is not accurate at the beginning of the production. After 2005 gas production rate matched the observed data reasonably. Overall, the calculated gas production is less than the field production. Oil production matches the field production quite well. For water production, the simulation result matched the breakthrough time quite well. The peak water production rate from the simulation is the production from well N469. We do not have any information from this well, and

this lack of data caused the significant mismatch with observed data. At the end of the production history, the water production rate from the simulation is acceptable.

7.5: Sensitivity Study

Sensitivity analysis can be used for various purposes, including model validation, evaluating model behavior, estimating model uncertainties, decision making using uncertain models, and determining potential areas of research. "Sensitivity analysis provides information about the effect of the errors and/or variations in the variables and/or parameters and models on the predicted behavior" (Lehr et al., 1994).

In this thesis, a sensitivity study was conducted on various modeling parameters to determine how each parameter would affect the production. This process provides a better understanding of how a specific property can affect the simulation result and the reliability of the geological model. During the sensitivity study, only one parameter was varied, and all other parameters were kept at their original values.

7.5.1: Relative Permeability

Relative permeability was measured from the core flood test. Conventional cores were obtained from one well. Core scale measurements are not representative of the entire field, so some modifications to core data are usually needed for a history match.

While processing core data before the simulation study, generalized Corey correlation was used. The exponents of oil and water are less than 1. In the base case simulation run, the Corey exponent value of 2 was used.

From lab data, the endpoint of k_{rw} is 0.1 and endpoint of k_{ro} is less than 0.5. The endpoint values will affect the production because the production rates are the function of relative permeabilities. The adjustment made on the relative permeability curves includes increasing the endpoint values and Corey exponents. A larger Corey exponent results in a higher curvature. The effect on water production is fairly obvious.

The final values applied in the simulation model are summarized in the table below.

Table 7-3. Relative Permeability in Simulation Study

S_{gcr}	0.0875	S_{orw}	0.3	S_{wmin}	0.3
Corey gas	4	S_{org}	0.32	S_{wcr}	0.3
k_{rg} at S_{wmin}	1	Corey O/W	2	Corey Water	3
k_{rg} at S_{org}	0.8	Corey O/G	2	k_{rw} at S_{orw}	0.15
		k_{ro} @ S_{omax}	0.8	k_{rw} @ S = 1	1

Water relative permeability endpoints which were tested varies between 0.1 to 0.5 with increments of 0.1. Figure 7-11 shows that higher the water relative permeability endpoint values, higher the simulated water production. However, for endpoint value from 0.3 to 0.5 increase of oil production is not obvious. The curves overlap on each other at different time periods. Figure 7-6 shows the effect of different endpoint values on the field oil production rate. A similar impact can be also found in water production.

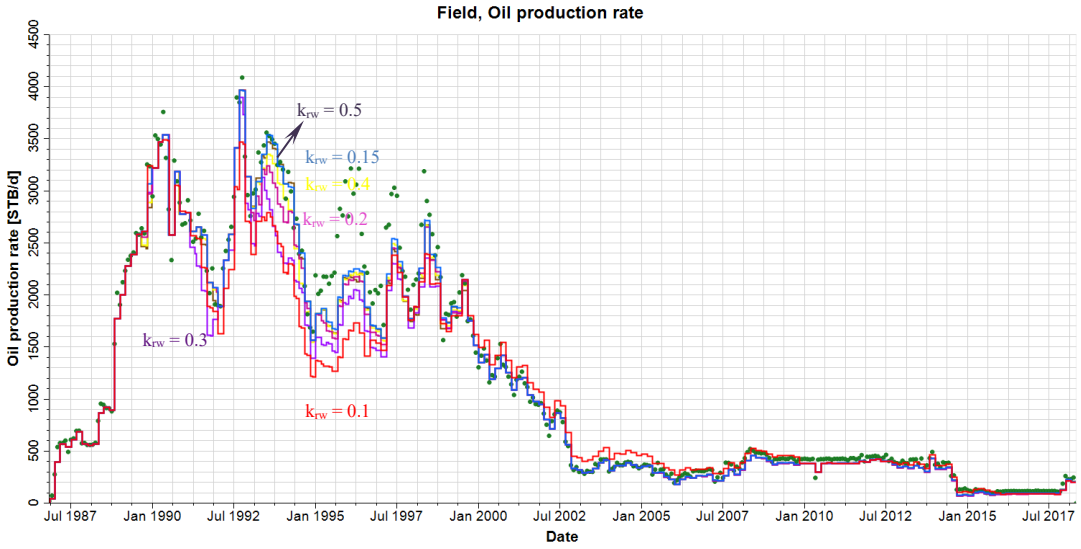

Figure 7-10. Field oil production using all k_{rw} variables.

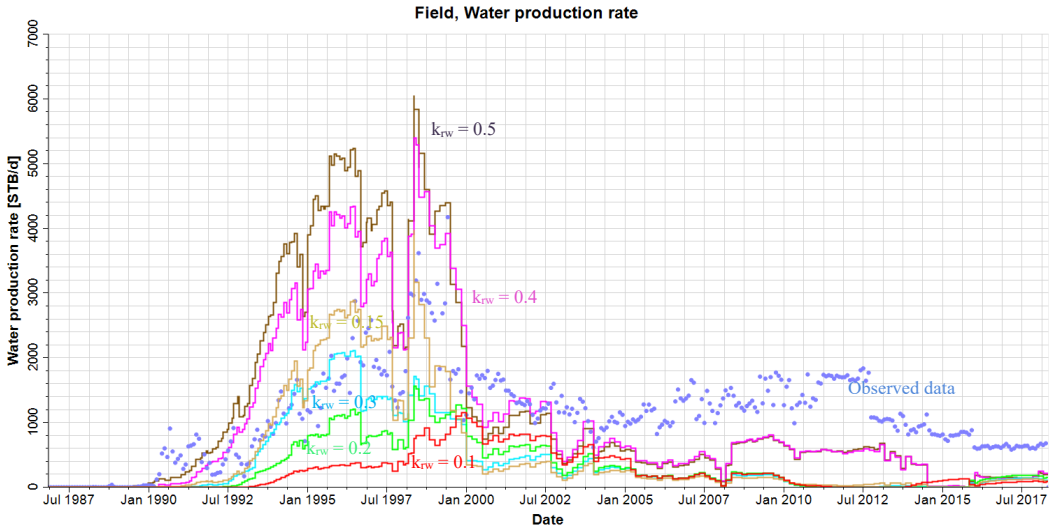

Figure 7-11. Field water production using k_{rw} variables

Some modifications to the endpoint values of gas relative permeability curve and its curvature were also applied. The original endpoint value of gas relative permeability was approximately 0.5 and Corey exponent was 2. The modification improved the early gas production performance in the simulation model. The current endpoint value for gas relative permeability is 0.8 and Corey exponent is 4. The higher

the curvature of the curve, the slower the gas can flow at low saturation. That is the reason why gas production matches better in an early time.

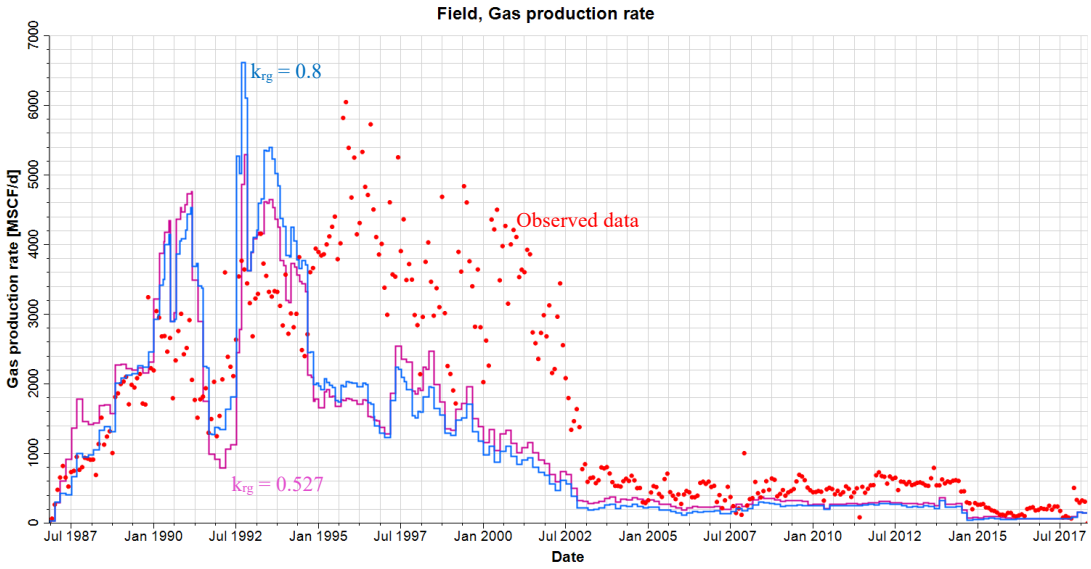

Figure 7-12. Field gas production rate using different k_{rg} endpoint value.

7.5.2: Pore Volume Multiplier

The pore volume multiplier is used below OWC to increase the pressure support from the aquifer. After several simulations runs, it was found that the pressure support from the aquifer varies from area to area. In the western part, the aquifer support is not as strong as in the east. In the middle part of the model, the pressure support from the aquifer is moderate. Therefore, using the same PV multiplier in the aquifer is not appropriate.

Initially, the PV multiplier used in the model is 10. After modifying the PV multiplier in different districts water production increased and aided in the match of oil production. The following plot illustrates the impact of the PV multiplier on the whole model.

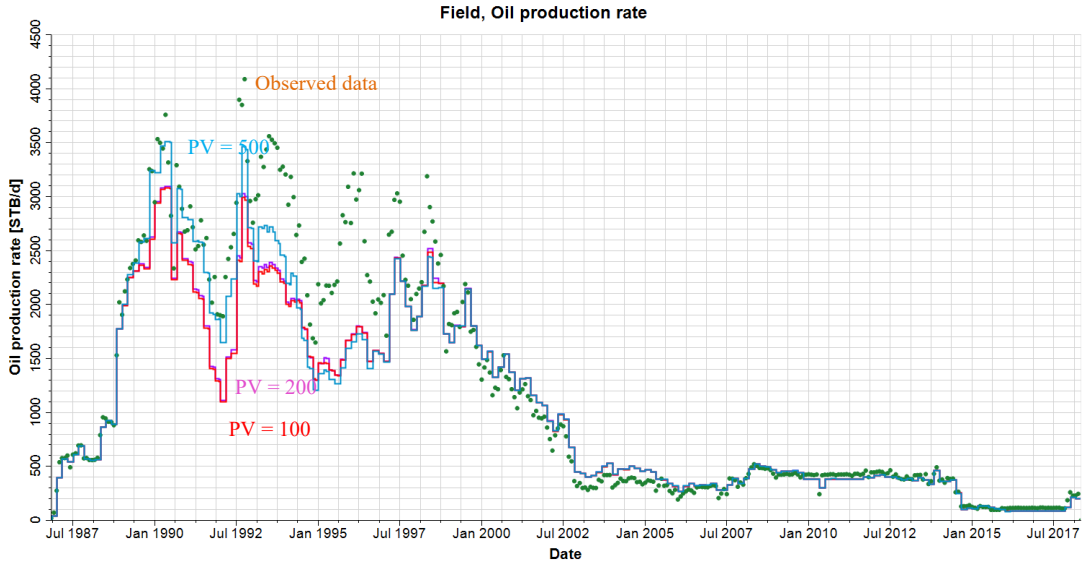

Figure 7-13. Field oil production using different PV multiplier on the entire model.

In the early time, the PV multiplier has a larger effect on oil production than late time. The higher aquifer PV multiplier results in the higher oil production. Because the water from the aquifer flooded the oil out.

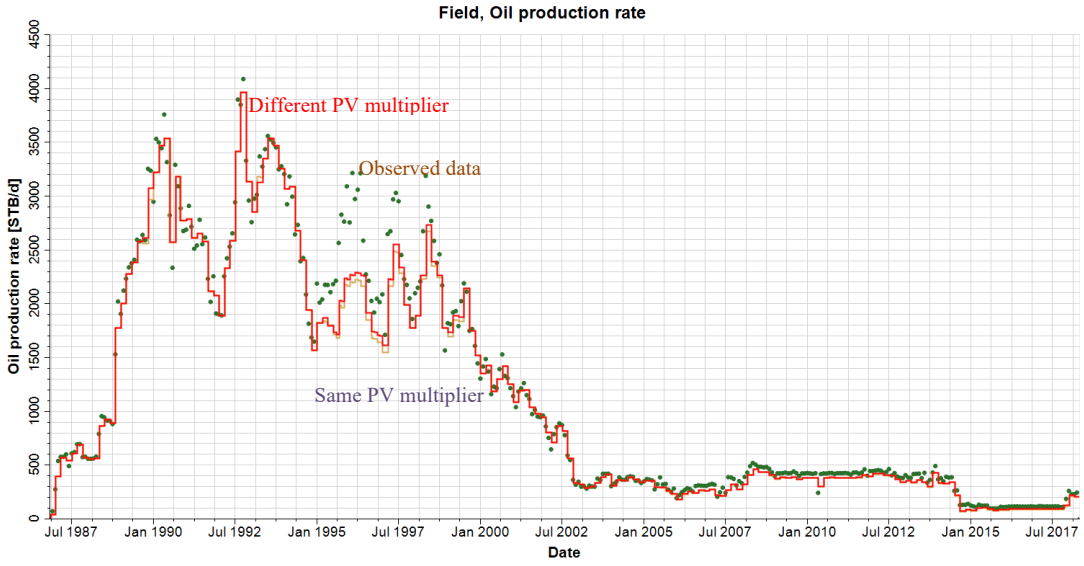

Figure 7-14. Field oil production comparison using different PV multiplier.

7.5.3: Permeability Anisotropy

Permeability was given as a property in the geological model. Initially, isotropic permeability is assumed which means the permeability is the same in all directions, i.e., horizontal and vertical. Sensitivity on permeability anisotropy was tested aiming to improve water production match. Like PV multiplier sensitivity analysis, firstly, k_V/k_H ratio change is consistent in the entire model. Zonal k_V/k_H ratio test was also conducted.

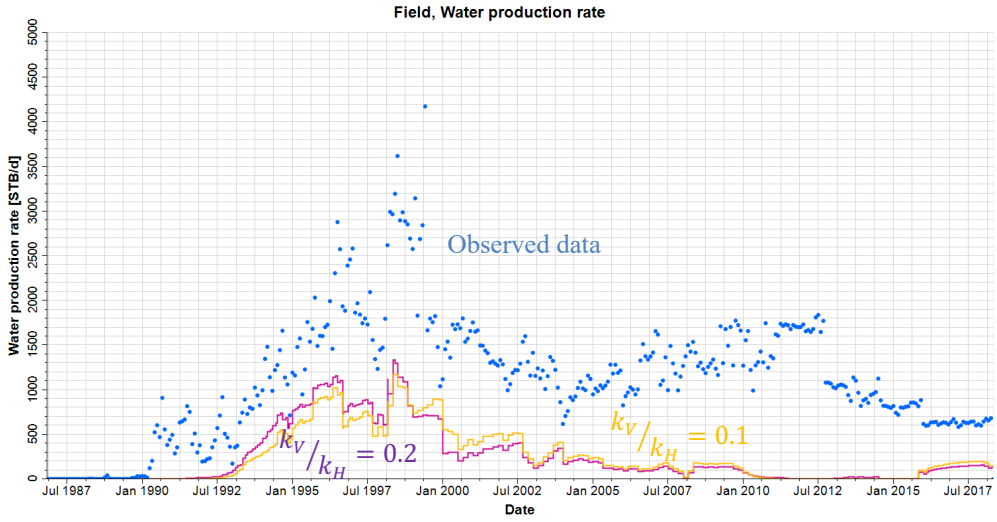

Figure 7-15. Field water production using different k_V/k_H ratio.

k_V/k_H ratio of 0.2 gives a higher production in early time but lower production at the end compared with k_V/k_H ratio of 0.1. Zonal k_V/k_H ratio was tested in the next step.

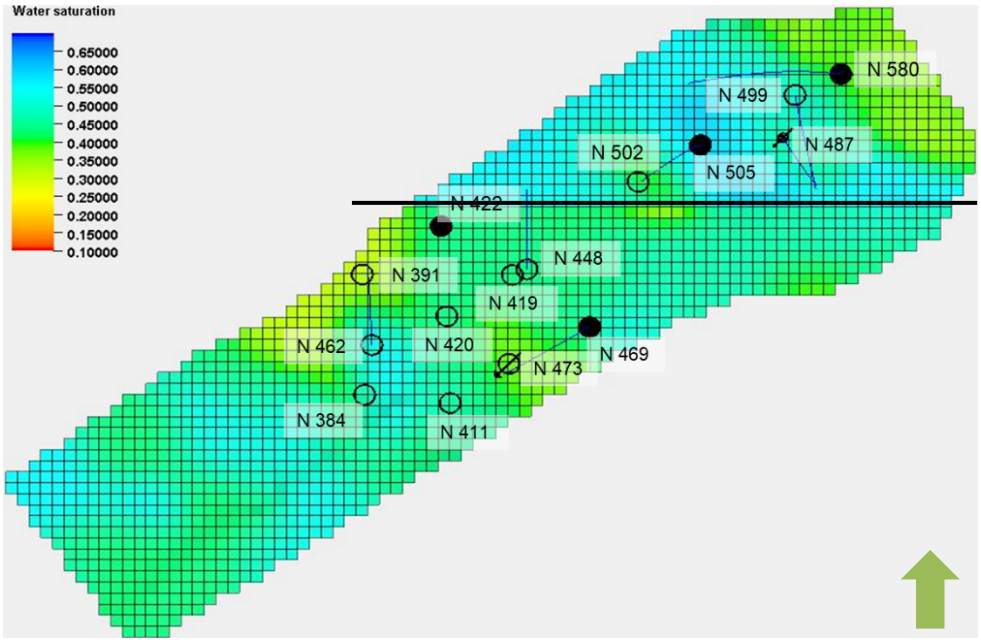

Figure 7-16. Water saturation map of the Field N-384.

Since the aquifer support is not evenly distributed on the entire field, using different k_V/k_H ratios in different areas was considered. As the above map illustrates, the wells in the lower part of the field (south) were depleted earlier than the ones in the upper part (north). Additionally, the wells in the south contributed to most of the production before 2000.

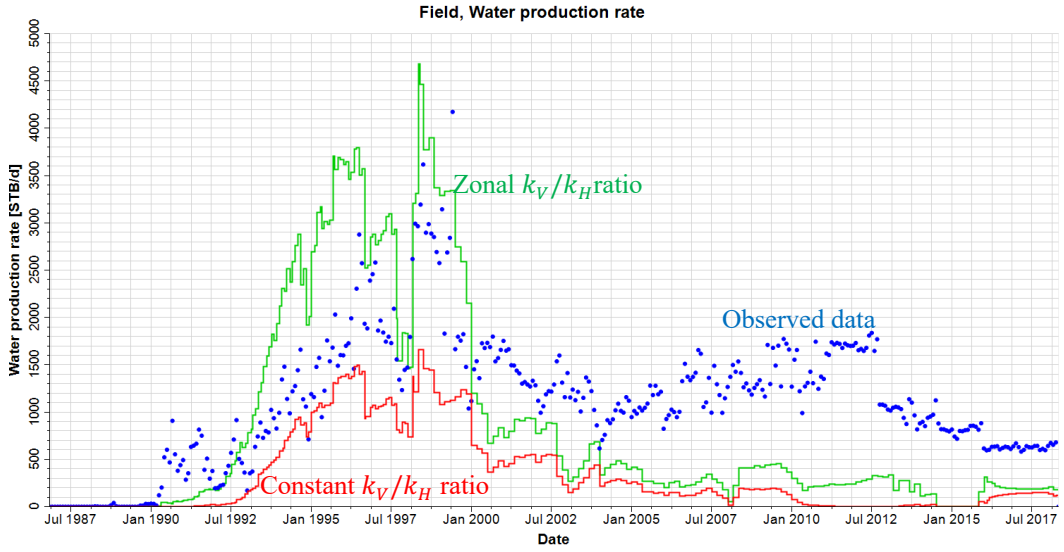

Figure 7-17. Field water production rate comparison.

Although the zonal k_V/k_H ratio does not give a decent water production match, water breakthrough time is better than the case using constant k_V/k_H ratio in the model.

A close match to historical data is a result of a combination of all different parameters. Based on the sensitivity study on each parameter some adjustments were made in the final history match. The values of all parameters used in the final history match are listed in Table 7-3.

Table 7-4. Summary of parameters in final history match

Parameters		Values
PV multiplier	Aquifer-east	100
	Aquifer-west	1000
	Aquifer-local	500
	Aquifer-middle	200
S_{gcr}, Critical gas saturation		0.0875
S_{orw}, Residual water saturation in water		0.3
S_{wmin}, Minimum water saturation		0
S_{org}, Residual water saturation in gas		0.32
S_{wcr}, Critical water saturation		0.3
k_{rg} at S_{wmin}		1
k_{rg} at S_{org}		0.8
k_{rw} at S_{orw}		0.15
k_{rw} @ S = 1		1
k_{ro} @ S_{omax}		0.8
Corey gas		4
Corey O/W		2
Corey O/G		2
Corey water		3
k_V/k_H	north	0.6
	south	0.9

Figure 7-18 illustrates the regional aquifer PV multiplier applied to obtain the final match. The modified oil-water and gas-oil relative permeability curves are shown in Figures 7-19 and Figure 7-20.

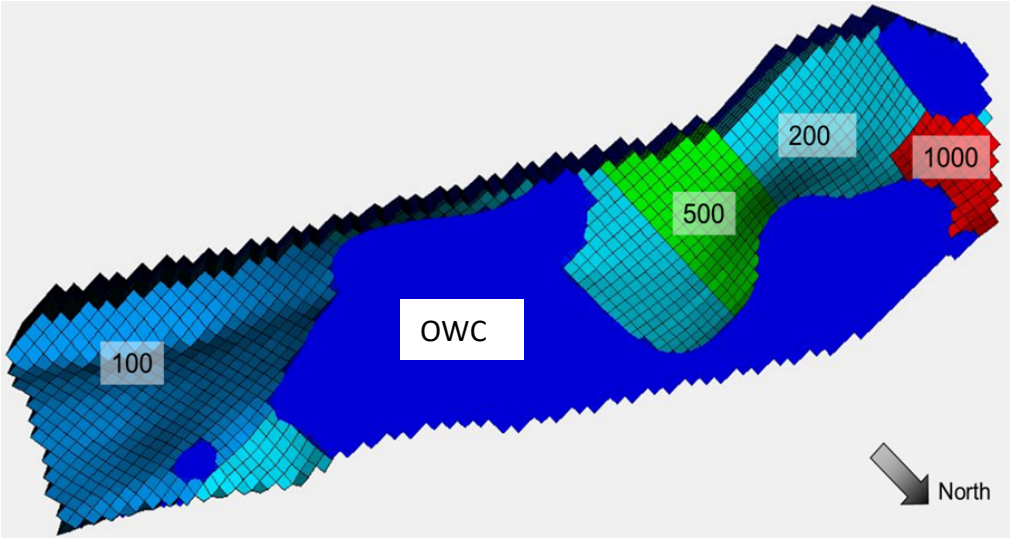

Figure 7-18. Areal PV multiplier adjustment in the aquifer.

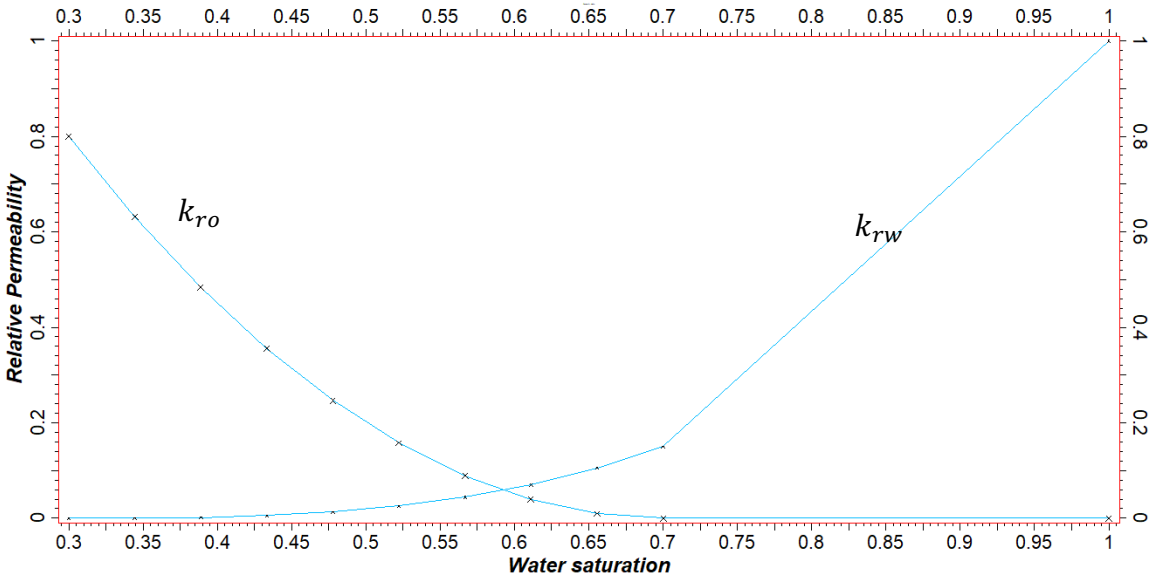

Figure 7-19. Oil-water relative permeability curve used in the final history match case.

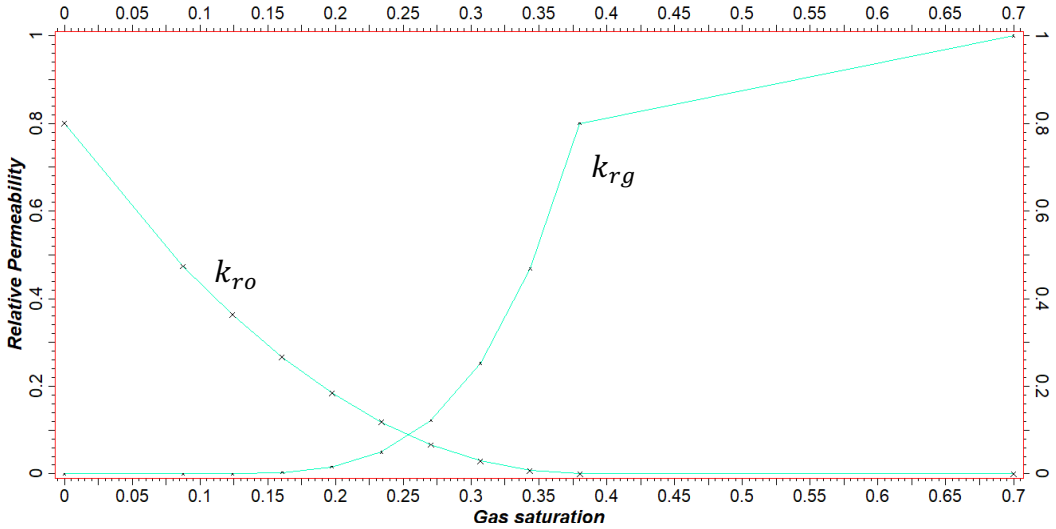

Figure 7-20. Oil-gas relative permeability curve used in the final history match case.

The results of the final history match for the field pressure, oil, water, and gas production based on the parameters listed in Table 7-4 are given in Figures 7-9.

7.6: Prediction Cases

The history matching simulation runs were performed using the geological model. The simulation results reasonably matched the observed field data, including production data of three phases and static and flowing bottom-hole pressure. Now the dynamic simulation model is ready for future performance prediction studies. A sum of six simulation cases was studied in detail. The constraints for each case were all set to be the flowing bottom hole pressure (FBHP) constraint. The simple description of each different case is summarized as Table 7-5. All prediction cases were run to forecast the reservoir production from May 2018 to May 2040. Meanwhile, the water injection rate was kept the same in all prediction cases as it was in the history match.

Table 7-5. Summary of Prediction Case Description

Cases	Description
1 - Base Case	FBHP was constant for every active producer at the end of the history match. Injection rate was the same as it was in history match
2 - Follow the trend	Let FBHP follow the trend of each active producers
3 - FBHP Decrease	FBHP of each active producer decrease 5 psi per year
4 - Infill Well	Base Case + one infill well (UH 1)
5 - Infill Well	Base Case + one infill well (UH 2)
6 - Infill Well	Base Case + two infill wells (UH 1, UH 2)

The following sections discuss each case in detail.

7.6.1: Prediction (Base case)

The first prediction case was run to forecast the reservoir production from May 2018 to 2040. The oil phase productivity index was calibrated before the prediction run. The prediction run was controlled by FBHP at the end of history match and FBHP was kept being constant till 2040. Figure 7-21 to Figure 7-23 present the results of base case prediction.

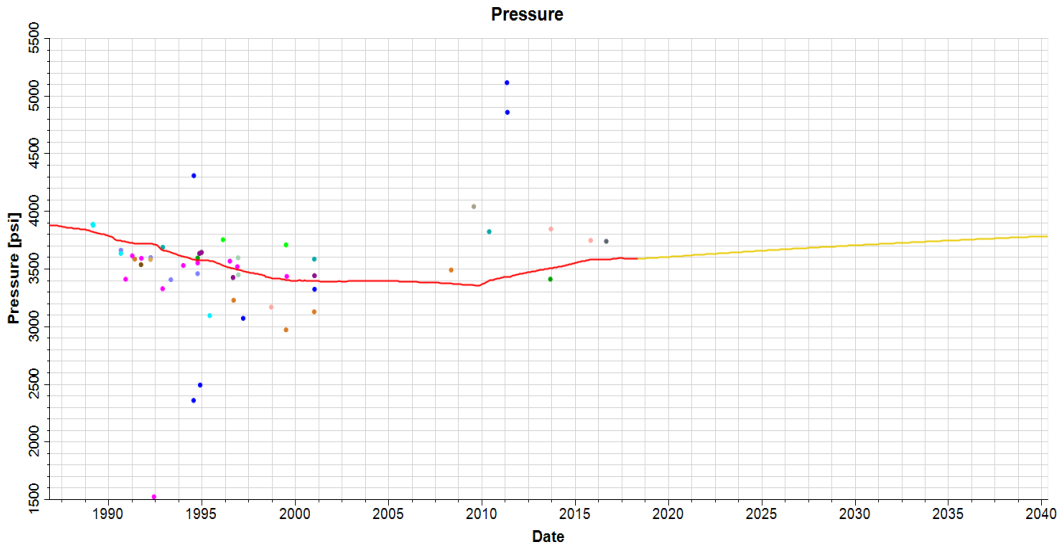

Figure 7-21. Field-wise reservoir pressure profile for prediction case 1.

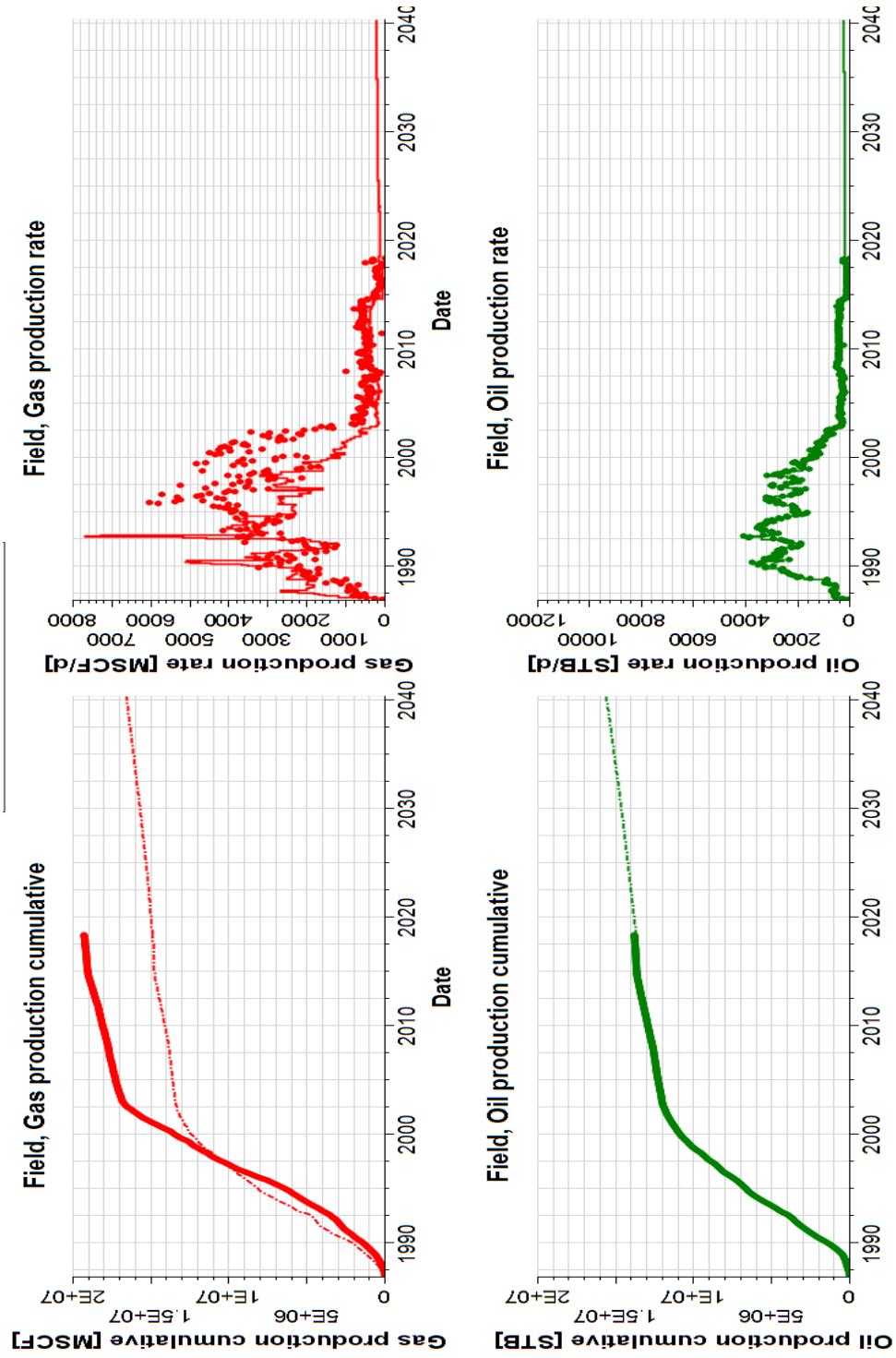

Figure 7-22. Field-wise oil and gas production profiles in base case study.

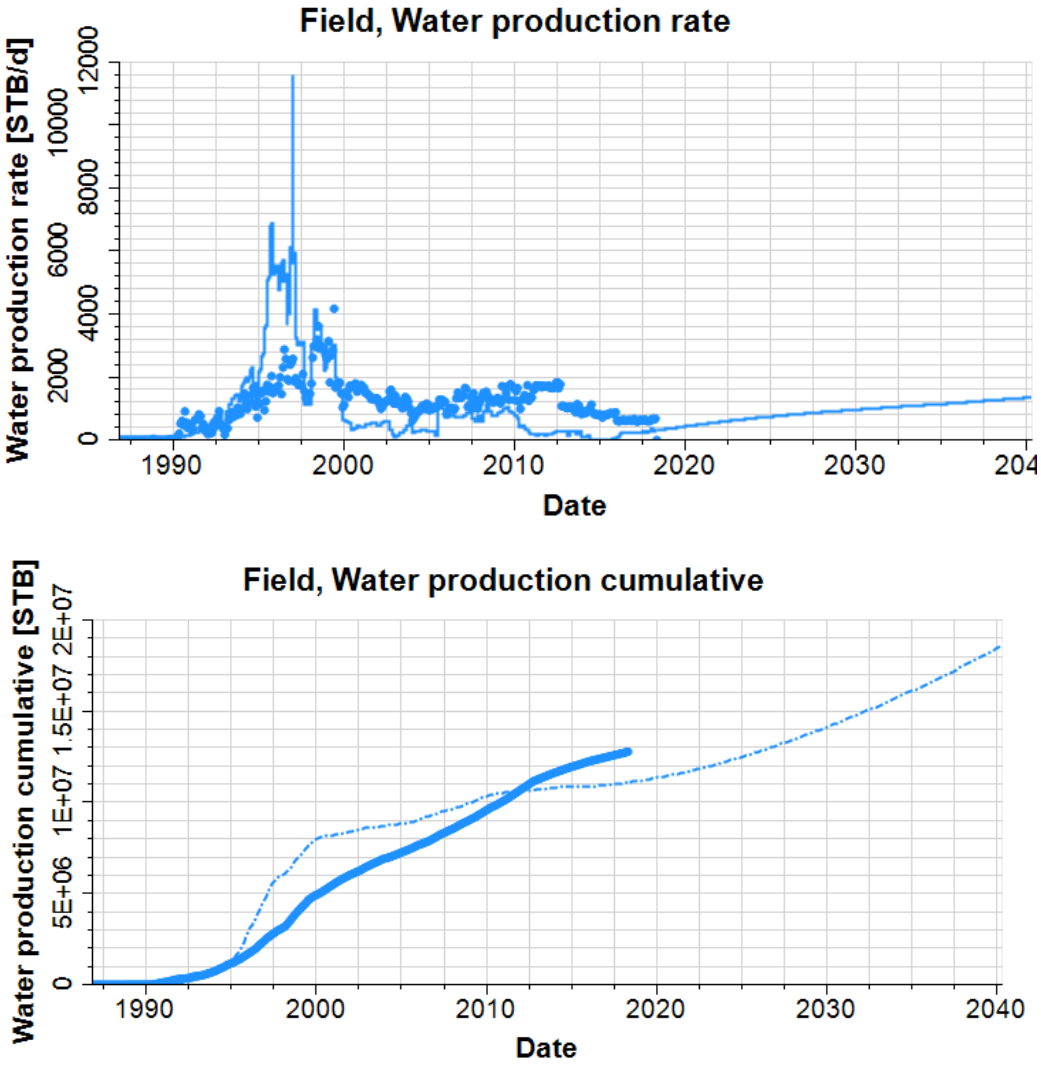

Figure 7-23. Field-wise water production profile in the base case.

Table 7-6. Comparison of History match and Prediction case 1 results

Production Parameters	End of History, 2018	End of Prediction 2040
Oil rate (stb/day)	238.7	269.78
Water rate (stb/day)	339.6	1379.3
Gas rate (Mscf/day)	174.6	246.88
Cumulative Oil Production (MMSTB)	13.74	15.65
Cumulative Water Production (MMSTB)	11.16	18.5
Cumulative Gas Production (MMSCF)	14.97	16.65

As shown in Table 7-6, it can be observed that at the end of prediction, cumulative oil production has increased from 13.74 to 15.65 MMSTB. The incremental oil recovery during the 20-year production was forecasted to be 1.91 MMSTB. Field pressure has increased a little because of the continuous response from the injection well.

7.6.2: Prediction Case 2 (follow the trend)

In this prediction case, FBHP was set to follow the trend of each active producer for the last few years of history match. Among the four producers, there are two wells with increasing FBHP, and two wells with decreasing FBHP. Overall, at the end of the prediction, the field pressure increased a little as shown in the following plot.

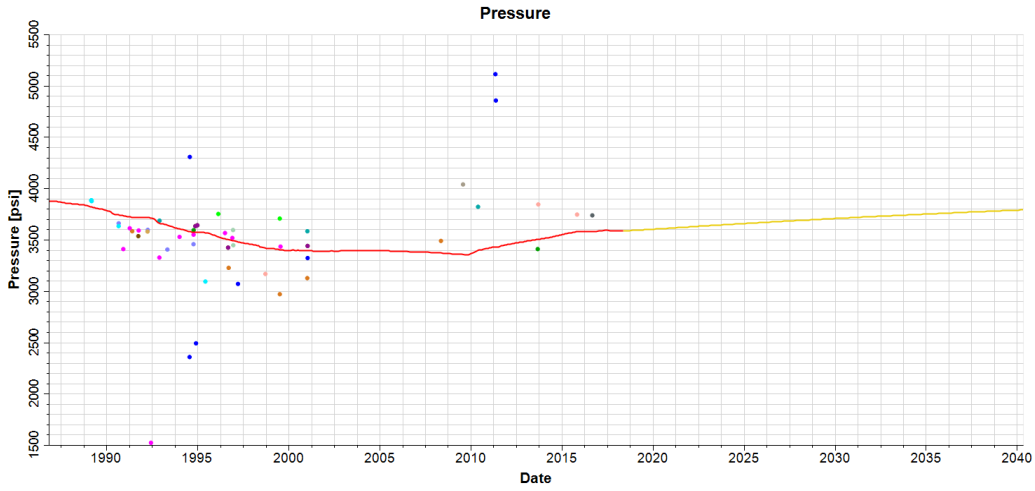

Figure 7-24. Field Pressure result from prediction case 2.

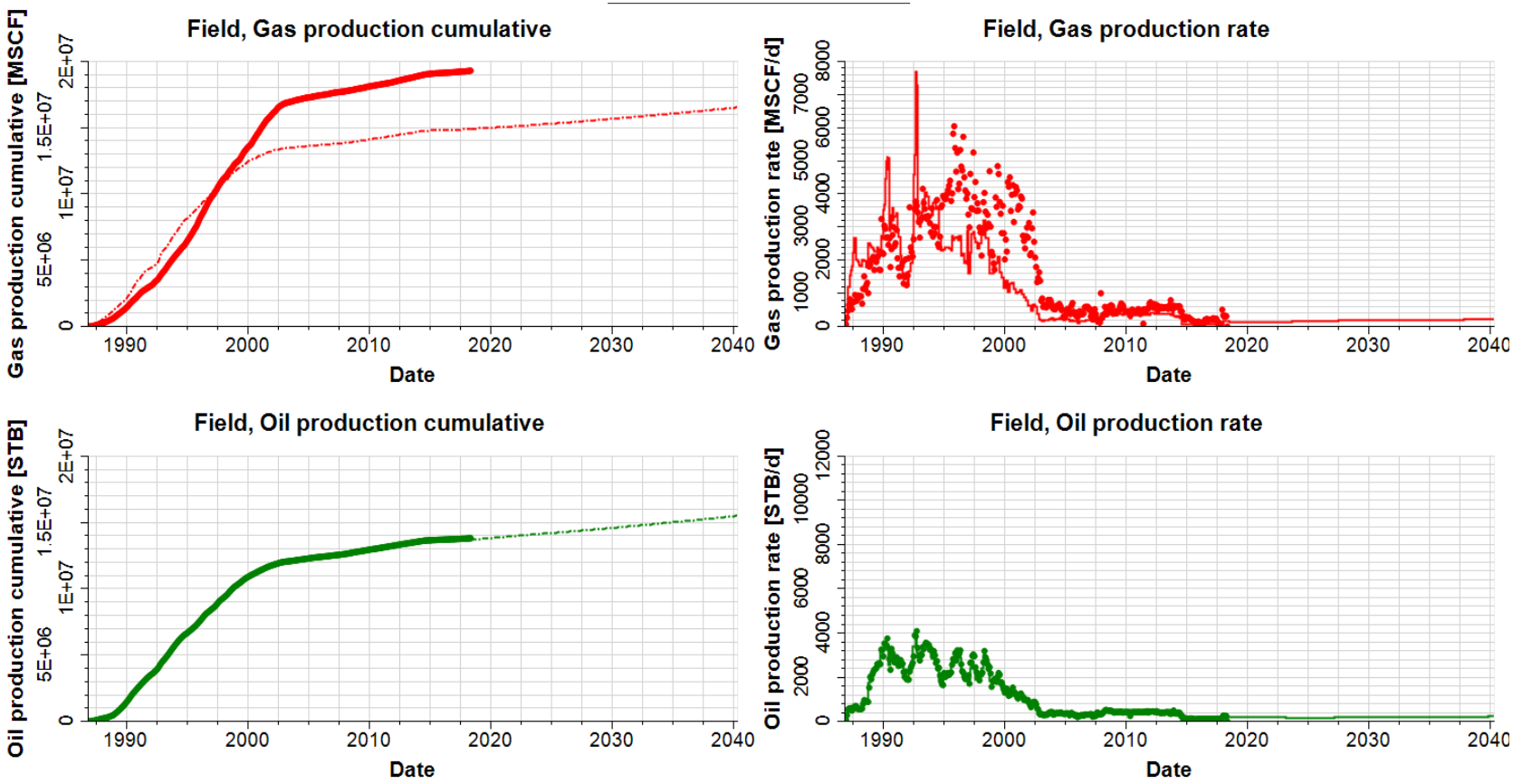

Figure 7-25. Field-wise oil and gas production profiles in case 2 study.

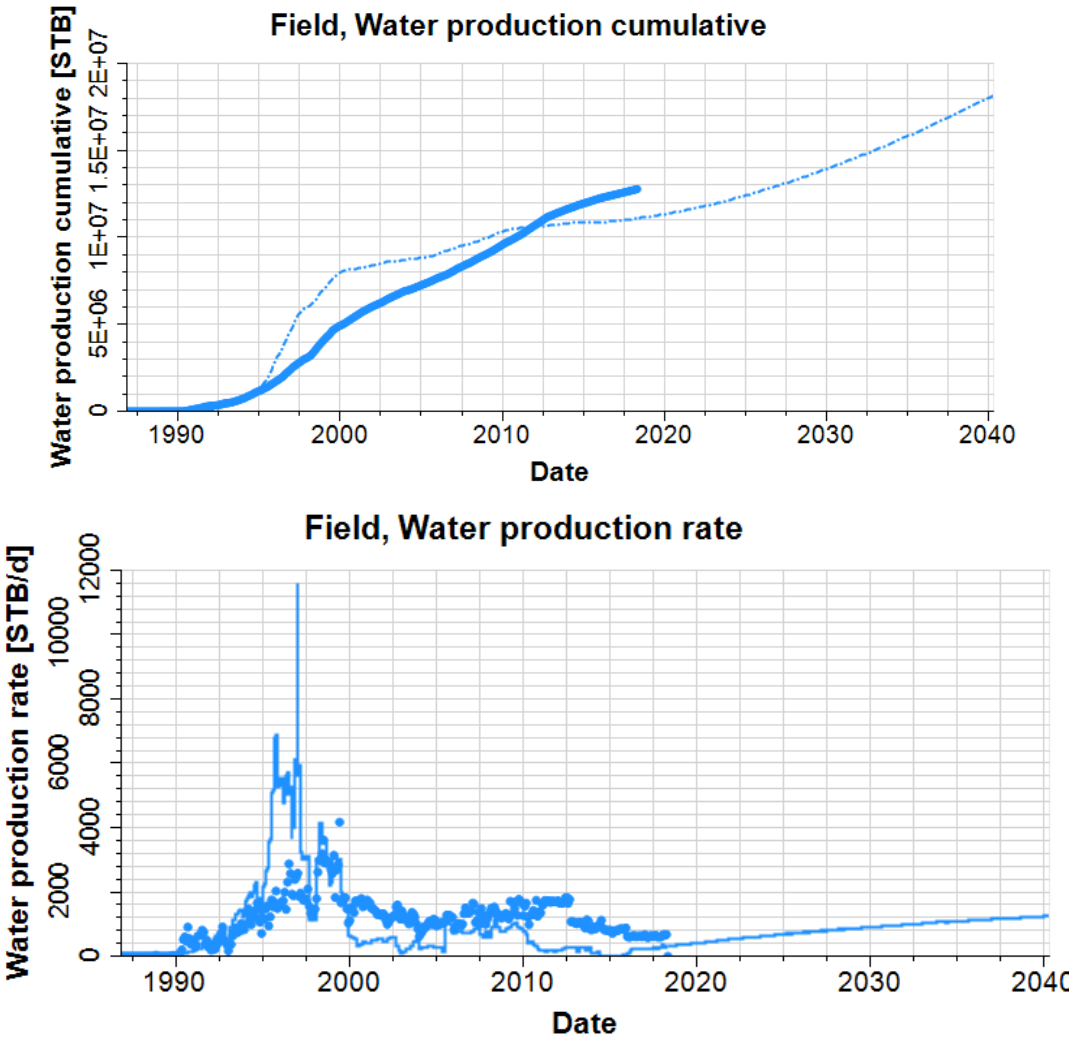

Figure 7-26. Field water production result from prediction case 2.

Table 7-7. Comparison of history match and prediction case 2

Production Parameters	End of History, 2018	End of Prediction 2040
Oil rate (stb/day)	238.7	262.32
Water rate (stb/day)	339.59	1278.5
Gas rate (Mscf/day)	174.6	248.81
Cumulative Oil Production (MMSTB)	13.74	15.55
Cumulative Water Production (MMSTB)	11.16	18.13
Cumulative Gas Production (MMSCF)	14.97	16.58

Table 7-7 shows that at the end of prediction, cumulative oil production has increased by 1.82 MMSTB. Field pressure increased slightly in prediction case-2 because of the pressure support from the injection wells.

7.6.3: Prediction Case 3 (FBHP decreases 5 psi per year)

In the prediction case 3, the flowing bottom-hole pressure (FBHP) of each active producer was set to decrease by 5 psi every year. The injection rate was kept to be the same as it was in the history match. Figure 7-27 shows the field pressure profile of this prediction case. With time, the field pressure gradually increases, which is partially due to the continuous water injection.

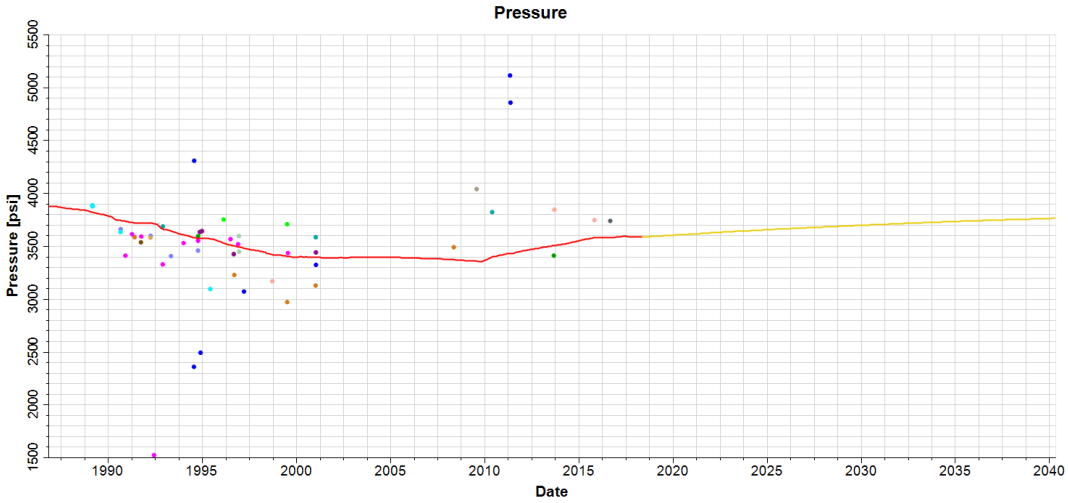

Figure 7-27. Field-wise reservoir pressure profile for prediction case 3.

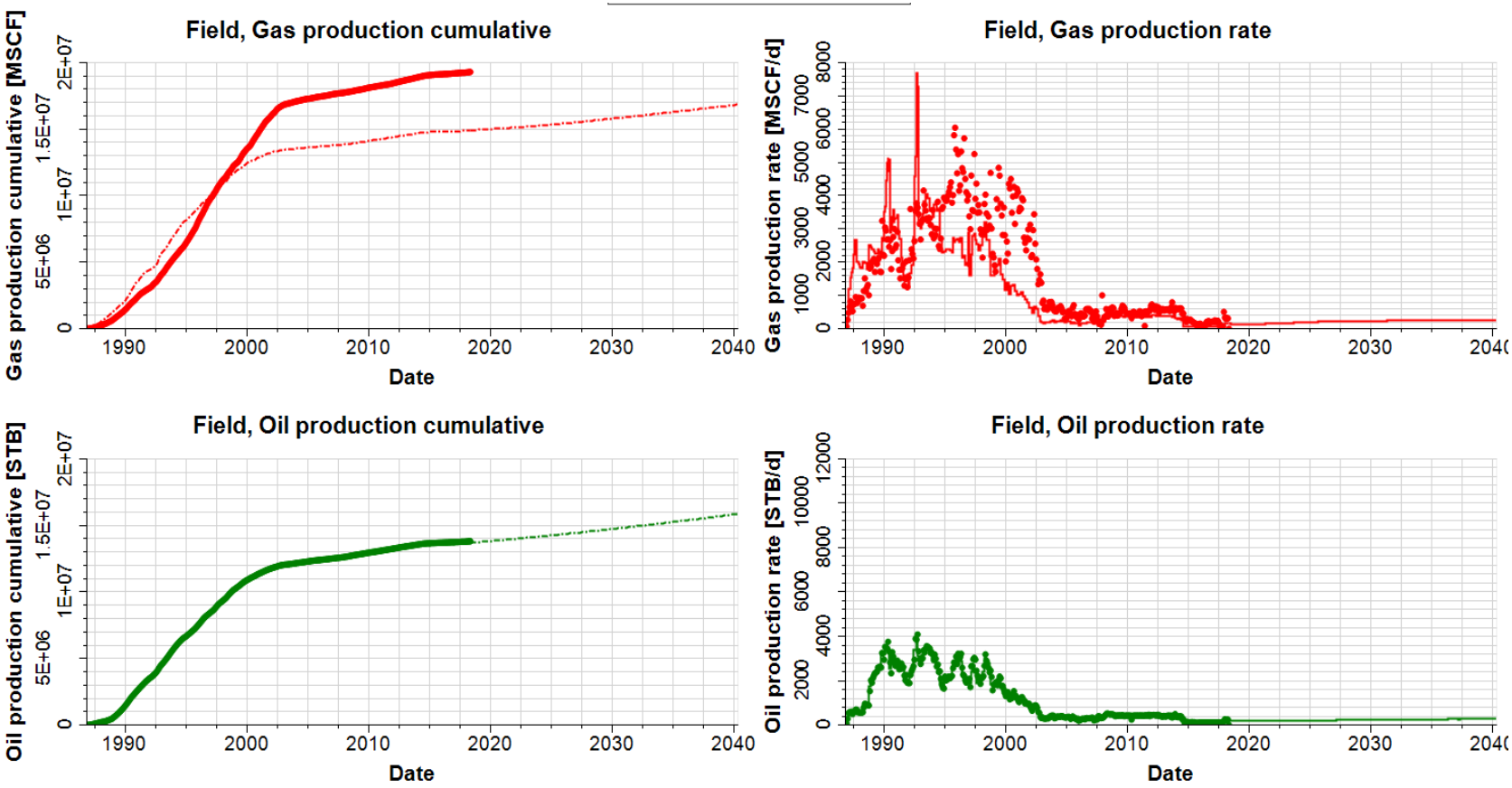

Figure 7-28. Field-wise oil and gas production profiles in case 3 study.

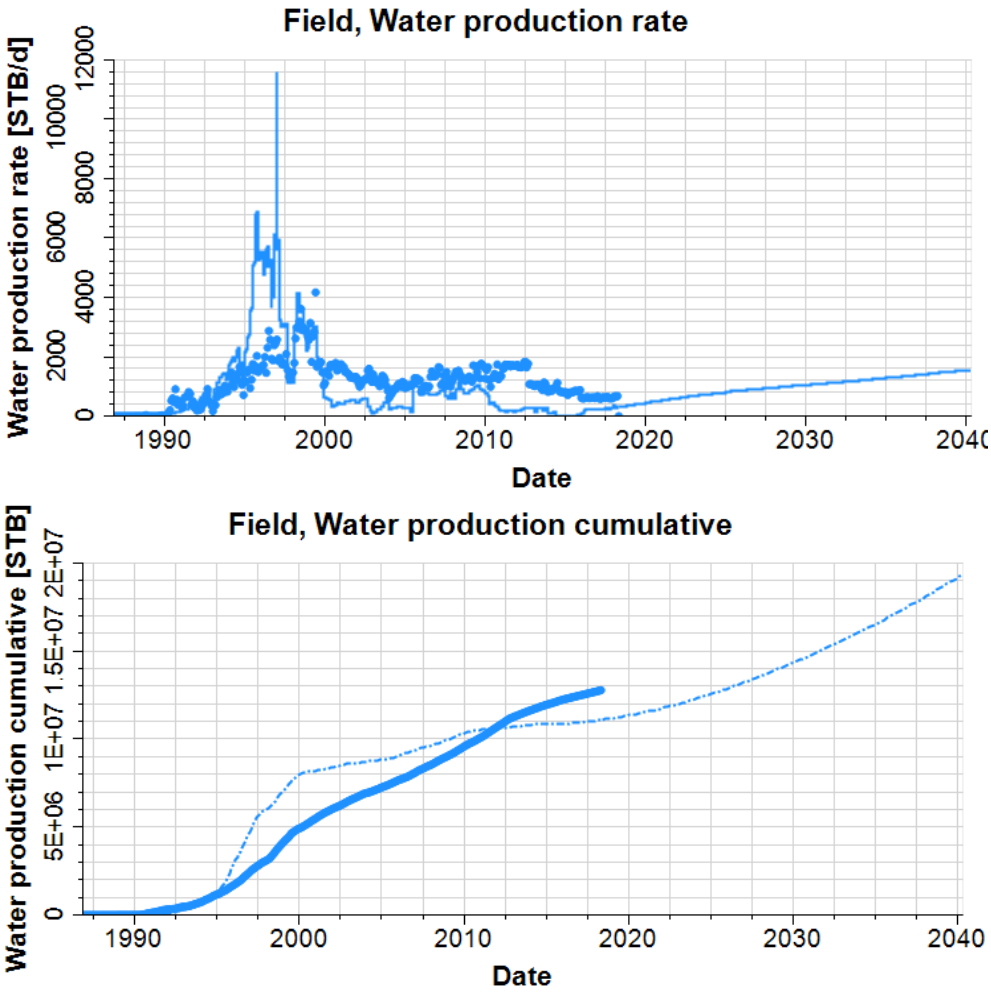

Figure 7-29. Field-wise water production profile in case 3 study.

Table 7-8. Comparison of history match and prediction case 3

Production Parameters	End of History, 2018	End of Prediction 2040
Oil rate (stb/day)	238.7	308.5
Water rate (stb/day)	339.59	1587.8
Gas rate (Mscf/day)	174.6	287.9
Cumulative Oil Production (MMSTB)	13.74	15.9
Cumulative Water Production (MMSTB)	11.16	19.4
Cumulative Gas Production (MMSCF)	14.97	16.88

In Table 7-8, it can be observed that by 2040, the cumulative oil production increases by 2.18 MMSTB. Compared with the previous two prediction cases, case 3

has the largest incremental oil production. This may be because the reservoir pressure in the simulator was decreased by 5 psi per year.

7.6.4: Prediction Case 4 (Base Case + one infill well)

In the history matching simulation study, the current remaining hydrocarbon map can be generated through Petrel RE. This map assists in detecting the location of bypassed oil. Figure 7-30 presents the net oil pay map. Net oil pay is a function of oil saturation at the end of history match, porosity, and cell thickness. One proposed well, UH-1, is recommended to be drilled in the high net oil pay area. The surrounding wells are N502 and N505. The properties and productivity of these two wells are considered as the constraints for the infill well in the prediction case. The distance between UH-1 and N505 is 879 ft. and the distance between UH-1 and N502 is 905ft. In the performance prediction simulation run, this new infill well was made to open from May 2018 to 2040. It was also controlled by FBHP which was kept constant till 2040. All other existing wells were in the same condition as they were in the prediction base case.

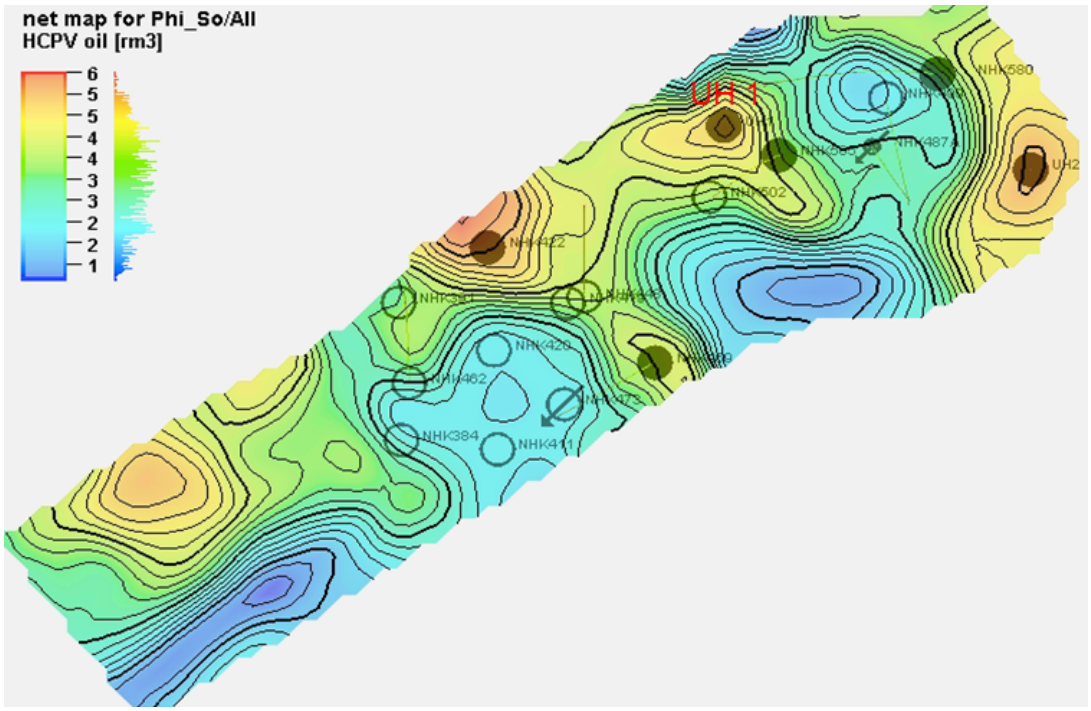

Figure 7-30. Infill well (UH-1) location.

Figure 7-31 shows that the field pressure of this infill prediction case. The field pressure does not increase as much as previous three prediction cases (without infill well) because oil is produced much more.

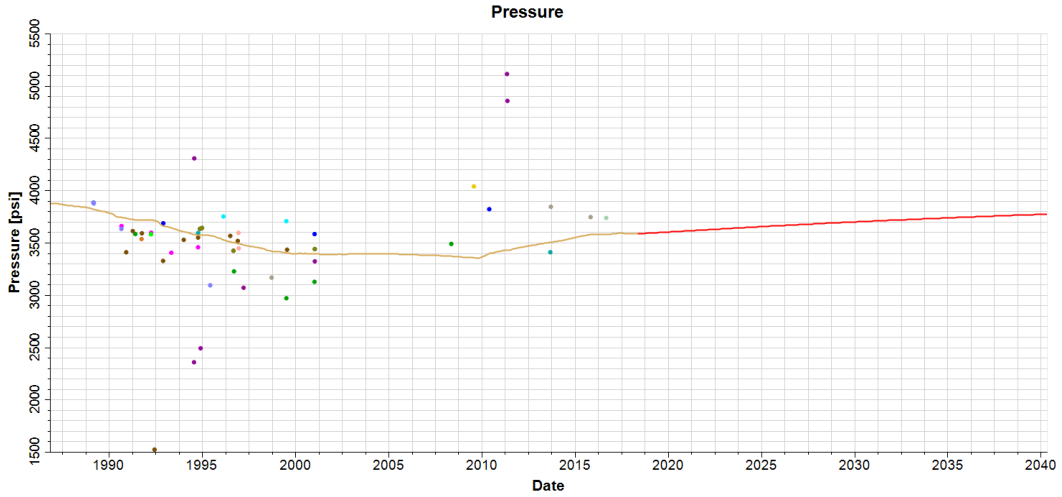

Figure 7-31. Field-wise reservoir pressure profile for prediction case 4.

Cumulative field production plots are shown in Figure 7-32 and Figure 7-33.

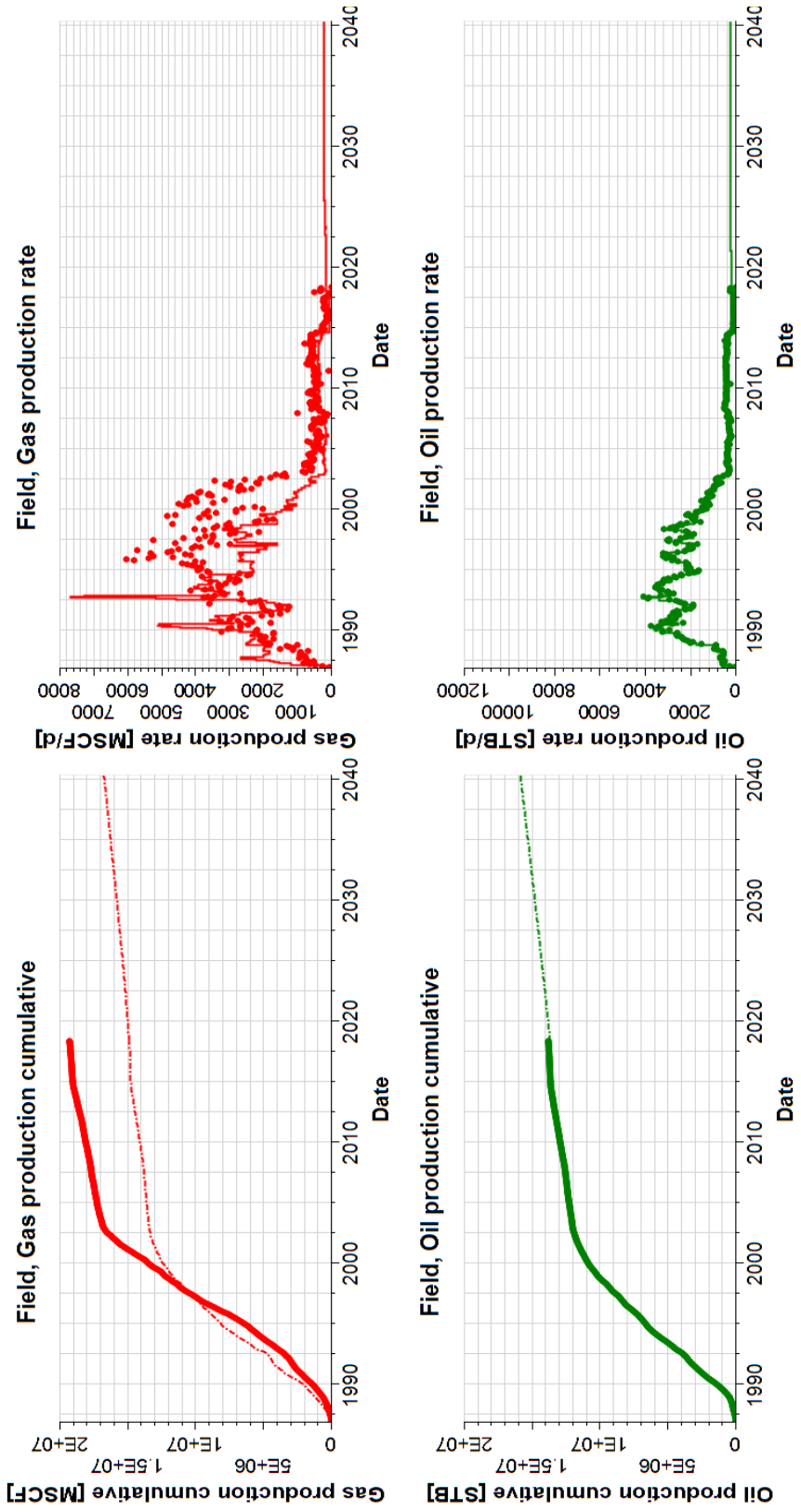

Figure 7-32. Field-wise oil and gas production profile in case 4 study.

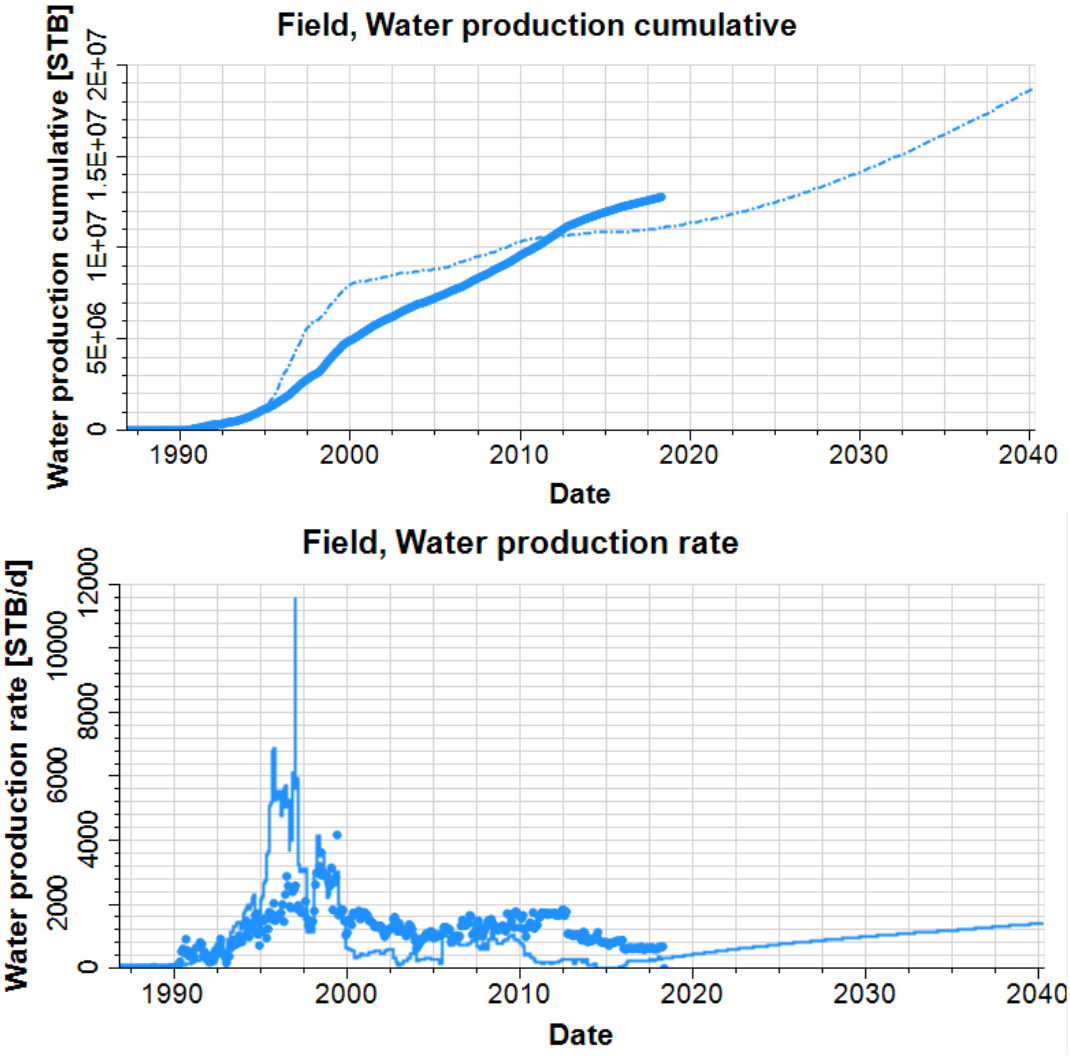

Figure 7-33. Field-wise water production profile in case 4 study.

Table 7-9. Comparison of history match and prediction case 2

Production Parameters	End of History, 2018	End of Prediction 2040
Oil rate (stb/day)	238.7	281.3
Water rate (stb/day)	339.6	1437.3
Gas rate (Mscf/day)	174.6	253.8
Cumulative Oil Production (MMSTB)	13.76	15.9
Cumulative Water Production (MMSTB)	11.16	18.71
Cumulative Gas Production (MMSCF)	14.97	16.83

In Table 7-9 shows that at the end of prediction in case-4, the cumulative oil production increases by 2.14 MMSTB.

7.6.5: Prediction Case 5 (Base Case + UH-2)

Similarly, in case-5, we proposed another promising infill well by utilizing the same net oil pay map as shown in Figure 7-34. This infill well, UH-2, will open to produce from May 2018 to 2040. Well UH-2 is controlled by FBHP, which is set as the average FBHP of two surrounding wells (N499 and N580). The distance between UH-2 and N499 is 2047 ft. and the distance between UH-2 and N580 is 1689 ft. All other existing wells will be kept under the same conditions as they are in the base case study.

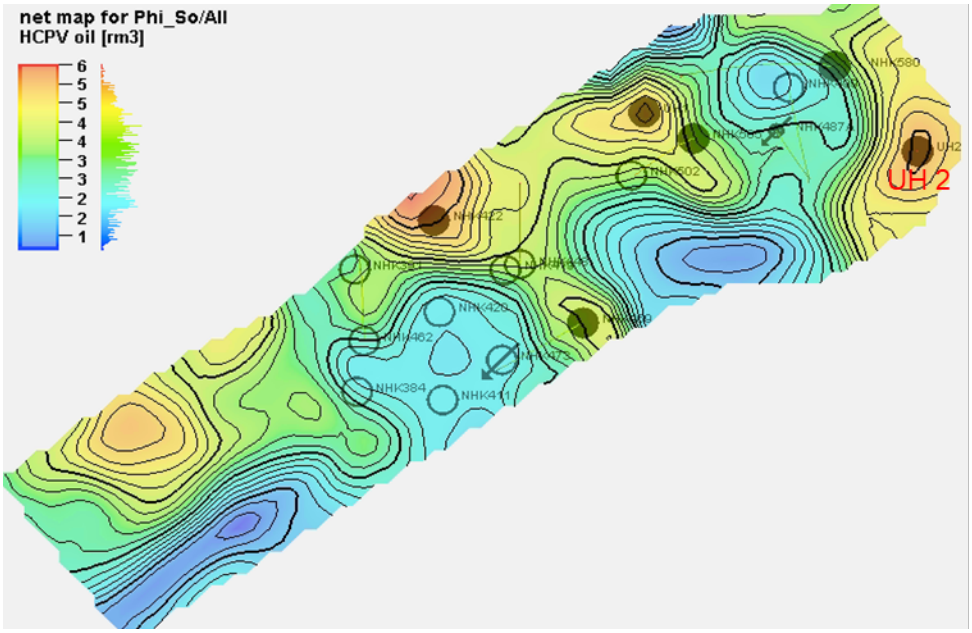

Figure 7-34. Infill well (UH-2) location.

The Figure 7-35 shows the field pressure for this infill prediction case. The field pressure increases less than it is in prediction case 4. The well UH-2 produces more oil than that from UH-1.

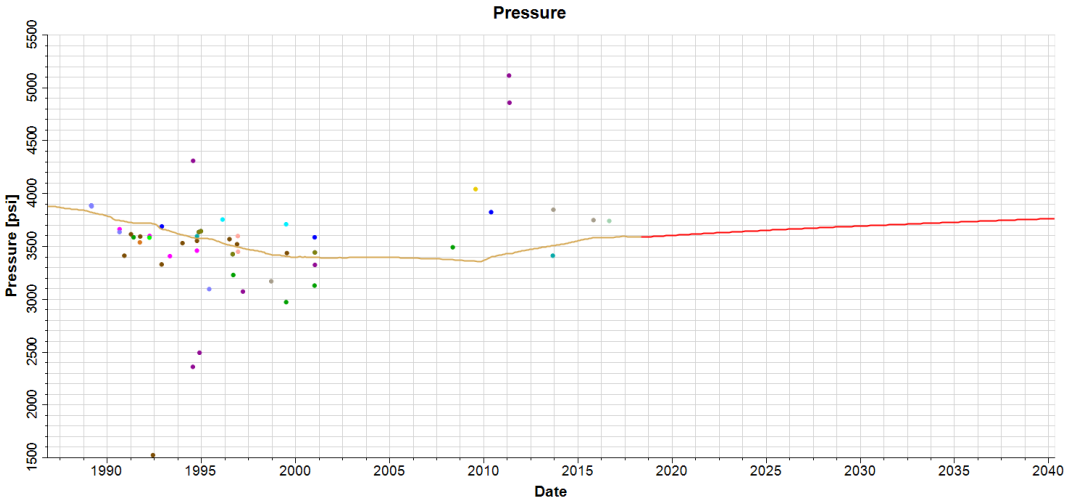

Figure 7-35. Field-wise reservoir pressure profile for prediction case 5.

Cumulative field production plots are shown in Figures 7-36 and 7-37.

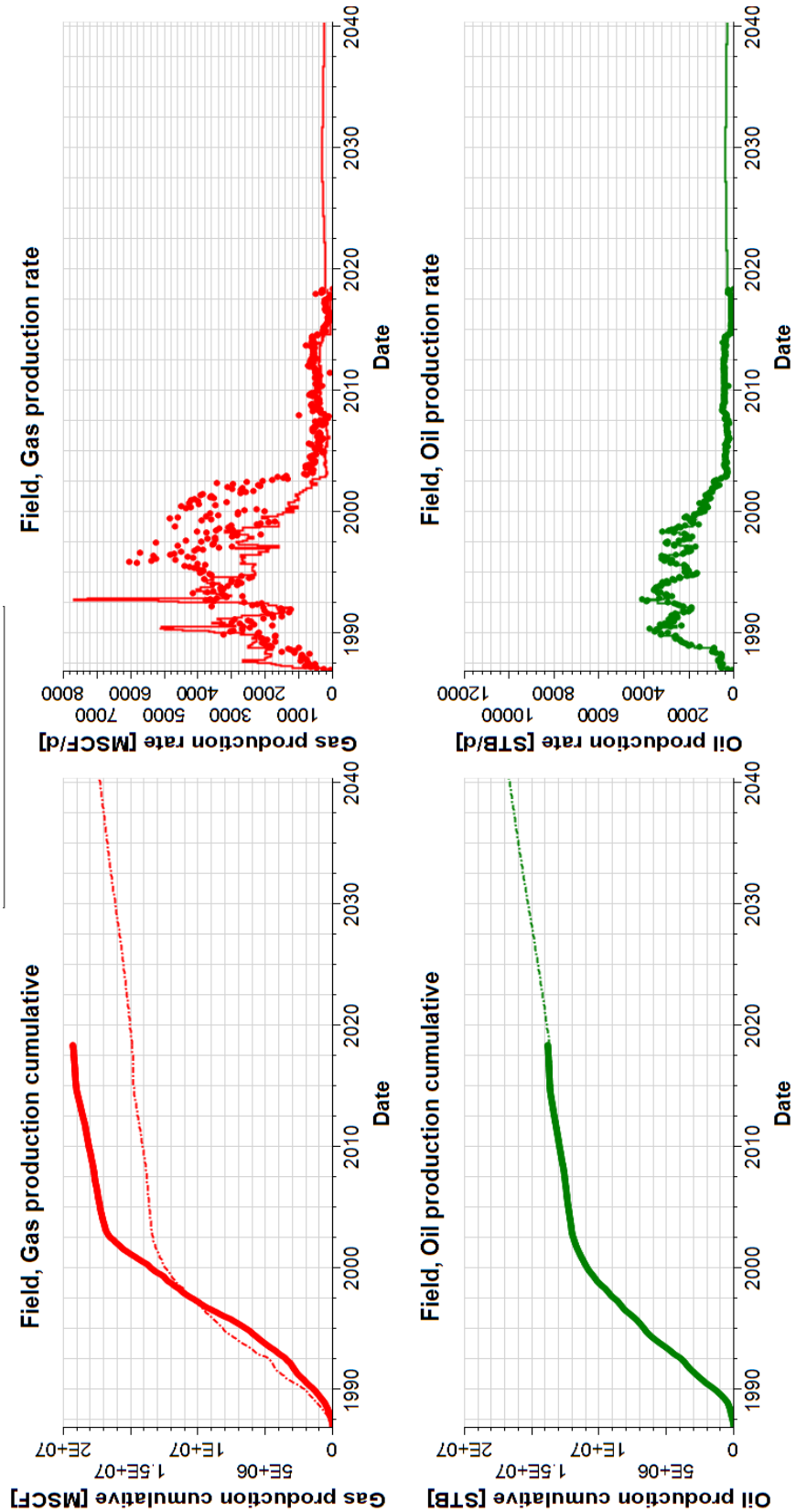

Figure 7-36. Field-wise oil and gas production profile in case 5 study.

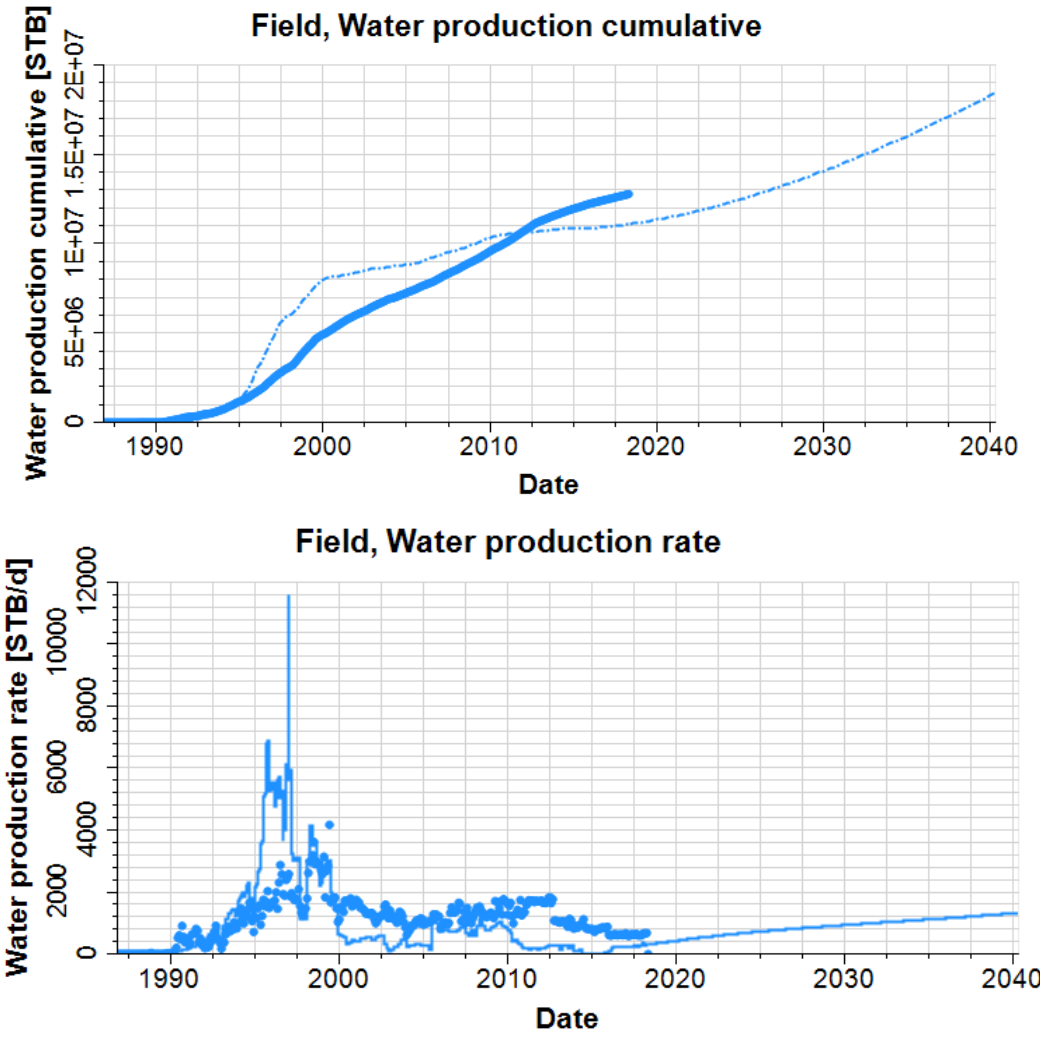

Figure 7-37. Field-wise water production profile in case 5 study.

Table 7-10. Comparison of history match and prediction case 5

Production Parameters	End of History, 2018	End of Prediction 2040
Oil rate (stb/day)	238.7	346.7
Water rate (stb/day)	339.59	1357.4
Gas rate (Mscf/day)	174.6	287.2
Cumulative Oil Production (MMSTB)	13.74	16.66
Cumulative Water Production (MMSTB)	11.16	18.35
Cumulative Gas Production (MMSCF)	14.97	17.34

Table 7-10 shows that at the end of the prediction run the cumulative oil production increases by 2.92 MMSTB.

7.6.6: Prediction Case 6 (Base Case + two infill wells)

In prediction case 6, two infill wells UH-1 and UH-2 were added together in the prediction simulation run. All other existing wells were kept under the same conditions as they were in the base case. The field pressure only increases slightly since these two infill wells together produced a significant amount of oil while water injection through one injector continued.

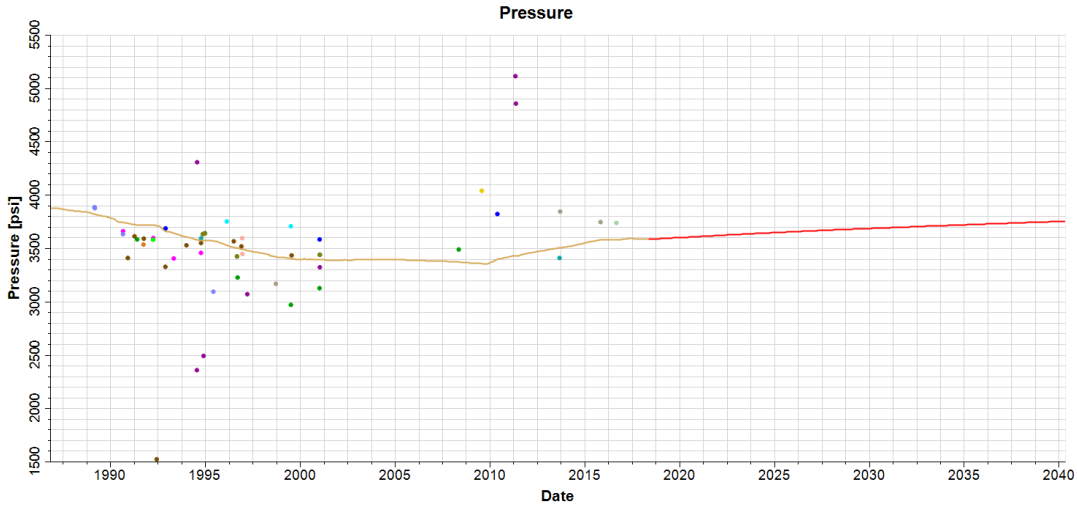

Figure 7-38. Field-wise reservoir pressure profile for prediction case 6.

Cumulative field production is shown in the figures 7-39 and 7-40.

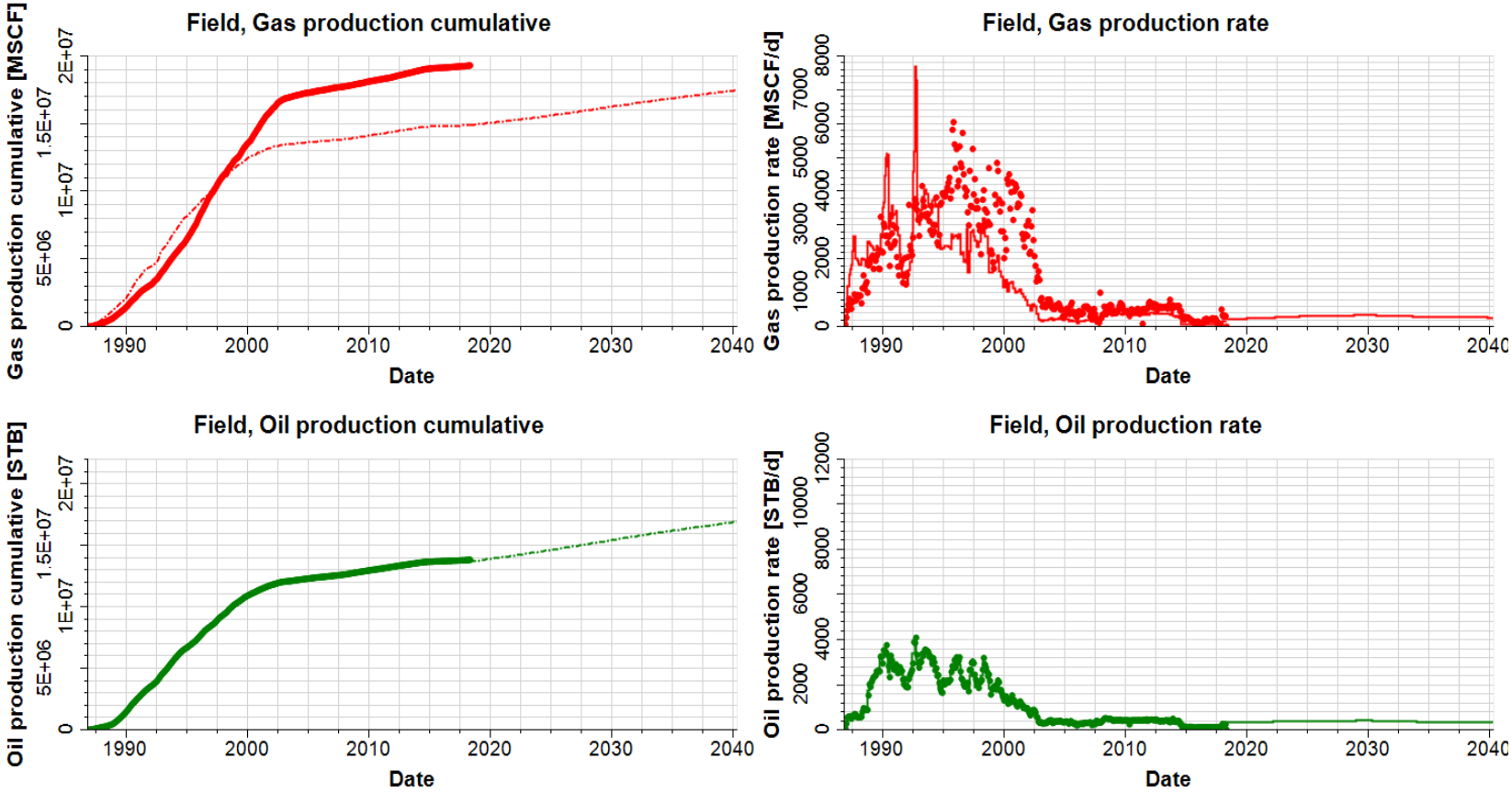

Figure 7-39. Field-wise oil and gas production profile in case 6 study.

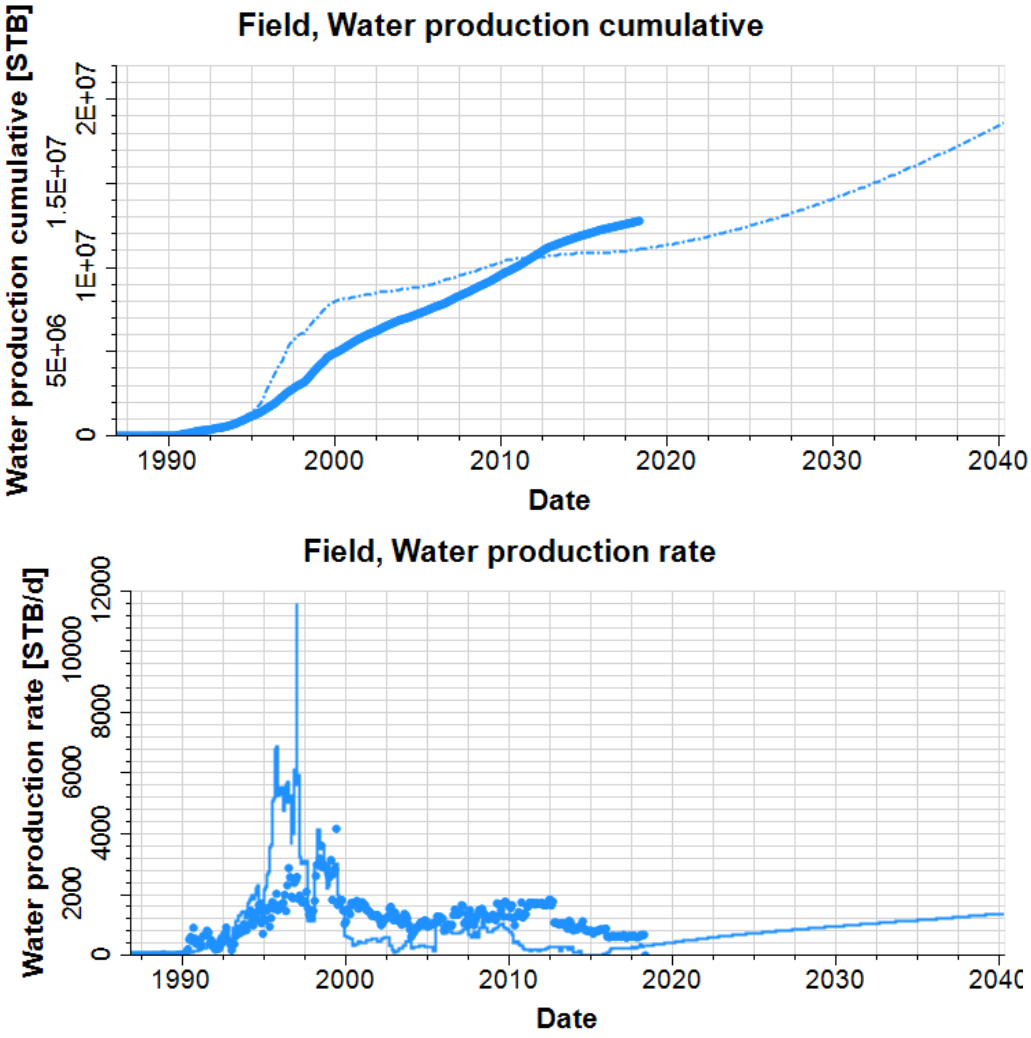

Figure 7-40. Field-wise water production profile in prediction case 6 study.

Table 7-11. Comparison of history match and prediction case 6

Production Parameters	End of History Match, 2018	End of Prediction 2040
Oil rate (stb/day)	238.7	359.37
Water rate (stb/day)	339.59	1412.4
Gas rate (Mscf/day)	174.6	296.53
Cumulative Oil Production (MMSTB)	13.74	16.95
Cumulative Water Production (MMSTB)	11.16	18.57
Cumulative Gas Production (MMSCF)	14.97	17.52

Table 7-11 shows that at the end of the prediction, the incremental oil production reaches 3.21 MMSTB.

7.6.7: Prediction Cases Comparison

In this section, all prediction cases are compared, and incremental oil production is calculated to systematically investigate the conditions under which cumulative oil recovery will be the highest. Comparison shows that the case with two infill wells gives the highest production and the case following FBHP trend of active producers gives the lowest incremental oil production.

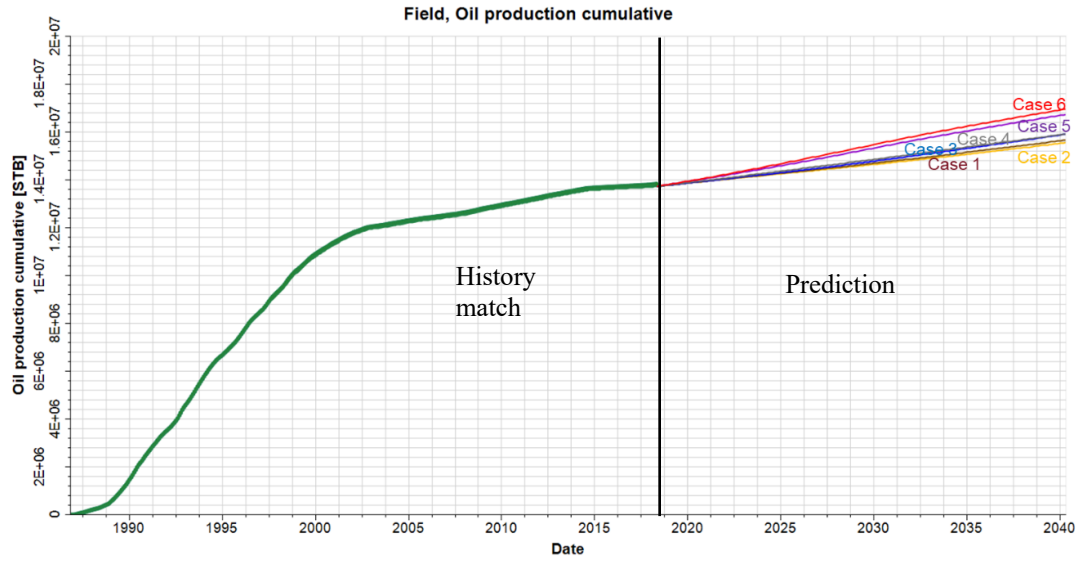

Figure 7-41. Cumulative oil production of prediction cases.

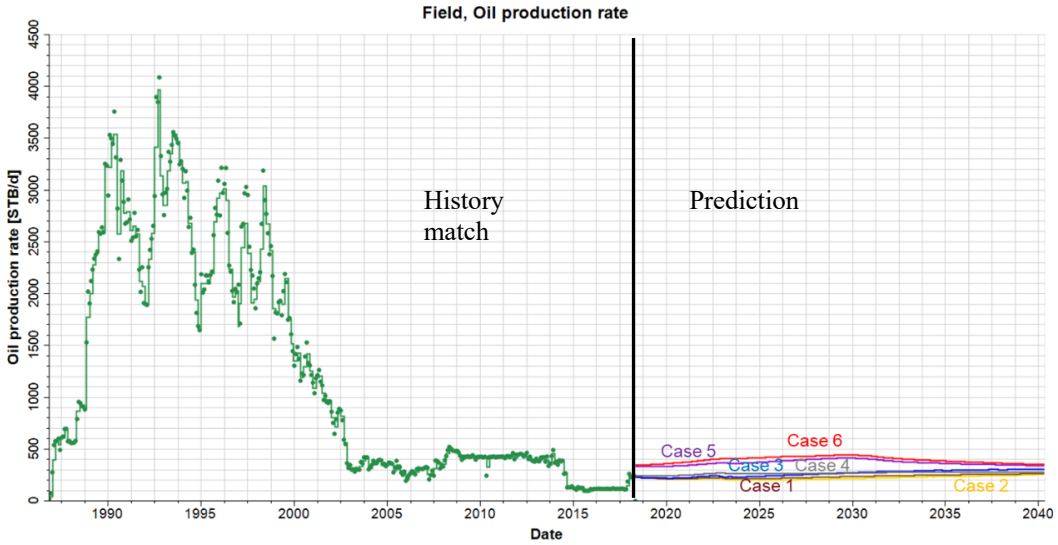

Figure 7-42. Oil rate comparison of prediction cases.

Table 7-12. Oil production comparison for prediction cases

Case	Current Cumulative Production (end of history), MMSTB	Cumulative Production by 2040, MMSTB	Incremental Production, MMSTB
1	13.76	15.7	1.94
2	13.76	15.58	1.82
3	13.76	15.94	2.18
4	13.76	15.95	2.19
5	13.76	16.77	3.01
6	13.76	16.99	3.23

In Table 7-12, cumulative production in all prediction cases are compared at the end of 2040 to the end of history match. It can be observed that the prediction case with two infill wells has the most promising production with 3.23 MMSTB incremental oil.

In Table 7-13, EUR estimation is compared from all methods used in the thesis. Analytical methods give the higher estimation than simulation base case.

Table 7-13. EUR comparison.

	Method	EUR, MMSTB
Analytical	Decline Curve Analysis	16.33
	WOR vs. Cum. Production	16
Simulation	Prediction Case 1	15.7
	Prediction Case 2	15.58
	Prediction Case 3	15.94
	Prediction Case 4	15.95
	Prediction Case 5	16.77
	Prediction Case 6	16.99

The above EUR numbers appear to be low for a mature water injection project. I suspect that our OOIP calculation is inaccurate. I recommend that further research be conducted in determining a more accurate OOIP value.

CHAPTER 8: CONCLUSIONS AND RECOMMENDATIONS

The work performed in this thesis is an attempt to apply reservoir engineering concepts with an aim to find IOR opportunities to improve well performance. All field data (geoscience, reservoir, production, wells) were reviewed in detail to accomplish this study. The major conclusions drawn from this study are as follows:

For active producers:

1. Well N422 and N469:
    a. Keep current status for future development to reach a higher recovery.
    b. A decreasing water cut indicates a positive response of waterflooding management.
    c. Measure current FBHP to determine whether they need to be decreased to obtain a higher oil production.
2. Well N505:
    a. Initially control the abrupt increasing water cut (from 60% to 77%) before move to waterflooding implementation (Investigate whether the injection rate should be decreased from surrounding wells).
    b. The reason for an abrupt decrease in oil rate at the end of history is needed. (Increasing water cut might be the reasons).Find out the reason for an increasing water cut and an abrupt decrease in oil rate at the end of history.
3. Well N580:
    a. The well was reopened in Dec. 2017. Production data for only 5 months is available.
    b. A longer observation is needed to make further recommendations.

4. Based on simulation prediction cases, infill well (UH2) has a higher potential in oil production (1.07 MMSTB), and it should be put in a higher priority in infill-well options.
5. New findings (alternative ABC Plot) assist in identifying specific issues of individual well. It is recommended to test on other fields.

REFERENCES

Baker, R., 1998. *Reservoir Management For Waterfloods-Part II*. Petroleum Society of Canada. DOI:10.2118/98-01-DA

Chen, P., Zhu, Y., Deka, A., Kuma, C., Kuma, M., Balasubramanian, S., & Thakur, G., 2019. *A Robust Reservoir Screening Approach to Identify IOR/EOR Opportunities from Mature Oilfields*. *SPE Western Regional Meeting, 23-26 April 2019, San Jose, California, USA*. Society of Petroleum Engineers. DOI:10.2118/195270-MS

Cobb, W. M., & Marek, F. J., 1997. *Determination of Volumetric Sweep Efficiency in Mature Waterfloods Using Production Data*. *SPE Annual Technical Conference and Exhibition, 5-8 October, 1997, San Antonio, Texas, USA*. Society of Petroleum Engineers. DOI:10.2118/38902-MS

Dyes, A.B., Caudle, B.H., and Erickson, R.A., 1954. *Oil production After Breakthrough as Influenced by Mobility Ratio*. JPT 27-32; Trans., AIME, 201

Fassihi, M. R., 1986. *New Correlations for Calculation of Vertical Coverage and Areal Sweep Efficiency*. Society of Petroleum Engineers. DOI:10.2118/13945-PA

Johnson, C. E., 1956. *Prediction of Oil Recovery by Waterflood - A Simplified Graphical Treatment of the Dykstra-Parsons Method*. Society of Petroleum Engineers. DOI:10.2118/733-G

Lee, A.L., Gonzales, M.H. and Eakin, B.E., 1966. *The Viscosity of Natural Gases*. Trans., AIME 237, 997-1000.

Lehr, W., Calhoun, D., Jones, R., Lewandowski, A., & Overstreet, R., 1994. "*Model Sensitivity Analysis in Environmental Emergency Management: A Case Study in Oil Spill Modeling,"* Proceeding of the 1994 Winter Simulation Conference, J. D. Tew, S. Manivannan, D. A. Sadowski, and A. F. Seila (eds), pp. 1198 – 1205.

Mattax, C. C., & Dalton, R. L., 1990. *Reservoir Simulation*. SPE Monograph 13

Satter, A., Varnon, J. E., & Hoang, M. T., 1994. *Integrated Reservoir Management.* Society of Petroleum Engineers. DOI:10.2118/22350-PA

Souza, A.O. de, Brigham, W.E., 1995. *A study of Dykstra-Parsons curves*. The United States. DOI: 10.2172/10115919

Terrado, R. M., Yudono, S., & Thakur, G. C., 2006. *Waterflooding Surveillance and Monitoring: Putting Principles into Practice*. *SPE Annual Technical Conference and Exhibition, 24-27 September, 2006, San Antonio, Texas, USA*. Society of Petroleum Engineers. DOI:10.2118/102200-MS

Thakur, G. C., 1990. *Reservoir Management: A Synergistic Approach*. Society of Petroleum Engineers. Permian Basin Oil and Gas Recovery Conference, 8-9 March, 1990, Midland, Texas, USA. DOI:10.2118/20138-MS

Thakur, G. C., 1991. *Waterflood surveillance Techniques - A Reservoir Management Approach*. Society of Petroleum Engineers. DOI:10.2118/23471-PA

Walsh, M. P., 1995. *A Generalized Approach to Reservoir Material Balance Calculations*. Petroleum Society of Canada. DOI:10.2118/95-01-07

William C. Lyons, Gary J. Plisga, Michael D. Lorenz., 2016. *Standard Handbook of Petroleum and Natural Gas Engineering (Third Edition)*. Gulf Professional Publishing, Pages 5-1-5-291. ISBN 9780123838469